Robust Control of the Contact Force of an Active Pantograph for High Speed Trains

Myat Thiri Ko

Graduate School of Science and Technology

Niigata University, Japan

2017

Acknowledgments

The work presented in this thesis was carried out between September 2014 and August 2017 at the graduate school of advanced science and engineering at Niigata University in Niigata, Japan.

Firstly, I would like to thank my supervisor, Associate professor Makoto Yokoyama in particular, for giving me the opportunity to work as a Ph.D. student and guiding me exploring the unknown world. Due to his devotion of immense amount of effort and time, the writing of this dissertation became possible. I would like to give special thanks to the Dr. Y. Yamashita, Dr. T. Usuda and Dr. S. Kobayashi of the Railway Technical Research Institute for their valuable contributions in the development of our active pantograph.

I also would like to thank all my colleges in our nonlinear laboratory, especially Nagayoshi and Miura who have been very helpful not only in laboratory but also in personal matters. Especially, Nagayoshi helped me on study of active pantograph for two years. I also would like to thank the people around me, due to their support, I survived in Japan. The writing of this dissertation become possible due to the financial support of Japan International Cooperation Agency (JICA), Tokyo.

In the end, I want to show my most heartfelt gratitude to my parents and my husband, for their encouragements and supports in the past three years.

Myat Thiri Ko

Contents:

List of Tables

Abbreviations

HILS	Hardware in the loop simulation
VSS	Variable structure system
SRL	Symmetric root locus
AC	Alternative current
DC	Direct current
LQR	Linear quadratic regulator

Chapter 1

Introduction

1.1 Introduction

High speed trains are a fast transport system in many countries and is getting popular all over the world. With the development of railway technology, electric field trains have proven to have many advantages over other forms of transport systems, i.e. high energy efficiency, high specific installed power, low maintenance cost, more responsive control, no emissions in urban areas, and energy-saving by regeneration brake systems. However, it also has some drawbacks: high capital cost of providing the energy distribution, complex to operate in regions with different electrical supply standards and poor current collecting quality when running above the originally intended operational speed. Today, electrically powered trains are widely used on the main railway lines in many countries. [1,2,3]

Fig 1.1 High Speed Train in Japan

Figure 1.1 shows a high-speed train with the pantograph and catenary system. The functions of pantograph is to collect the electric energy from the catenary and transfer it to the locomotives motors, so that they have enough energy to operate. The pantograph-catenary system is an elaborately-designed system which can keep a good quality of electricity transmission at relatively high speeds. The pantograph can automatically be raised from the folded position and work at a certain range of the height while sustaining a constant uplift force. The catenary is a well-suspended structure kept in a desired geometry.

For high-speed trains, active control of the pantograph is crucial technology to collect electrical current from the overhead contact wire supported by vertical droppers, hangers and cantilevers. When the pantograph runs along the catenary, it is fluctuated due to aerodynamic force, propagation and reflection of the wave on the catenaries, changes in the dynamics characteristics of the catenary system depending on the position, etc. An excessively large contact force can damage both in the pantograph and the catenary or may cause a severe accident like contact wire breaking in the worst case. On the other hand, if the contact force is too small, the pantograph and catenary easily lose their contact state. The state the pantograph and catenary are in the non-contact state is called contact loss.

If the dynamic interaction between pantograph and catenary is not constrained within an acceptable range, in some extreme cases, not only a high maintenance cost can be expected but also serious structural damage can appear. With the development of the railway technology in recent years, the operational speeds for most railway line have significantly been increased world-widely, so the pantograph-catenary becomes one of the key factors which decide the cost of infrastructure and maintenance, and limit the operational speed. Therefore, it is quite important for both engineers and researchers to investigate the dynamic behavior of the pantograph-catenary system to keep the contact tight and stable. The increase of the static contact force, which might be considered as a possible solution for this problem, is not an efficient way, because it increases mechanical abrasive wear and produces an excessive uplift of the contact wire.

Therefore, maintaining the contact force in an admissible region is crucial for high speed trains and thus modeling and control of active pantograph-catenary systems have been taken much attention from many researchers. So far, some models and controllers for the systems have been proposed. For example, Arnold and Simeon

developed a rather rigorous model with PDEs and DAEs and then proposed a numerical solution method [4], Makino et al. developed a wing-shaped low-noise collector and proposed an H_∞ controller with a disturbance observer [5], Yamashita et al. developed a low-noise active pantograph, and then applied a PID controller or an impedance control method [6], Chartter et al. proposed a controller based on the back-stepping method together with a high-gain observer [7], Allota, Pisano, et al. proposed higher order sliding mode controllers [8]-[10], Sanchez-Rebollo et al. proposed a hardware-in-the-loop strategy with a PID controller [11].

In order to regulate the contact force, the authors and the Railway Technical Research Institute have developed an active pantograph using a pneumatic actuator, and presented modelling and a robust regulator with a rigid frame model. In this thesis, three different types of control strategies are introduced. The design and performance of an active pantograph which collects current for high-speed train are considered. A dynamic model of the pantograph/catenary system is described and control objectives are established.

1.2 Objectives

As mentioned above, the modelling and the study of the pantograph-catenary system enables the saving of time and cost. By modelling these elements, engineers can make modifications and test new implementation to improve the quality of real pantographs, making them more perfect. The main objectives of this project can be summarized as presented below:

- Modelling the active pantograph with flexibility: to maintain the contact force in an admissible region
- Analyzing the pantograph-catenary system
- Applying different kinds of control theory to the controller design to regulate the more robust contact force
- Developing the best control configuration and control strategy

1.3 Contributions

This thesis investigates a dynamic behavior of the contact force variations of pantograph-catenary system based on numerical studies. There are three different types of controller together with an observer, which are introduced. They are

(1) Linear state feedback controller with sliding mode observer,

(2) Sliding mode servo controller with sliding mode observer and

(3) Optimal servo system based on sliding mode control with sliding mode observer. Although the first two control methods of the active pantograph systems in this thesis only regulate the contact force under model uncertainty or disturbance, but the last controller, optimal servo system, can realize to track the reference signal optimally by making efficient use of the active force.

The model of the pantograph was recovered from the work developed by the master student *Shun Nagayoshi*. Once the model has been obtained, the next stage is to investigate the dynamic properties both analytically from a systems-theory point of view and numerically. The system is studied with the computational tool *Matlab / Simulink* that enables knowing the response of the pantograph to the catenary's action.

1.4 Thesis Organization

This thesis is organized into five chapters:

Chapter 1 describes an introduction to all worked about the high speed train.

In Chapter 2, a basic structure of the pantograph head and the contact wire (catenary system) is described. The mathematical model of the pantograph head and the catenary system are constructed. Furthermore, a mathematical model of the pantograph and catenary has integrated to get the contact state because the train is considered as moving state. The stiffness of the overhead contact wire in catenary system is a main source of the variation of the pantograph-catenary system. Hence, it is emphasized that the fluctuation of the equivalent stiffness between the pantograph head and the overhead contact wire, makes it difficult to control the contact state of the system.

Chapter 3 proposes the linear state feedback controller together with the sliding mode observer, taking account of the flexibility of the articulated frame in our

pantograph. It is emphasized that one of the key points is to regulate the contact force in the nominal model without perturbation. A physical interpretation of the pole-zero cancellation in the transfer function is also given.

Chapter 4 is composed of two different sections. In the first section, we propose a sliding mode controller together with the sliding mode observer, taking account of the flexibility of the articulated frame in the actual pantograph. An introduction to the variable structure system (VSS) is described. The condition to ensure the switching surface, so-called reachability condition, is also described. The reduced order sliding dynamics is formulated. The proposed controller achieves the robust output (contact force) by pole-zero cancellation during sliding mode. Secondly, we analyze the robust stability of the active pantograph system using Lyapunov method.

Chapter 5 describes an optimal servo system based sliding mode controller together with a sliding mode observer. It is pointed out through our analysis of the plant and the closed-loop system using SRL (symmetric root locus) technique that pole-zero cancellations play an important role to control the contact force.

Chapter 6 summarizes the contribution of the thesis and points out some key ideas proposed in this thesis.

Chapter 2

Mathematical Model of the Pantograph and Problem Formulation

2.1 Pantograph Catenary interaction

Figure 2.1 shows a high-speed train with the overview of the pantograph and catenary system. The stationary system that consists of poles and the wires with the electric power supply is called catenary. The train is connected to the catenary system via pantograph which is mounted on the roof of the train. The catenary has two wires, the contact wire which is connected to the pantograph and the messenger wire above the contact wire is linked together over the droppers. The pantograph catenary is designated to transfer electric current to the train. As a contact pair is always moving, it is important to keep the contact between pantograph and catenary tight and stable.

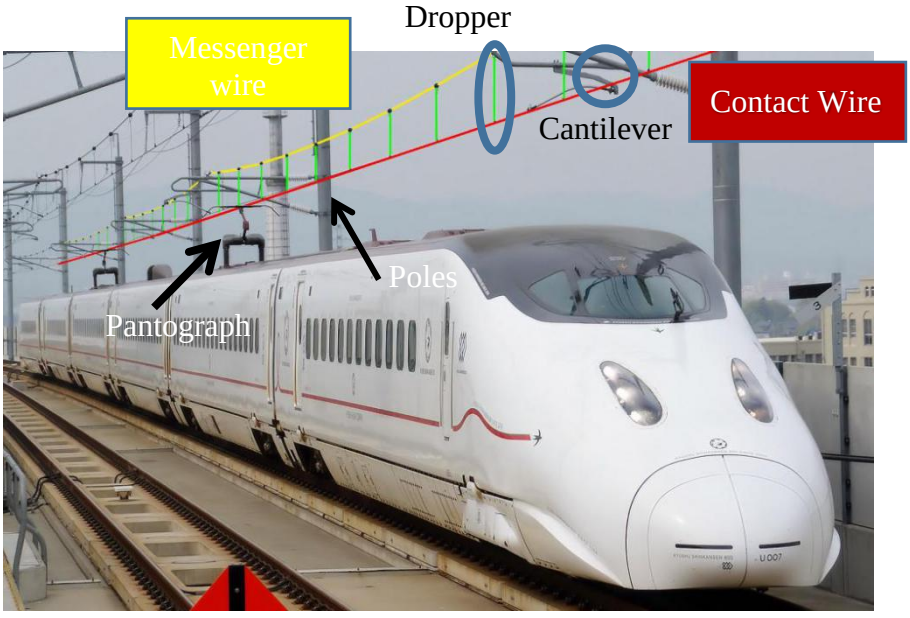

Fig 2.1 The train with pantograph and catenary system

2.1.1 Pantograph

The aim of pantograph system is to collect electrical current from the catenary cable system. In order to collect the current and not to interfere with the passing non-electric train under the overhead lines, the main frame is fold-able and can vertically raise the pantograph head a significant distance. To achieve good current collection, the pantograph head is sprung and is pushed against the overhead line. The drive, usually operated by compressed air from the brake system, is used to power the system to raise or fall, and provides sufficient uplift force to keep the contact between overhead line and pantograph head. Nowadays, there are several types of pantographs existing, but the principles are nearly the same. [2]

The pantograph consists of a part of body that come in contact with the overhead catenary and a frame that supports it. The frame is divided into upper frame and lower frame. The main spring acts to lift the entire pantograph upwards. For a passive pantograph, the only way to avoid the loss of contact at higher speed is to reduce both the mass of the pantograph head and the frame, but this is limited by the required current-carrying capacity of the pantograph.

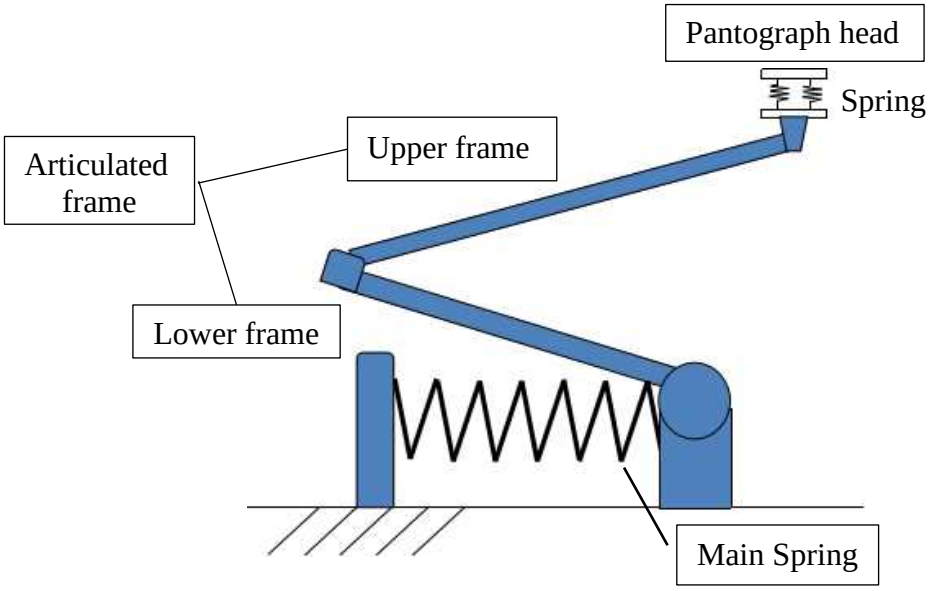

Fig 2.2 Pantograph

2.1.1.1 Force exerted on the pantograph

The pantograph suffers different types of forces which have different natures. They can be classified as static loads [12], dynamic loads and aerodynamic loads. The

application point of these forces is established in the contact point with the catenary wire. A summarized explanation of these forces is presented below:

1. Static contact forces: These loads are exerted on the pantograph when it raised still. This force is applied on the point where the overhead's strips contact with the catenary wire. A perfect pantograph should keep a constant static contact force across its route.
2. Dynamic contact forces: This component of the force depends on the nature of the contact and on the speed of the train.
3. Aerodynamic contact forces: This force must be differentiated from the aerodynamic force that opposes to the train's course. This aerodynamic force is a vertical force and it opposite to the vertical movement of the pantograph as consequence of the aerodynamic effects. These aerodynamic effects increase with the train speed, therefore a proper design both of the train and the pantograph needs to take account to them.

2.1.2 Active Pantograph

As mentioned above, the pantograph doesn't control the variations of the contact force by itself. In order to control the contact force between the pantograph and the catenary, the active pantograph with the pneumatic actuator have been developed. It was found through some experiments that the frame had flexibility which could not be ignored to control the contact force.

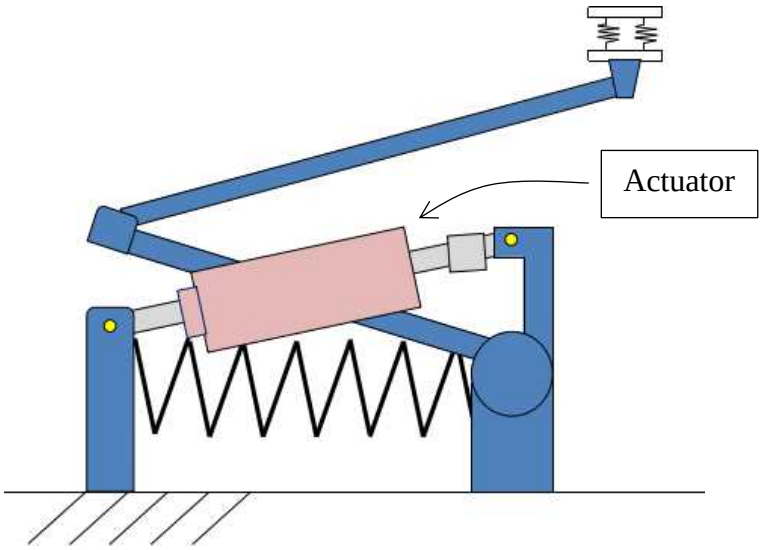

Fig 2.3 Active pantograph

2.1.3 Catenary

The catenary mainly consists of the contact wire, a continuous conduction which transfers electric current to the moving train through the pantograph, and some other supporters to support the weight of the contact line and to keep the contact wire in a certain shape at certain positions. [3] The structure of the catenary shown in fig 2.4. In general, a catenary is composed of one or two wires that ensure the power transmission to the pantograph, and it also counts with one or two complementary wires that are charged of maintaining the horizontality of the contact wire, as observed in fig 2.4.

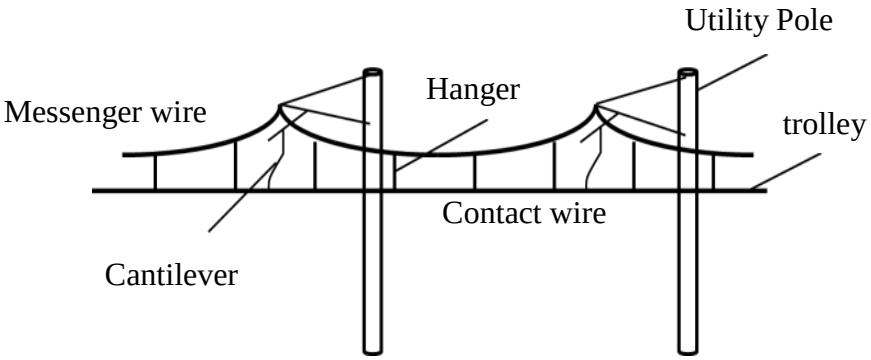

Fig 2.4 Catenary system

The upper wire is the messenger wire and the lower wire is the contact wire where the contact with the pantograph take places. The catenary is widely used in railways permitting operation at voltages above AC 1000V and DC 1500V, by which trains get sufficient power to run at a high speed. To achieve good current collection, it is necessary to keep the contact wire geometry within the definite limits. This is usually achieved by supporting the contact wire from above by a second wire known as catenary wire (or messenger wire).

2.1.3.1 Types of catenaries

1 (Tramway) Catenary

It is the simplest catenary, it consist on a wire tended between two supports. It is used in low speed tracks. It greatest advantage is the presence of stiff points

at the supports, what leads to the interruption of the contact between the pantograph and the catenary.

2 AC Catenary

When running at high speeds becomes, the use of tramway catenaries is no longer an option. This is due to the fact that catenaries start oscillating when the train starts to run at high speeds. This can be solved by using an additional wire which positioned over the contact wire with the mission of holding the latter. Two kinds of catenary can be used, AC (Alternative current) or DC (Direct current) catenaries. It is easier to boost the AC voltage than the DC voltage, so it is send more power with AC lines. As AC is easier to transmit over long distances, it is an ideal medium for electric railway's supply. This catenary is the most used in long lines requiring from trains running at high speeds.

3 DC Catenary

DC catenary, is preferred in shorter lines, urban systems and tramways. As shorter line trains required less power, DC catenaries supply the enough power to the railway's traction. It must be mentioned that corrosion is an important factor to be considered in DC systems.

2.2 Mathematical Model of the System

2.2.1 Mathematical model of the catenary system`

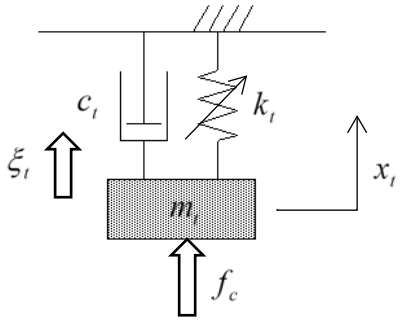

Fig 2.5 Catenary model

A catenary is a complex periodic structure. The catenary model described here is use a simplified spring, mass and damper model as shown in fig 2.5. The catenary mass and the damper are time-invariant elements and the spring is as the time-varying element k_t. The equation of motion can be written as

$$m_t \ddot{x}_t = -c_t \dot{x}_t - k_t x_t + f_c + \xi_t \tag{2.1}$$

where $\xi_t = \Delta k_t x_t$ defines as the uncertainty/ disturbance due to the change of the equivalent stiffness k_t of the catenary system. The state equation can be expressed as

$$\begin{aligned} \begin{bmatrix} \dot{x}_t \\ \ddot{x}_t \end{bmatrix} &= \begin{bmatrix} 0 & 1 \\ -\frac{k_t}{m_t} & -\frac{c_t}{m_t} \end{bmatrix} \begin{bmatrix} x_t \\ \dot{x}_t \end{bmatrix} + \begin{bmatrix} 0 \\ \frac{1}{m_t} \end{bmatrix} f_c + \begin{bmatrix} 0 \\ \frac{1}{m_t} \end{bmatrix} \xi_t \\ &= \mathbf{A}\mathbf{x}_t + \mathbf{h}_t f_c + \mathbf{d}_t \xi_t \end{aligned} \tag{2.2}$$

where t is taken as the short form of the trolley (Catenary).

2.2.2 Mathematical model of pantograph system

Taking account of the flexibility in the frame, a three degree of freedom model is developed as shown in fig 2.6, where m_s, m_{f1} and m_{f2} are masses of the pantograph head, the upper frame and lower frame, respectively, f_a is static uplift force generated by the main spring which is denoted as the actuator force (the other variables are defined as shown below in table 2.1). In this research, the disturbance such as aerodynamic fore, static loads, etc… which are neglected.

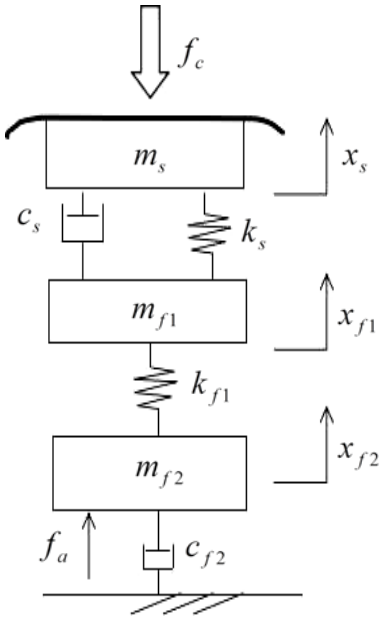

Fig 2.6 Pantograph model

The equation of motion of the system can be written as

$$
\begin{aligned}
m_s\ddot{x}_s &= -c_s(\dot{x}_s - \dot{x}_{f1}) - k_s(x_s - x_{f1}) - f_c \\
m_{f1}\ddot{x}_{f1} &= -c_s(\dot{x}_{f1} - \dot{x}_s) - k_s(x_{f1} - x_s) - c_{f1}(\dot{x}_{f1} - \dot{x}_{f2}) - k_{f1}(x_{f1} - x_s) \\
m_{f2}\ddot{x}_{f2} &= -c_{f1}(\dot{x}_{f2} - \dot{x}_{f1}) - k_{f1}(x_{f2} - x_{f1}) - c_{f2}\dot{x}_{f2} + f_a
\end{aligned}
\tag{2.3}
$$

Hence the following linear and time-invariant of the state space representation was derived to

$$\begin{bmatrix} \dot{x}_s \\ \ddot{x}_s \\ \dot{x}_{f1} \\ \ddot{x}_{f1} \\ \dot{x}_{f2} \\ \ddot{x}_{f2} \end{bmatrix} = \begin{bmatrix} 0 & 1 & 0 & 0 & 0 & 0 \\ -\frac{k_s}{m_s} & -\frac{c_s}{m_s} & \frac{k_{f1}}{m_s} & \frac{c_{f1}}{ms} & 0 & 0 \\ 0 & 0 & 0 & 1 & 0 & 0 \\ \frac{k_s}{m_{f1}} & \frac{c_s}{m_{f1}} & -\frac{(k_s+k_{f1})}{m_{f1}} & -\frac{(c_s+c_{f1})}{m_{f1}} & \frac{k_{f1}}{m_{f1}} & \frac{c_{f1}}{m_{f1}} \\ 0 & 0 & 0 & 0 & 0 & 1 \\ 0 & 0 & \frac{k_{f1}}{m_{f2}} & \frac{c_{f1}}{m_{f2}} & -\frac{k_{f2}}{m_{f2}} & -\frac{(c_{f1}+c_{f2})}{m_{f2}} \end{bmatrix} \begin{bmatrix} x_s \\ \dot{x}_s \\ x_{f1} \\ \dot{x}_{f1} \\ x_{f2} \\ \dot{x}_{f2} \end{bmatrix} + \begin{bmatrix} 0 \\ -\frac{1}{m_s} \\ 0 \\ 0 \\ 0 \\ 0 \end{bmatrix} f_c + \begin{bmatrix} 0 \\ 0 \\ 0 \\ 0 \\ 0 \\ \frac{1}{m_{f2}} \end{bmatrix} f_a \tag{2.4}$$

$$= \mathbf{A}_p \mathbf{x}_p + \mathbf{h}_p \mathbf{f}_c + \mathbf{b}_p \mathbf{f}_a$$

where p is used as the short form of the pantograph model. The physical parameters used here are shown in Table 2.1.

Table 2.1 Physical parameters					
Catenary stiffness	k_t	[N/m]	Catenary damping	c_t	[Ns/m]
Mass of catenary	m_t	[kg]			
Shoe-upper frame stiffness	k_s	[N/m]	Shoe-upper frame damping	c_s	[Ns/m]
Mass of shoe	m_s	[kg]	Mass of upper frame	m_{f1}	[kg]
Upper frame-lower frame stiffness	k_{f1}	[N/m]	Upper frame-lower frame damping	c_{f1}	[Ns/m]
Mass of lower frame	m_{f2}	[kg]	Lower frame damping	c_{f2}	[Ns/m]
Contact force	f_c	[N]	Axis force	f_a	[N]
Displacement of contact wire/shoe	x_{ts}	[m]	Displacement of upper frame	x_{f1}	[m]
Displacement of lower frame	x_{f2}	[m]	Uncertainty/disturbance due to catenary's stiffness variation	ξ_t	[N]

2.2.3 Composite model of pantograph and catenary

Consider the train situation is always moving, it is desired to control the contact force variations and not to get the contact losses between the pantograph and catenary system, the overhead contact wire and pantograph have to keep in contact with each other. Therefore, it is determined to combine the catenary model which described in fig 2.5 and pantograph model which described in fig 2.6. Figure 2.7 shows the combine model when the contact wire and the pantograph are in contact state. Assuming that the overhead contact wire and the shoe on the pantograph head are connected all the time, the state vectors can be redefined as

$$x_t = x_s = x_{ts} \tag{2.5}$$

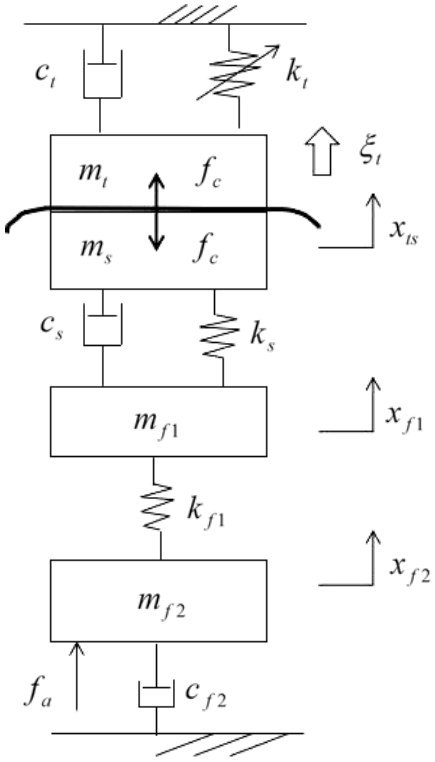

Fig 2.7 pantograph-catenary model

The origin in the coordinates is the equilibrium point, the equations of motion of the masses are given by

$$(m_t + m_s)\ddot{x}_{ts} = -(-c_t + c_s)\dot{x}_{ts} - (k_t + k_s)x_{ts} + c_s\dot{x}_{f1} + k_s x_{f1} + \xi_t \tag{2.6}$$

$$m_{f1}\ddot{x}_{f1} = c_s\dot{x}_{ts} + k_s x_{ts} - (c_s + c_{f1})\dot{x}_{f1} - (k_s + k_{f1})x_{f1} + c_{f1}\dot{x}_{f2} + k_{f1}x_{f2} \tag{2.7}$$

$$m_{f2}\ddot{x}_{f2} = c_{f1}\dot{x}_{f1} + k_{f1}x_{f1} - (c_{f1} + c_{f2})\dot{x}_{f2} - k_{f1}x_{f2} + f_a \tag{2.8}$$

Taking the state vector as,

$$\mathbf{x} = \begin{bmatrix} x_{ts} & \dot{x}_{ts} & x_{f1} & \dot{x}_{f1} & x_{f2} & \dot{x}_{f2} \end{bmatrix}^T \tag{2.9}$$

The state equation is

$$\dot{\mathbf{x}} = \begin{bmatrix} 0 & 1 & 0 & 0 & 0 & 0 \\ -\frac{k_t + k_s}{m_t + m_s} & -\frac{c_t + c_s}{m_t + m_s} & \frac{k_s}{m_t + m_s} & \frac{c_s}{m_t + m_s} & 0 & 0 \\ 0 & 0 & 0 & 1 & 0 & 0 \\ \frac{k_s}{m_{f1}} & \frac{c_s}{m_{f1}} & -\frac{k_s + k_{f1}}{m_{f1}} & -\frac{c_s + c_{f1}}{m_{f1}} & \frac{k_{f1}}{m_{f1}} & \frac{c_{f1}}{m_{f1}} \\ 0 & 0 & 0 & 0 & 0 & 1 \\ 0 & 0 & \frac{k_{f1}}{m_{f2}} & \frac{c_{f1}}{m_{f2}} & -\frac{k_{f1}}{m_{f2}} & -\frac{c_{f1} + c_{f2}}{m_{f2}} \end{bmatrix} \mathbf{x} \qquad (2.10)$$

$$+ \begin{bmatrix} 0 \\ 0 \\ 0 \\ 0 \\ 0 \\ \frac{1}{m_{f2}} \end{bmatrix} f_a + \begin{bmatrix} 0 \\ \frac{1}{m_t + m_s} \\ 0 \\ 0 \\ 0 \\ 0 \end{bmatrix} \xi_t$$

$$= \mathbf{A}\mathbf{x} + \mathbf{b}u + \mathbf{d}_t \xi_t$$

Since the contact force includes inertial force of the overhead contact wire and pantograph head, in order to obtain an expression of the contact force, we need the following equations of motion with respect to each mass independently.

$$m_t \ddot{x}_t = -c_t \dot{x}_t - k_t x_t + f_c - \Delta k_t x_t \qquad (2.11)$$

$$m_s \ddot{x}_s = -c_s (\dot{x}_s - \dot{x}_{f1}) - k_s (x_s - x_{f1}) - f_c \qquad (2.12)$$

From these equations, it follows the contact force equation can be represented by

$$f_c = \frac{1}{m_t + m_s} \left\{ (c_t m_s - m_t c_s) \dot{x}_{ts} + (k_t m_s - m_t k_s) x_{ts} + m_t c_s \dot{x}_{f1} + m_t k_s x_{f1} \right\} \qquad (2.13)$$

$$- \frac{m_s}{m_t + m_s} \xi_t$$

The contact force state equation can be given by

$$f_c = \frac{1}{m_t + m_s}\begin{bmatrix} k_t m_s - m_t k_s & c_t m_s - m_t c_s & m_t k_s & m_t c_s & 0 & 0 \end{bmatrix}\mathbf{x} - \frac{m_s}{m_t + m_s}\xi_t = \mathbf{c}\mathbf{x} + d\xi_t \tag{2.14}$$

2.2.4 Stiffness variations of the catenary

Figure 2.8 shows the diagram of the catenary stiffness, when the train speed is 360km/h. The distance between two poles is set to 50meters. The wire length is usually from 1 km to 1.5 km, depending on the temperature ranges. When the pantograph moves along the overhead wire, its stiffness variation produces a periodic excitation which leads to the vibration of the pantograph and the fluctuation of the contact force. A main source of vibration is the stiffness variation of the contact wire along the span. The stiffness of the overhead wire is the minimum at the middle of the span and it is the maximum at the around the support tower, which means that the catenary stiffness k_t is always change with the time. In this thesis, the variations of the catenary stiffness is treated as the disturbance. And then consider the fluctuation range of the contact force due to the changes of the stiffness variations. The catenary stiffness k_t varies between

$$200 \le k_t \le 2000 \tag{2.15}$$

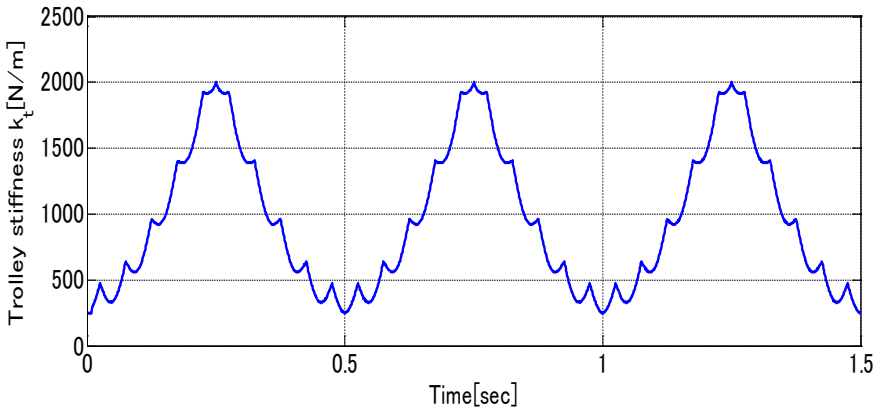

Fig 2.8 Catenary Stiffness

2.3 System analysis of the open loop control system

In this section, we do analyze the state equation of the pantograph catenary system (eq 2.10) and the output equation (eq 2.13). The parameters are set according to the values from Table (2.2) and d stands for the disturbance input to the pantograph-catenary model. From the identification experiments of these parameters, the equivalent stiffness coefficient of the catenary, k_t is defined as a time varying parameters. But in this thesis, we take $k_t = 1100N/m$ as for the nominal case.

Table (2.2) Designated parameter values

m_t	$100kg$	m_s	$2.13kg$	m_{f1}	$6kg$	m_{f2}	$10kg$
k_t	$200N/m$	k_s	$3800N/m$	k_{f1}	$19218N/m$		
c_t	$100Ns/m$	c_s	$60Ns/m$	c_{f1}	0	c_{f2}	$80Ns/m$

Design on the open loop control system of the pantograph-catenary system, we can consider the control system in two different ways as follow;

(1) Control analysis from disturbance input *d* to the output *y* and

(2) Control analysis from control input *u* to the output *y*.

2.3.1 From Disturbance input to Output

The equation of the open loop gain from the disturbance input to contact force (output of the system) can be written as

$$G(s) = \mathbf{c}(s\mathbf{I} - \mathbf{A})^{-1}(-\mathbf{D}) + (-d) \tag{2.16}$$

From (eq 2.16), the poles and zeros of the transfer function from the disturbance input to the contact force are obtained as follows

$$p_{dy} = \begin{bmatrix} -5.17 \pm 102.27i & -3.85 \pm 36.39i & -0.76 \pm 1.05i \end{bmatrix}$$

$$z_{dy} = \begin{bmatrix} -18.94 \pm 157.53i & -1.93 \pm 64.0i & -4.43 & 0 \end{bmatrix}$$

Figure 2.9 shows the bode diagram of the transfer function from the disturbance input to the contact force.

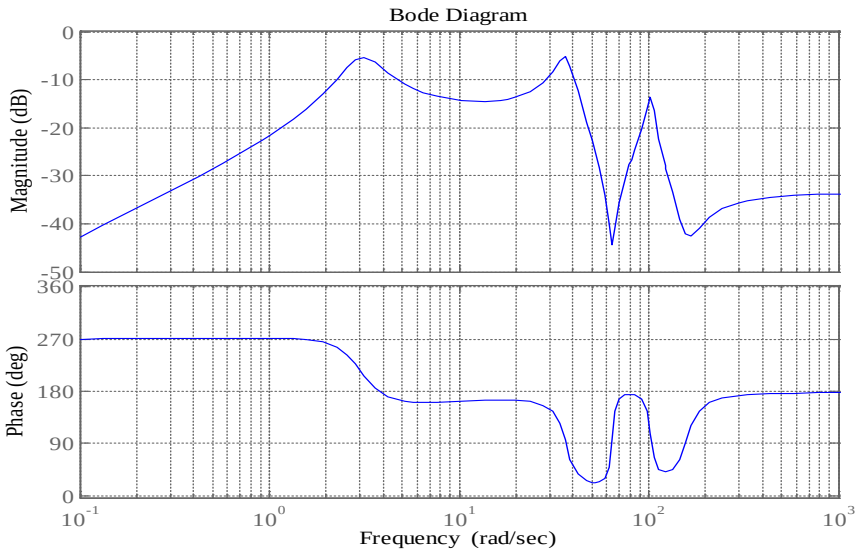

Fig 2.9 Bode plot for the open loop transfer function from the disturbance input to the contact force output

According to this diagram, it can be seem that the gain continues to decrease in the low frequency until it reaches to the zero point of the origin because of the direct term which we mentioned in (eq 2.14). It also should be noted that the relative degree between the uncertainty/ disturbance ξ_t and the contact force f_c is zero because the uncertainty ξ_t appears in the output equation (eq 2.14).

2.3.2 From Control input to Contact force

The equation of the open loop gain from the control input to contact force (output of the system) can be written as

$$G(s) = \mathbf{c}(\mathbf{s}I - \mathbf{A})^{-1}\mathbf{b} \tag{2.17}$$

From (eq 2.17), the poles and zeros of the transfer function from the control input to the contact force are obtained as follows

$$p_{uy} = \begin{bmatrix} -5.17 \pm 102.27i & -3.85 \pm 36.39i & -0.76 \pm 1.05i \end{bmatrix}$$

$$z_{uy} = \begin{bmatrix} -633.33 & -0.50 \pm 1.32i \end{bmatrix}$$

Figure 2.10 shows the bode diagram of the transfer function from the disturbance input to the contact force.

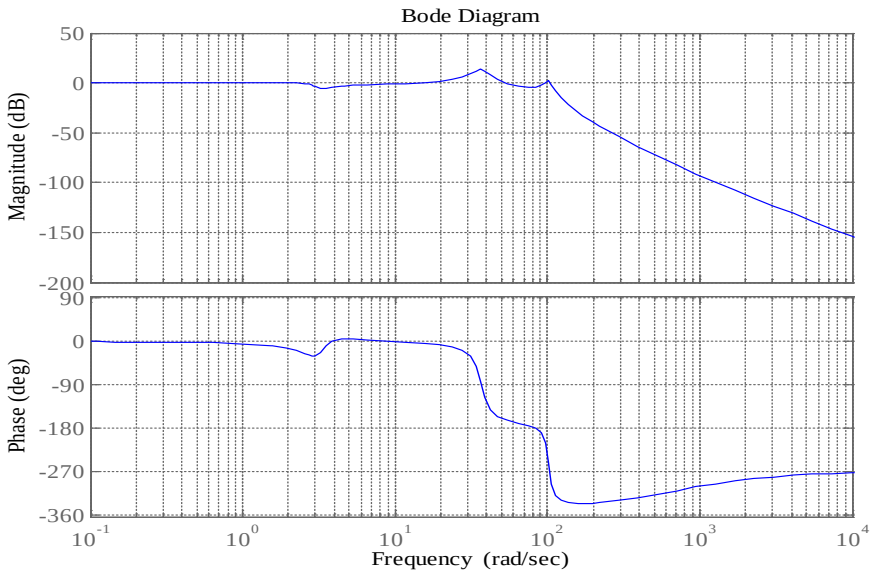

Fig 2.10 Bode plot for the open loop transfer function from the control input to the contact force output

With the state equation (eq 2.10) and the output equation (eq 2.14), the numerator polynomial of the transfer function from the control input to the contact force is given by

$$\begin{vmatrix} \mathbf{A} - s\mathbf{I} & -\mathbf{b} \\ \mathbf{c} & 0 \end{vmatrix} = (m_t s^2 + c_t s + k_t)(c_s s + k_s)(c_{f1} s + k_{f1}) \tag{2.18}$$

where $c_{f1} = 0$ from our identification experiments, and thus the zeros of the transfer function are obtained as follows

$$s = -\frac{k_s}{c_s}, \frac{-c_t \pm \sqrt{c_t^2 - 4m_t k_t}}{2m_t} \tag{2.19}$$

It should be noted that two complex zeros of the transfer function are the same as the poles of the nominal catenary subsystem given by (eq 2.11), and that the relative degree is three. If $c_{f1} \neq 0$, the relative degree would be four. On the other hand, the relative degree of the transfer function from the disturbance ξ_t to the contact force is zero as mentioned above. In general output regulation or disturbance rejection problems, the relative degree and pole-zero cancellation play an important role in controller design. That is, from the above observations, we can see that it is impossible to reject the disturbance completely in our system, because the relative degree of the transfer function from the control input to the contact force is less than that of the transfer function of the disturbance. Furthermore, in order to reduce the effect of the disturbance on the contact force, some of the closed-loop poles should be assigned in exactly the same location as the catenary poles, yielding pole-zero cancellation.

2.4 Problem formulation

The main reason of the implementation of an active control system is the reduction of the standard deviation of the contact force between the pantograph and catenary, hence reducing the contact variation and holding the contact force as constant as possible. The disturbances are mainly caused by the droppers and poles.

In control theory, the disturbance is normally considered in the way as shown in fig 2.11. As the exact input of the disturbance into the pantograph-catenary model is known from section (2.2.3).

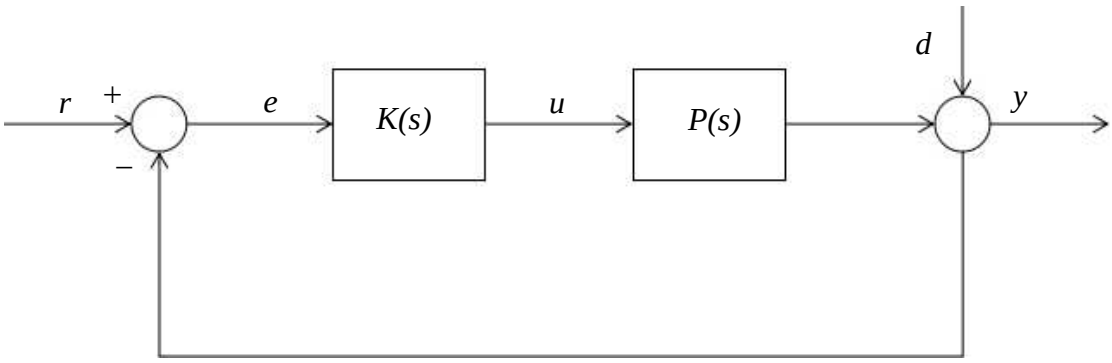

Fig 2.11 Closed loop control system with the disturbance added to the output signal

The active pantograph control system is mainly used closed-loop feedback control, in which it is difficult to keep the contact force constant. Because of the comprise between the stability and the performance of a feedback control system. For an active pantograph, different control strategies will lead to different results. Here in this thesis, we introduce three different types of control strategies. They are

(1) Linear state feedback controller with sliding mode observer,

(2) Sliding mode servo controller with sliding mode observer and

(3) Optimal servo system based on sliding mode control with sliding mode observer.

Each of them above gives a good performance of the pantograph catenary interaction which will be discussed in chapter 3, 4 and 5.

2.5 Summary

In this chapter, a basic structure of the pantograph head and the contact wire (catenary system) is described. The mathematical model of the pantograph head and the catenary system are constructed. Furthermore, a mathematical model of the pantograph and catenary has integrated to get the contact state because the train is considered as moving state. The stiffness of the overhead contact wire in catenary system is a main source of the variation of the pantograph. Hence, the fluctuation of the equivalent stiffness between the pantograph head and the overhead contact wire, make it happen a problem to control the contact state of the system. In section 2.3, a problem formulation of the pantograph-catenary system proposed and then a numerical analysis of the open-loop pantograph-catenary system has described. Moreover, the relative degree of the transfer function and the pole-zero cancellation plays as an important role from the viewpoint of output system are also discussed.

Chapter 3

Linear State Feedback Controller Design

3.1 Introduction

The performance of the high speed trains depend critically on the quality of the contact in the pantograph-catenary interaction. Maintaining a constant contact force needs taking special measures and one of the methods is to utilize active control to optimize the contact force. Therefore, maintaining the control of the contact force becomes the main problem for the high-speed train transportation system. The force exerted by the pantograph on the contact wire oscillates, such oscillations can cause contact losses, electric arc formations that damage the structure of the pantograph and reduce the system performance.

In order to regulate the contact force, we have been developing an active pantograph with a pneumatic actuator which described in chapter (2). Based on that model design, an optimal control strategy with the aim of maintaining the constant contact force are investigated in this chapter. The active pantograph using optimal strategy can resist the disturbances because of the optimal control force is derived from feedback, and achieves the best theoretical performance.

In this chapter, a design of the linear state feedback controller for the pantograph-catenary system and a sliding mode observer are mainly discussed. First, design an optimal type 1 servo system by full state feedback where the controlled variable is the contact force f_c between the pantograph overhead and the contact wire, and then design a sliding mode observer is proposed to regulate the contact force in the presence of variation with respect to the equivalent stiffness of the catenary system.

The overall block diagram of the control design will be discussed. In section 3.3, the function of the optimal control theory by full state feedback law will be introduced. In section 3.5, a sliding mode observer design will be discussed. Numerical simulation is carried out and the output reduction will be discussed in section 3.8.

3.2 Overall control design

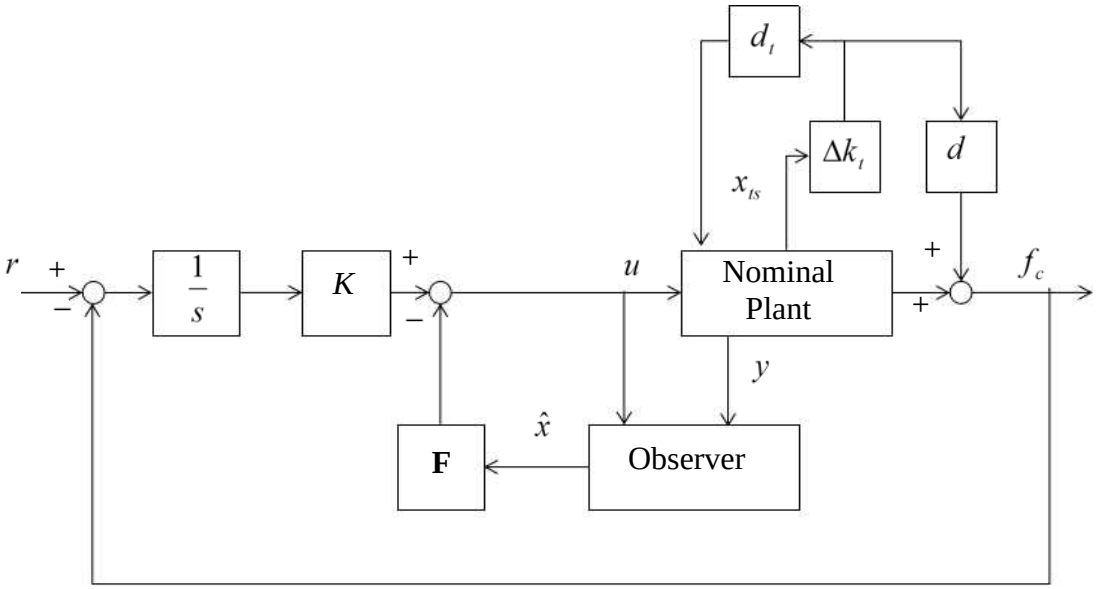

Fig 3.1 Overall block diagram of the control system

First we design an optimal servo controller and then design a sliding mode observer to regulate the contact force. Figure 3.1 shows the overall block diagram of the control system of pantograph-catenary system, where r is the reference contact force and u is the control input. At first, assuming that all the state variables are available, we design an optimal controller and then design a sliding mode observer to estimate the state.

This controller design can divided into two parts, a nominal controller plant and an observer. A nominal controller plant is designed with the optimal control theory and an observer is designed with sliding mode theory. The state error is used as an input to the system in closed-loop system. Because of the main reason is that the disturbance or uncertainty, which is directly effect to the contact force, output of the system which make the system much more difficult.

3.3 Theoretical background of linear optimal controller

This is the short summary on optimal full-state feedback control theory. [14] The plant for the linear time invariant system to be written in the controllable state-space form represented by

$$\dot{x}(t) = Ax(t) + Bu(t) \tag{3.1}$$

and that all of the *n* states *x* are available for the controller. The feedback gain is a matrix *k*, represented as

$$u = -K(x(t) - \hat{x}(t)) \tag{3.2}$$

The system dynamics of the closed loop system are written as

$$\dot{x}(t) = (A - BK)x(t) + BK\hat{x}(t) \tag{3.3}$$

$\hat{x}$ represented the vector of the closed loop system, and serves as the external input to the closed loop system. As the system is controllable, the closed-loop poles can be allocated to any desired location by appropriate choice of K. The schematic diagram of the full-state feedback controller is as shown in fig 3.2.

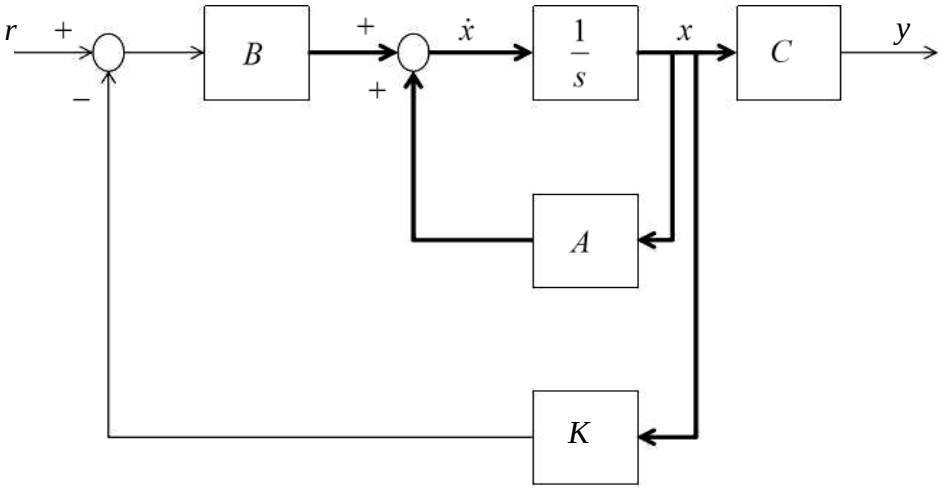

Fig 3.2 Schematic design of full-state feedback controller

In order to design an optimal controller for the pantograph-catenary system, the linear quadratic regulator (LQR) is used in this chapter. This method depends on minimizing criteria using the feedback $u = -Kx(t)$. The performance index that is used for minimizing both the control effort and the states is given as

$$J = \frac{1}{2}\int_0^\infty \left[x(t)^T Qx(t) + u(t)^T Ru(t)\right]dt \tag{3.4}$$

$\|x\| = x(t)^T x(t)$ and x is an $n \times 1$ state vector. The given norm that depends on the state can be used as a measure of the system response. The index also includes u input to control the system. The Q and R matrices in J are called the weight matrix. The weight matrix allow to define the effect of each state and control input in the controller response when the feedback is used for designing the controller. The Q and R are positive definite symmetric matrices and design parameter R is designed as a scalar which is greater than 0.

According to the eq (3.1) and (3.4), the required optimal solution for the feedback gain is calculated by

$$u(t) = -R^{-1}B^T Px(t) \tag{3.5}$$

where $P(t)$ is the positive semidefinite solution of the matrix differential Riccati equation

$$P^T A + AP - PBR^{-1}B^T P + Q = 0 \tag{3.6}$$

3.4 Design of Linear Optimal Controller

First, we design an optimal type I servo system by full state feedback where the controlled variable is the contact force f_c. An optimal servo controller is designed with integral action which shown in the overall block diagram fig (3.1). Considering the optimal controller, we assume all the state variables for the controller design, the parameter K is the integral gain and F is the feedback gain.

The plant to be controlled is given by

$$\dot{\mathbf{x}}(t) = \mathbf{A}\mathbf{x}(t) + \mathbf{b}u(t) + d_t\xi_t \tag{3.7}$$

$$y = \mathbf{c}x(t) + d\xi_t \tag{3.8}$$

where $A \in \Re^{6\times 6}$. This controller design is denoted as a (SISO) system, the input is the reference signal *r* and the output is the contact force f_c.

In order to apply the linear quadratic regulator (LQR) technique to the tracking problem, we consider the deviation system from the steady state to the contact reference signal. Then the time derivative of the control input is given by

$$\begin{aligned}
\dot{u} &= -\mathbf{F}\dot{\mathbf{x}} + K\dot{\mathbf{z}} \\
&= -\mathbf{F}(\mathbf{A}\mathbf{x} + \mathbf{b}u) + K(-\mathbf{c}\mathbf{x} + r) - \mathbf{F}\mathbf{d}_t\xi_t \\
&= -\begin{bmatrix}\mathbf{F} & K\end{bmatrix}\begin{bmatrix}\mathbf{A} & \mathbf{b} \\ \mathbf{c} & 0\end{bmatrix}\begin{bmatrix}\mathbf{x} \\ u\end{bmatrix} + Kr - \mathbf{F}\mathbf{d}_t\xi_t
\end{aligned} \tag{3.9}$$

In order to formulate the tracking problem to LQR, the state vector of the linear servo system is defined as $[\mathbf{x} \quad u]$. Using the above equation, we can derive the deviation system from the steady state for the linear servo system as follows;

$$\begin{bmatrix}\dot{\mathbf{x}} \\ \dot{u}\end{bmatrix} = \begin{bmatrix}\mathbf{I} & \mathbf{0} \\ -\mathbf{F} & K\end{bmatrix}\begin{bmatrix}\mathbf{A} & \mathbf{b} \\ \mathbf{c} & 0\end{bmatrix}\begin{bmatrix}\mathbf{x} \\ u\end{bmatrix} + \begin{bmatrix}\mathbf{0} \\ K\end{bmatrix}r + \begin{bmatrix}\mathbf{d}_t \\ \mathbf{F}\mathbf{d}_t\end{bmatrix}\xi_t \tag{3.10}$$

$$y = \begin{bmatrix} \mathbf{c} & 0 \end{bmatrix} \begin{bmatrix} \mathbf{x} \\ u \end{bmatrix} + d\xi_t \tag{3.11}$$

Letting E as;

$$\mathbf{E} = \begin{bmatrix} \mathbf{A} & \mathbf{b} \\ \mathbf{c} & 0 \end{bmatrix} \tag{3.12}$$

Assuming that both the reference signal and the disturbance are constant in the steady state $\dot{\mathbf{x}} = 0, \dot{u} = 0$, the equilibrium point can be obtained as follows:

$$\begin{bmatrix} 0 \\ 0 \end{bmatrix} = \begin{bmatrix} \mathbf{I} & \mathbf{0} \\ -\mathbf{F} & K \end{bmatrix} \begin{bmatrix} \mathbf{A} & \mathbf{b} \\ \mathbf{c} & 0 \end{bmatrix} \begin{bmatrix} \mathbf{x}(\infty) \\ u(\infty) \end{bmatrix} + \begin{bmatrix} \mathbf{0} \\ K \end{bmatrix} r + \begin{bmatrix} \mathbf{d}_t \\ \mathbf{F}\mathbf{d}_t \end{bmatrix} \xi_t$$

$$\begin{aligned} \begin{bmatrix} \mathbf{x}(\infty) \\ u(\infty) \end{bmatrix} &= -\begin{bmatrix} \mathbf{A} & \mathbf{b} \\ \mathbf{c} & 0 \end{bmatrix}^{-1} \begin{bmatrix} \mathbf{I} & \mathbf{0} \\ -\mathbf{F} & K \end{bmatrix}^{-1} \left\{ \begin{bmatrix} \mathbf{0} \\ K \end{bmatrix} r + \begin{bmatrix} \mathbf{d}_t \\ \mathbf{F}\mathbf{d}_t \end{bmatrix} \xi_t \right\} \\ &= \mathbf{E}^{-1} \begin{bmatrix} \mathbf{0} \\ 1 \end{bmatrix} r - \mathbf{E}^{-1} \begin{bmatrix} \mathbf{I} & \mathbf{0} \\ -K^{-1}\mathbf{F} & -K^{-1} \end{bmatrix} \begin{bmatrix} \mathbf{d}_t \\ \mathbf{F}\mathbf{d}_t \end{bmatrix} \xi_t \end{aligned} \tag{3.13}$$

$$y(\infty) = \begin{bmatrix} \mathbf{c} & 0 \end{bmatrix} \begin{bmatrix} \mathbf{x}(\infty) \\ u(\infty) \end{bmatrix} + d\xi_t \tag{3.14}$$

Substituting eq (3.13) into eq (3.14)

$$y(\infty) = r - \mathbf{E}^{-1} \begin{bmatrix} \mathbf{I} & \mathbf{0} \\ -K^{-1}\mathbf{F} & -K^{-1} \end{bmatrix} \begin{bmatrix} \mathbf{d}_t \\ \mathbf{F}\mathbf{d}_t \end{bmatrix} \xi_t \tag{3.15}$$

Define the new state and output, which are perturbations from the equilibrium.

$$\begin{aligned} &\mathbf{x}_e = \mathbf{x} - \mathbf{x}(\infty), u_e = u - u(\infty) \\ &e = r - y \end{aligned} \tag{3.16}$$

Defining $\mathbf{x}_e$ and u_e as the deviation of the state and the control, respectively, and taking $x_w = [x_e \quad u_e]^T$ as the augmented state vector. The augmented deviation system can be represented by

$$\begin{aligned}\begin{bmatrix}\dot{\mathbf{x}}_e \\ \dot{u}_e\end{bmatrix} = \begin{bmatrix}\dot{\mathbf{x}} \\ \dot{u}\end{bmatrix} &= \begin{bmatrix}\mathbf{I} & \mathbf{0} \\ -\mathbf{F} & -K\end{bmatrix}\mathbf{E}\left\{\begin{bmatrix}\mathbf{x}_e \\ u_e\end{bmatrix} - \mathbf{E}^{-1}\begin{bmatrix}\mathbf{0} \\ 1\end{bmatrix}r - \mathbf{E}^{-1}\begin{bmatrix}\mathbf{I} & \mathbf{0} \\ -K^{-1}\mathbf{F} & -K^{-1}\end{bmatrix}\begin{bmatrix}\mathbf{d}_t \\ \mathbf{F}\mathbf{d}_t\end{bmatrix}\xi_t\right\} \\ &\quad + \begin{bmatrix}\mathbf{0} \\ K\end{bmatrix}r + \begin{bmatrix}\mathbf{d}_t \\ \mathbf{F}\mathbf{d}_t\end{bmatrix}\xi_t \\ &= \begin{bmatrix}\mathbf{I} & \mathbf{0} \\ -\mathbf{F} & -K\end{bmatrix}\begin{bmatrix}\mathbf{A} & \mathbf{b} \\ \mathbf{c} & 0\end{bmatrix}\begin{bmatrix}\mathbf{x}_e \\ u_e\end{bmatrix} \\ &= \begin{bmatrix}\mathbf{A} & \mathbf{b} \\ \mathbf{0} & 0\end{bmatrix}\begin{bmatrix}\mathbf{x}_e \\ u_e\end{bmatrix} - \begin{bmatrix}0 \\ 1\end{bmatrix}\begin{bmatrix}\mathbf{F} & K\end{bmatrix}\mathbf{E}\begin{bmatrix}\mathbf{x}_e \\ u_e\end{bmatrix}\end{aligned} \tag{3.17}$$

$$\begin{aligned}e &= r - y \\ &= r - \left\{\begin{bmatrix}\mathbf{c} & 0\end{bmatrix}\begin{bmatrix}\mathbf{x} \\ u\end{bmatrix} + d\xi_t\right\} \\ &= r - \left[\begin{bmatrix}\mathbf{c} & 0\end{bmatrix}\left\{\begin{bmatrix}\mathbf{x}_e \\ u_e\end{bmatrix} + \mathbf{E}^{-1}\begin{bmatrix}0 \\ 1\end{bmatrix}r - \mathbf{E}^{-1}\begin{bmatrix}\mathbf{I} & \mathbf{0} \\ -K^{-1}\mathbf{F} & -K^{-1}\end{bmatrix}\begin{bmatrix}\mathbf{d}_t \\ \mathbf{F}\mathbf{d}_t\end{bmatrix}\xi_t\right\} + d\xi_t\right]\end{aligned} \tag{3.18}$$

For this controller design,we neglected the effect of the disturbance, the perturbation term from the plant system and consider as a nominal pantograph-catenary system. Removing the disturbance yields

$$\begin{aligned}\begin{bmatrix}\dot{\mathbf{x}}_e \\ \dot{u}_e\end{bmatrix} &= \begin{bmatrix}\mathbf{A} & \mathbf{b} \\ \mathbf{0} & 0\end{bmatrix}\begin{bmatrix}\mathbf{x}_e \\ u_e\end{bmatrix} - \begin{bmatrix}0 \\ 1\end{bmatrix}v \\ &= \mathbf{A}_w\begin{bmatrix}\mathbf{x}_e \\ u_e\end{bmatrix} - \mathbf{b}_w v\end{aligned} \tag{3.19}$$

$$e = \begin{bmatrix}\mathbf{c} & 0\end{bmatrix}\begin{bmatrix}\mathbf{x}_e \\ u_e\end{bmatrix} = \mathbf{c}_w\begin{bmatrix}\mathbf{x}_e \\ u_e\end{bmatrix} \tag{3.20}$$

where e is the tracking error, and $v = \dot{u}_e$ which can be seen as the control input in the regulator given in eq (3.19). Thus, for this plant, the following state feedback is employed.

$$v = -\begin{bmatrix}\mathbf{F} & K\end{bmatrix}\mathbf{E}\begin{bmatrix}\mathbf{x}_e \\ u_e\end{bmatrix} = -\mathbf{F}_e\begin{bmatrix}\mathbf{x}_e \\ u_e\end{bmatrix} \tag{3.21}$$

To obtain the optimal regulator gain $\mathbf{F}_e$, the following performance index is used.

$$\begin{aligned} J &= \int_0^\infty \left\{e^T We + v^T Rv\right\}dt \\ &= \int_0^\infty \left\{\begin{bmatrix}\mathbf{x}_e^T & u_e^T\end{bmatrix}\begin{bmatrix}\mathbf{c}^T W\mathbf{c} & \mathbf{0} \\ \mathbf{0} & 0\end{bmatrix}\begin{bmatrix}\mathbf{x}_e \\ u_e\end{bmatrix} + v^T Rv\right\}dt \end{aligned} \tag{3.22}$$

The design parameters are the weighting matrices W, R on the tracking error. The optimal regulator gain $\mathbf{F}_e$ can be obtained with 'LQR' function in Matlab, then it changed to the original state equation as follows:

$$v^o = -\mathbf{F}_e^o\begin{bmatrix}\mathbf{x}_e \\ u_e\end{bmatrix} \tag{3.23}$$

Finally, the actual optimal gain is given by

$$\begin{bmatrix}\mathbf{F} & K\end{bmatrix} = \mathbf{F}_e^o\mathbf{E}^{-1} \tag{3.24}$$

3.5 Sliding Mode Observer

An observer is a system that provides an estimate of the internal state driven by the input of the system and a signal representing discrepancy between the estimated and the actual states. In most practical cases, the state of the real system cannot be determined by direct observation, therefore, the internal state is observed from the system outputs instead. The sliding mode observer, based on the same idea of sliding mode control, employs a switching function of the sliding variable to steer the system trajectory to the sliding manifold and maintain the motion on the manifold thereafter. [16,17,18] The ideal sliding motion is shown in fig (3.3).

The sliding mode observer uses non-linear high-gain feedback to force estimated states to reach a predetermined surface, which is called sliding surface (Hyper-surface) where there is no difference between the estimated output to the measured output. When the states reach on the switching surface, observer trajectories slide along the origin where the estimated output matches the measured output that means the sliding variable is chosen to ensure the observed states converge to the actual stages. [16-18]

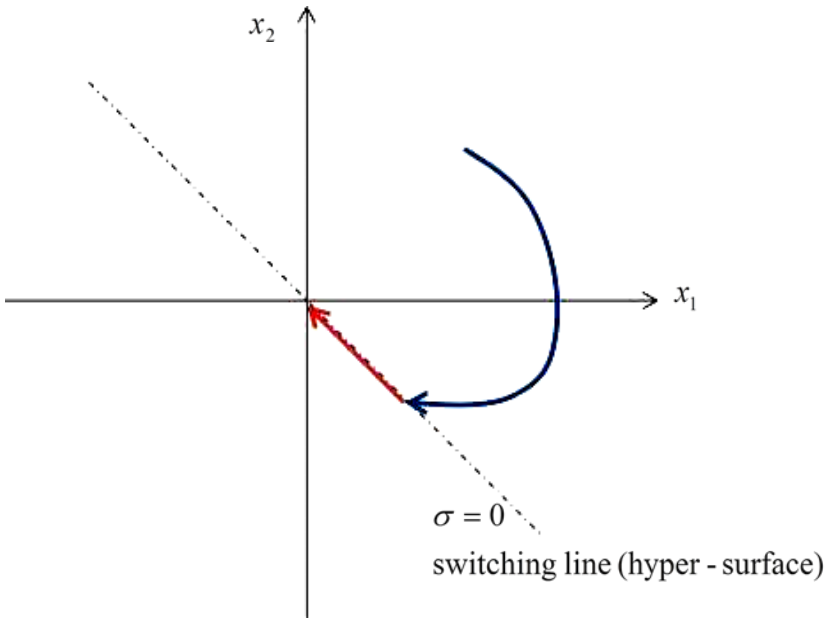

Fig 3.3 Ideal sliding motion

The main problem of the sliding mode observer is the chattering which makes the high frequency variations output. Chattering effects in the sliding motion which is described in fig (3.4).

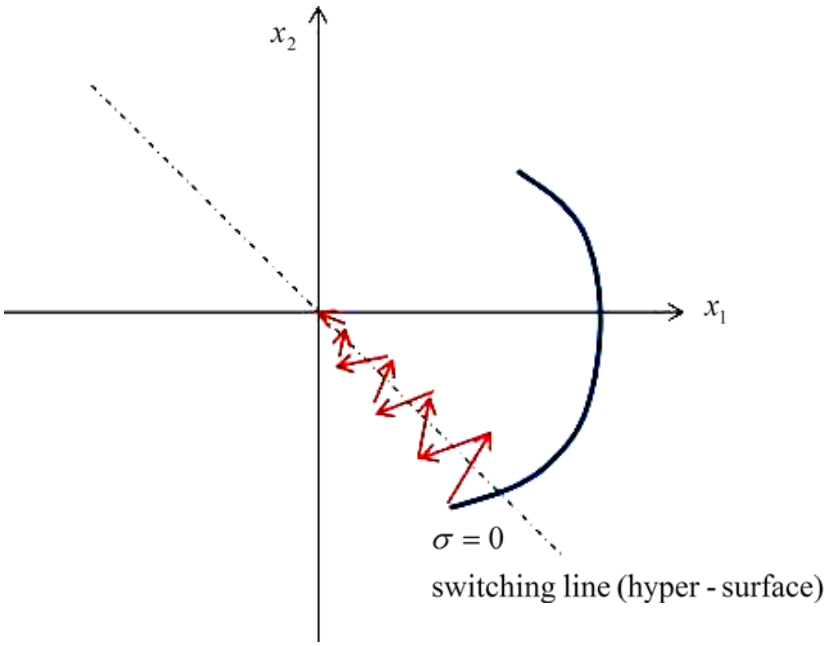

Fig 3.4 Chattering effect on sliding mode

In such a case, we can design to add various control theories, such as boundary layer, adaptive switching function and low pass filtering. Among the various solutions to reduce chattering: the boundary layer control is the most popular approach.

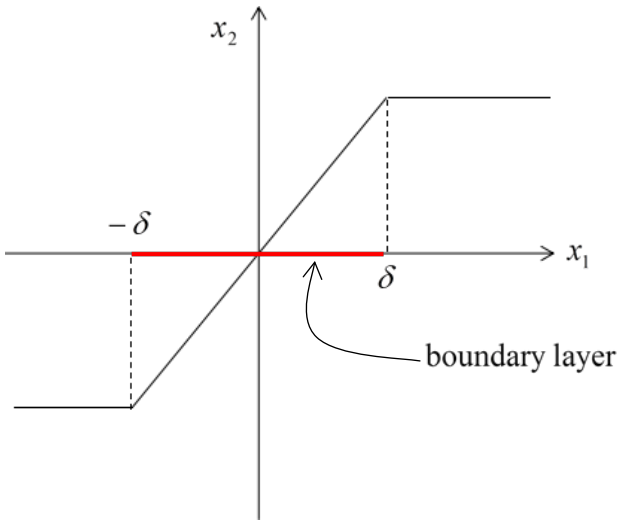

Fig 3.5 Boundary layer control

In a boundary layer design, a smooth continuous function is used to approximate the discontinuous sign function in a region called the boundary layer around the sliding surface. By using the sign of the error to drive the sliding mode observer, the

observer trajectories become insensitive to many forms of noise. Once the sliding mode is achieved, the sliding mode observer can reject certain external disturbances and internal parameter uncertainties. [16,17,18]

3.5.1 Theoretical background of a sliding mode observer

This is the short summary on sling mode observer design using variable structure control system [13]. Sliding mode observer can be used in the design of state observer. The nonlinear high-gain observers have the ability to bring coordinates of the estimation error dynamics to zero in finite time. The plant for the linear time invariant system to be written in the controllable state -space form represented by

$$\dot{x}(t) = Ax(t) + Bu(t)$$
$$y(t) = cx(t) \tag{3.25}$$

where $A \in \Re^n, B \in \Re^m, c \in \Re^p$ and the system is observable. A schematic diagram of the controller with an observer is shown below

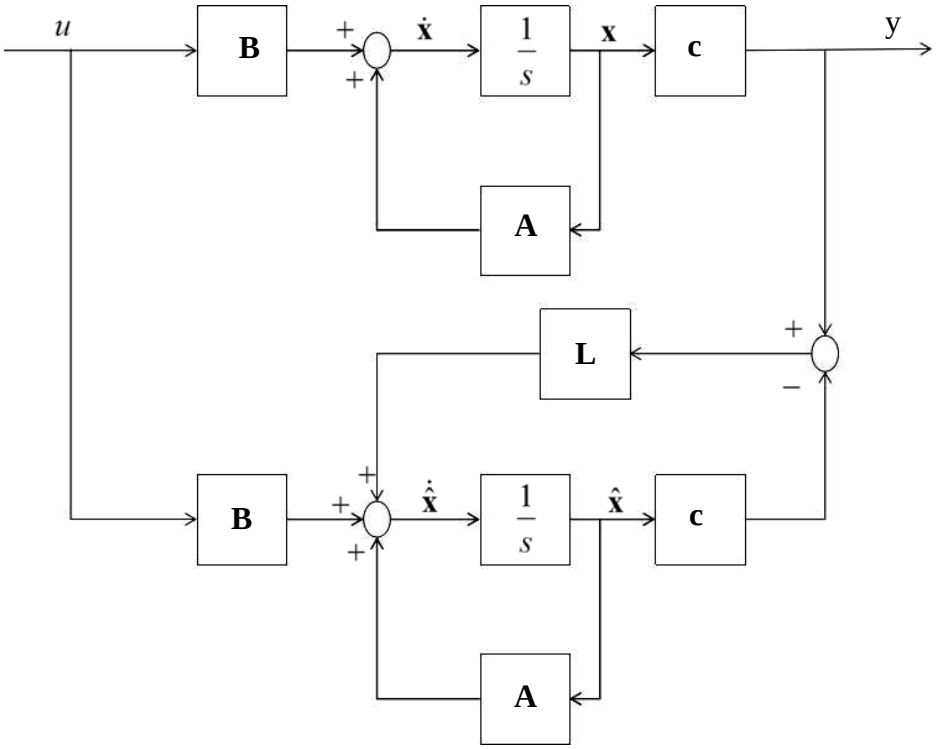

Fig 3.6 Schematic diagram of the controller with an observer

Based on the diagram, the dynamics of the state estimate are described by changing the new coordinate system as follows:

$$\dot{\hat{x}}_1(t) = A_{11}\hat{x}_1(t) + A_{12}\hat{x}_2(t) + B_1u(t) + Lv \tag{3.26}$$

$$\dot{\hat{y}}(t) = A_{21}\hat{x}_1(t) + A_{22}\hat{y}(t) + B_2u(t) - v \tag{3.27}$$

where L is the observer feedback gain and the vector v is defined by

$$v = M\,\mathrm{sgn}(\hat{y} - y) \tag{3.28}$$

where $M \in \Re_+$. Representing the mismatch in the process by state reconstruction error

$$e_1 = \hat{x}_1 - x_1 \tag{3.29}$$

$$e_y = \hat{y} - y \tag{3.30}$$

The following error dynamic is obtained

$$\dot{e}_1(t) = A_{11}e_1(t) + A_{12}e_y(t) + Lv \tag{3.31}$$

$$\dot{e}_y(t) = A_{21}e_1(t) + A_{22}e_y(t) - v \tag{3.32}$$

If the original plant system is observable, the pair (A_{11}, A_{12}) is also observable. After that change the coordinates dependent on L and let $\tilde{e}_1 = e_1 + Ly$. The error system with respect to the new coordinates can be written as

$$\dot{\tilde{e}}_1(t) = \tilde{A}_{11}\tilde{e}_1(t) + \tilde{A}_{12}e_y(t) \tag{3.33}$$

$$\dot{e}_y(t) = A_{21}\tilde{e}_1(t) + \tilde{A}_{22}e_y(t) - v \tag{3.34}$$

where $\tilde{A}_{11} = A_{11} + LA_{21}$, $\tilde{A}_{12} = A_{12} + LA_{22} - \tilde{A}_{11}L$ and $\tilde{A}_{22} = A_{22} - A_{21}L$. With an appropriate L, $\tilde{e}_1$ decays exponentially and observer stage converge to the actual

stages. Therefore, the goal of state reconstruction using sliding mode is achieved. An ideal sliding motion will take place on the surface

$$S_o = \{ (e_1, e_y): \quad e_y = 0 \} \tag{3.35}$$

In this research, we consider the problem of designing sliding mode observer using Variable Structure Control (VSS) system. Variable structure control system comprise feedback control and a decision rule. Depending on the states of the system, the decision rule, often termed the switching function, determines which of the control law. The dynamical behavior of the system when confined the surface is described as the ideal sliding motion. The latter property of invariance towards so-called matched uncertainty makes the methodology as an attractive one for designing robust controller for uncertain systems. The advantages of obtaining such a motion are twofold: firstly, there is a reduction in order and secondly the sliding motion is insensitive to parameters variations. [13,15,16,17]

3.6 Design of Sliding Mode observer

In this thesis, we introduce a sliding mode observer using variable structure control (VSS) system. A variable structure system (VSS) of a nonlinear uncertain system is well known for its robust property and simplicity of control law. In this section, the problem of designing an observer of state estimation using variable structure system (VSS) is discussed. The state equation of the pantograph-catenary plant system is given by

$$\dot{\mathbf{x}} = \mathbf{A}\mathbf{x} + \mathbf{b}u + \mathbf{d}_t \xi_t \tag{3.36}$$

There are six state variables in the plant system which described in eq. (2.9). To estimate the state variables for the observer system, we could not estimate the full state of the system. In general servo systems, the controlled variables are used for the observer. However, the contact force is not appropriate for the observer, because it is directly influenced by the uncertainty as seen from eq (2.14). Taking account of robustness against the uncertainty and the existence of the sliding mode, we use two

parameter measurements, $\dot{x}_{ts}$ the velocity of the pantograph head and x_{f2} the displacement of the lower frame, for the observer design.

$$\mathbf{y} = \mathbf{c}_2\mathbf{x} = \begin{bmatrix} 0 & 1 & 0 & 0 & 0 & 0 \\ 0 & 0 & 0 & 0 & 1 & 0 \end{bmatrix}\mathbf{x} \tag{3.37}$$

To simplify the design procedure, the state vector is redefined for the observer design as

$$\tilde{\mathbf{x}} = \begin{bmatrix} x_{ts} & x_{f1} & \dot{x}_{f1} & \dot{x}_{f2} & x_{f2} & \dot{x}_{ts} \end{bmatrix} \tag{3.38}$$

where the last two variables are available for the observer (only change of the order). With this new state vector, the system equation eq. (2.10) can be written by

$$\begin{aligned} \dot{\tilde{\mathbf{x}}} = & \begin{bmatrix} 0 & 0 & 0 & 0 & 0 & 1 \\ 0 & 0 & 1 & 0 & 0 & 0 \\ \dfrac{k_s}{m_{f1}} & -\dfrac{k_s + k_{f1}}{m_{f1}} & -\dfrac{c_s + c_{f1}}{m_{f1}} & \dfrac{c_{f1}}{m_{f1}} & \dfrac{k_{f1}}{m_{f1}} & \dfrac{c_s}{m_{f1}} \\ 0 & \dfrac{k_{f1}}{m_{f2}} & \dfrac{c_{f1}}{m_{f2}} & -\dfrac{c_{f1} + c_{f2}}{m_{f2}} & -\dfrac{k_{f1}}{m_{f2}} & 0 \\ 0 & 0 & 0 & 1 & 0 & 0 \\ -\dfrac{k_t + k_s}{m_t + m_s} & \dfrac{k_s}{m_t + m_s} & \dfrac{c_s}{m_t + m_s} & 0 & 0 & -\dfrac{c_t + c_s}{m_t + m_s} \end{bmatrix}\tilde{\mathbf{x}} \\ & + \begin{bmatrix} 0 \\ 0 \\ 0 \\ \dfrac{1}{m_{f2}} \\ 0 \\ 0 \end{bmatrix} f_a + \begin{bmatrix} 0 \\ 0 \\ 0 \\ 0 \\ 0 \\ \dfrac{1}{m_t + m_s} \end{bmatrix} \xi_t \\ = & \tilde{\mathbf{A}}\tilde{\mathbf{x}} + \tilde{\mathbf{b}}u + \tilde{\mathbf{d}}_t\xi_t \end{aligned} \tag{3.39}$$

Furthermore, the system matrix is partitioned as follows:

$$\tilde{\mathbf{A}} = \begin{bmatrix} \tilde{\mathbf{A}}_{11} & \tilde{\mathbf{A}}_{12} \\ \tilde{\mathbf{A}}_{21} & \tilde{\mathbf{A}}_{22} \end{bmatrix} \tag{3.40}$$

where $\mathbf{A}_{11} \in \Re^{(n-m)\times(n-m)}$, n is the number of the system states and m is the number of the measured states. If there are any invariant zeros present in the system then they must appear in matrix $\tilde{A}_{11}$. It can be partitioned accordingly, so that the sub-block has the structure as;

$$\tilde{\mathbf{A}} = \left[\begin{array}{c|c} \tilde{\mathbf{A}}_{11} & \tilde{\mathbf{A}}_{12} \\ \hline \tilde{\mathbf{A}}_{211} & \\ \tilde{\mathbf{A}}_{212} & \tilde{\mathbf{A}}_{22} \end{array}\right] \tag{3.41}$$

, $\mathbf{A}_{11} \in \Re^{4\times4}$, $\mathbf{A}_{12} \in \Re^{4\times2}$, $\mathbf{A}_{211} \in \Re^{4\times2}$, $\mathbf{A}_{212} \in \Re^{1\times4}$, $\mathbf{A}_{22} \in \Re^{2\times2}$

The pair $(\tilde{\mathbf{A}}_{22}, \tilde{\mathbf{A}}_{21})$ is completely observable. The output equation with respect to the measurements for the observer is give by

$$\begin{aligned} \tilde{\mathbf{y}} &= \begin{bmatrix} 0 & 0 & 0 & 0 & 1 & 0 \\ 0 & 0 & 0 & 0 & 0 & 1 \end{bmatrix} \tilde{\mathbf{x}} \\ &= \begin{bmatrix} \mathbf{0} & \mathbf{I} \end{bmatrix} \tilde{\mathbf{x}} \\ &= \tilde{\mathbf{C}} \tilde{\mathbf{x}} \end{aligned} \tag{3.42}$$

where $\mathbf{I} \in \Re^{2\times2}$.

In this research, we design a variable structure system (VSS) of sliding mode observer based on the Walcott-Zak observer theory. Figure 3.7 shows a block diagram of the Variable structure system (VSS) observer.

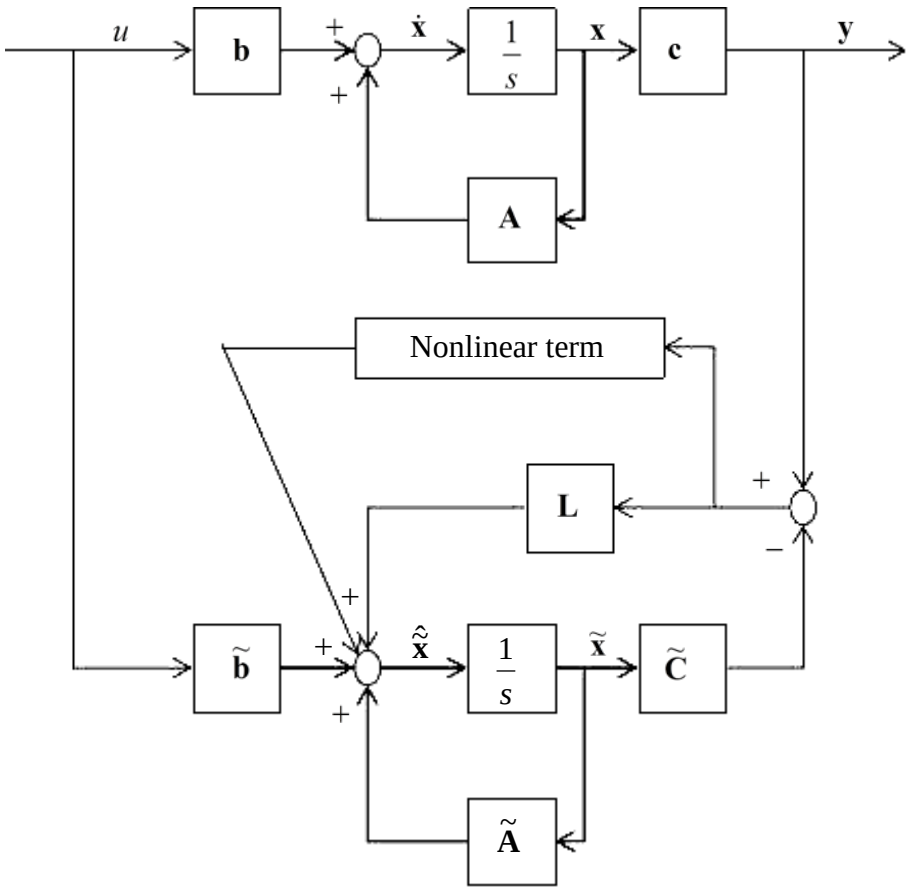

Fig 3.7 Schematic diagram of the VSS observer

The (VSS) sliding mode observer is designed as

$$\dot{\hat{\tilde{\mathbf{x}}}} = \tilde{\mathbf{A}}\hat{\tilde{\mathbf{x}}} + \tilde{\mathbf{b}}u - \mathbf{G}_l\mathbf{e}_y + \mathbf{G}_n\mathbf{v} \tag{3.43}$$

$$\hat{\tilde{\mathbf{y}}} = \tilde{\mathbf{C}}\hat{\tilde{\mathbf{x}}} \tag{3.44}$$

where, $\mathbf{e}_y = \hat{\tilde{\mathbf{y}}} - \tilde{\mathbf{y}}$, $\mathbf{v} = -\rho\dfrac{\mathbf{e}_y}{\|\mathbf{e}_y\|}$

$\mathbf{G}_l \in \Re^{6\times 2}$ and $\mathbf{G}_n \in \Re^{6\times 2}$ are the design parameters.

The third term of the eq (3.43) is the linear observer term and the last term is the nonlinear observer term, where, $\mathbf{e}_y$ is an error and it is used as a switching function of the observer. Therefore, when system is enter to the sliding mode control, the error ($\mathbf{e}_y$) becomes zero.

3.6.1 Design of a linear observer gain

In order to design the linear optimal observer gain for the system, the optimal observer theory (Kalman filter) is used. To consider the parameter of the linear observer gain $\mathbf{G}_l$, the nonlinear term from the observer state equation eq (3.43) is excluded. Therefore, the observer state equation can be rewritten as

$$\dot{\hat{\tilde{\mathbf{x}}}} = \tilde{\mathbf{A}}\hat{\tilde{\mathbf{x}}} + \tilde{\mathbf{b}}u - \mathbf{G}_l\mathbf{e}_y \tag{3.45}$$

By using the optimal observer theory (Kalman filter), the optimal observer gain $\mathbf{G}_l$ is calculated as

$$\mathbf{G}_l = \mathbf{P}\tilde{\mathbf{C}}^T\mathbf{R}^{-1} \tag{3.46}$$

where $\mathbf{P}$ is the positive semidefinite solution of the matrix differential Riccati equation

$$\mathbf{P}^T\tilde{\mathrm{A}} + \tilde{\mathbf{A}}\mathbf{P} - \mathbf{P}\tilde{\mathbf{C}}^T\mathbf{R}_l^{-1}\tilde{\mathbf{C}}\mathbf{P} + \mathbf{Q}_l = 0 \tag{3.47}$$

To find the optimal observer gain, we consider the system as dual system. It means that the output feedback is used as the system input to the observer design. The state equation of the dual system is given by

$$\dot{\tilde{\mathbf{x}}} = \tilde{\mathbf{A}}^T\tilde{\mathbf{x}}(t) + \tilde{\mathbf{C}}^T\mathbf{u}(t) \tag{3.48}$$

The performance index that is used for minimizing both the system error and the states is given as

$$J = \int_0^\infty \left[\tilde{x}(t)^T Q_l \tilde{x}(t) + u(t)^T R_l u(t)\right]dt \tag{3.49}$$

The index includes u input to control the system. The Q and R matrices in J are called the weight matrix. From eq (3.48) and eq (3.49), the required optimal solution to calculate the observer gain $\mathbf{G}_l$ is achieved. The optimal observer gain matrix is

$$\mathbf{G}_l = \tilde{\mathbf{F}}^T \tag{3.50}$$

The weight matrix in the Riccati equation is defined as follows:

$$\mathbf{Q}_l = \begin{bmatrix} 0 & 0 & 0 & 0 & 0 & 0 \\ 0 & 0 & 0 & 0 & 0 & 0 \\ 0 & 0 & 0.1 & 0 & 0 & 0 \\ 0 & 0 & 0 & 0.1 & 0 & 0 \\ 0 & 0 & 0 & 0 & 0 & 0 \\ 0 & 0 & 0 & 0 & 0 & 0.8 \end{bmatrix}, \quad \mathbf{R}_l = \begin{bmatrix} 10^{-4} & 0 \\ 0 & 10^{-4} \end{bmatrix}$$

3.6.2. Design of a nonlinear observer gain

In this observer, the nonlinear term on the right hand side from eq (3.43) is a discontinuous function to bring about the sliding mode. In order to analyze the error dynamics of the system, the state equation of the estimation error is defining as,

$$\begin{aligned} \mathbf{e} &= \hat{\tilde{\mathbf{x}}} - \tilde{\mathbf{x}} \\ &= \begin{bmatrix} \mathbf{e}_1 \\ \mathbf{e}_y \end{bmatrix} \end{aligned} \tag{3.51}$$

where an error dynamics is divided into two error states, e_1 is the unmeasured state vector which is not sensed by an observer and e_y is the measured state vector which is sensed by an observer. The state equation of the estimation error dynamics for the sliding mode observer is designed as

$$\dot{\mathbf{e}} = \tilde{\mathbf{A}}\mathbf{e} - \mathbf{G}_l\mathbf{e}_y + \mathbf{G}_n\mathbf{v} - \tilde{\mathbf{d}}\xi_t \tag{3.52}$$

$$= \begin{bmatrix} \tilde{\mathbf{A}}_{11} & \tilde{\mathbf{A}}_{12} \\ \tilde{\mathbf{A}}_{21} & \tilde{\mathbf{A}}_{22} \end{bmatrix}\mathbf{e} - \begin{bmatrix} \mathbf{G}_{l1} \\ \mathbf{G}_{l2} \end{bmatrix}\mathbf{e}_y - \begin{bmatrix} -\mathbf{L} \\ \mathbf{I}_2 \end{bmatrix}\mathbf{P}_o^{-1}\mathbf{v} - \begin{bmatrix} \mathbf{0} \\ \tilde{\mathbf{d}}_2 \end{bmatrix}\xi_t$$

where $\mathbf{G}_{l1} \in \Re^{4\times 2}$ and $\mathbf{G}_{l2} \in \Re^{2\times 2}$. As seem from the eq (3.52), one of the points to determine the design parameter $\mathbf{G}_n$ is that if $\tilde{\mathbf{d}}$ belongs to the range space of $\mathbf{G}_n$, i.e. the matching condition holds, then the estimation error dynamics during sliding mode is insensitive to the uncertainty. Although this requirement can be easily fulfilled, there is another obstacle such as the existence of the sliding mode, which is highly depend on $\mathbf{G}_n$ but also on the linear gain $\mathbf{G}_l$ as another design parameter. Taking the matching condition into account, firstly $\mathbf{G}_n$ is parameterized as

$$\mathbf{G}_n = \begin{bmatrix} -\mathbf{L} \\ \mathbf{I}_2 \end{bmatrix}\mathbf{P}_o^{-1} \tag{3.53}$$

and $\mathbf{L}$ is defined as, $\mathbf{L} = \begin{bmatrix} \mathbf{l}_o & 0 \end{bmatrix}$

where $\mathbf{P} \in \Re^{2\times 2}$, $\mathbf{l}_o \in \Re^{4\times 1}$.

It should be noted that the last column in $\mathbf{G}_n$ is taken for $\tilde{\mathbf{d}}$ to belong to the range space of $\mathbf{G}_n$.

As the error dynamics are divided into two states, then we convert the control variables to the regular form and divide it into two states also, which are Null space and Range space. In order to change the error dynamics eq (3.53) into a regular form, using the linear transformation as

$$\mathbf{e} \mapsto \mathbf{T}_l\mathbf{e} = \bar{\mathbf{e}}$$

$$\bar{\mathbf{e}} = \begin{bmatrix} \bar{\mathbf{e}}_1 & \bar{\mathbf{e}}_y \end{bmatrix}^T \tag{3.54}$$

The transformation matrix $\mathbf{T}_l$ is defined as

$$\mathbf{T}_l = \begin{bmatrix} \mathbf{I}_4 & \mathbf{L} \\ \mathbf{0} & \mathbf{I}_2 \end{bmatrix}$$

And the inverse form of the transformation matrix is as follows:

$$\mathbf{T}_l^{-1} = \begin{bmatrix} \mathbf{I}_4 & -\mathbf{L} \\ \mathbf{0} & \mathbf{I}_2 \end{bmatrix} \tag{3.55}$$

After applying a change of the state, the state equation for the error dynamics can be rewritten as

$$\dot{\bar{\mathbf{e}}} = \mathbf{T}_l \tilde{\mathbf{A}} \mathbf{T}_l^{-1} \bar{\mathbf{e}} - \mathbf{T}_l \mathbf{G}_l \mathbf{e}_y + \mathbf{T}_l \mathbf{G}_n \mathbf{v} - \mathbf{T}_l \tilde{\mathbf{d}} \xi_t \tag{3.56}$$

The estimation error dynamics of the measure state vector in the change state is $\bar{\mathbf{e}}_y = \mathbf{e}_y$. Then, It follows:

$$\begin{aligned} \mathbf{T}_l \tilde{\mathbf{A}} \mathbf{T}_l^{-1} &= \begin{bmatrix} \mathbf{I}_4 & \mathbf{L} \\ \mathbf{0} & \mathbf{I}_2 \end{bmatrix} \begin{bmatrix} \tilde{\mathbf{A}}_{11} & \tilde{\mathbf{A}}_{12} \\ \tilde{\mathbf{A}}_{21} & \tilde{\mathbf{A}}_{22} \end{bmatrix} \begin{bmatrix} \mathbf{I}_4 & -\mathbf{L} \\ \mathbf{0} & \mathbf{I}_2 \end{bmatrix} \\ &= \begin{bmatrix} \tilde{\mathbf{A}}_{11} + \mathbf{L}\tilde{\mathbf{A}}_{21} & \tilde{\mathbf{A}}_{12} + \mathbf{L}\tilde{\mathbf{A}}_{22} \\ \tilde{\mathbf{A}}_{21} & \tilde{\mathbf{A}}_{22} \end{bmatrix} \begin{bmatrix} \mathbf{I}_4 & -\mathbf{L} \\ \mathbf{0} & \mathbf{I}_2 \end{bmatrix} \\ &= \begin{bmatrix} \tilde{\mathbf{A}}_{11} + \mathbf{L}\tilde{\mathbf{A}}_{21} & -(\tilde{\mathbf{A}}_{11} + \mathbf{L}\tilde{\mathbf{A}}_{21})\mathbf{L} + \tilde{\mathbf{A}}_{12} + \mathbf{L}\tilde{\mathbf{A}}_{22} \\ \tilde{\mathbf{A}}_{21} & -\tilde{\mathbf{A}}_{21}\mathbf{L} + \tilde{\mathbf{A}}_{22} \end{bmatrix} \\ &= \begin{bmatrix} \bar{\tilde{\mathbf{A}}}_{11} & \bar{\tilde{\mathbf{A}}}_{12} \\ \bar{\tilde{\mathbf{A}}}_{21} & \bar{\tilde{\mathbf{A}}}_{22} \end{bmatrix} \end{aligned} \tag{3.57}$$

where the element (1×1) of the eq (3.57) is

$$\begin{aligned}\overline{\tilde{\mathbf{A}}}_{11} &= \tilde{\mathbf{A}}_{11} + \mathbf{L}\tilde{\mathbf{A}}_{21} \\ &= \tilde{\mathbf{A}}_{11} + \begin{bmatrix}\mathbf{l}_o & \mathbf{0}\end{bmatrix}\begin{bmatrix}\tilde{\mathbf{A}}_{211} \\ \tilde{\mathbf{A}}_{212}\end{bmatrix} \\ &= \tilde{\mathbf{A}}_{11} + \mathbf{l}_o\tilde{\mathbf{A}}_{211}\end{aligned} \tag{3.58}$$

Parametrization;

$$\mathbf{T}_l\mathbf{G}_l = \begin{bmatrix}\mathbf{I}_4 & \mathbf{L} \\ \mathbf{0} & \mathbf{I}_2\end{bmatrix}\begin{bmatrix}\mathbf{G}_{l1} \\ \mathbf{G}_{l2}\end{bmatrix} = \begin{bmatrix}\mathbf{G}_{l1} + \mathbf{L}\mathbf{G}_{l2} \\ \mathbf{G}_{l2}\end{bmatrix} = \begin{bmatrix}\overline{\mathbf{G}}_{l1} \\ \overline{\mathbf{G}}_{l2}\end{bmatrix} \tag{3.59}$$

$$\mathbf{T}_l\mathbf{G}_n = \begin{bmatrix}\mathbf{I}_4 & \mathbf{L} \\ \mathbf{0} & \mathbf{I}_2\end{bmatrix}\begin{bmatrix}-\mathbf{L} \\ \mathbf{I}_2\end{bmatrix}\mathbf{P}_o^{-1} = \begin{bmatrix}\mathbf{0} \\ \mathbf{P}_o^{-1}\end{bmatrix} \tag{3.60}$$

$$\mathbf{T}_l\tilde{\mathbf{d}} = \begin{bmatrix}\mathbf{I}_4 & \mathbf{L} \\ \mathbf{0} & \mathbf{I}_2\end{bmatrix}\begin{bmatrix}\mathbf{0} \\ \tilde{\mathbf{d}}_2\end{bmatrix} = \begin{bmatrix}\mathbf{0} \\ \tilde{\mathbf{d}}_2\end{bmatrix} \tag{3.61}$$

According to eq (3.60) and eq (3.61), It can be seen that the disturbance/ uncertainty term $\mathbf{T}_l\tilde{\mathbf{d}}$ is satisfied with the Range space of the nonlinear term $\mathbf{T}_l\mathbf{G}_n$. This condition is defined as the matching condition. Consequently, it follows the null space dynamics and range space dynamics,

$$\dot{\tilde{\mathbf{e}}}_1 = (\tilde{\mathbf{A}}_{11} + \mathbf{l}_o\tilde{\mathbf{A}}_{211})\mathbf{e}_1 + (\overline{\tilde{\mathbf{A}}}_{12} - \overline{\mathbf{G}}_{l1})\mathbf{e}_y \tag{3.62}$$

$$\dot{\tilde{\mathbf{e}}}_y = \overline{\tilde{\mathbf{A}}}_{21}\mathbf{e}_1 + (\overline{\tilde{\mathbf{A}}}_{22} - \overline{\mathbf{G}}_{l2})\mathbf{e}_y + \mathbf{P}_o^{-1}\mathbf{v} - \tilde{\mathbf{d}}_2\xi_t \tag{3.63}$$

The null space dynamics eq (3.62) is insensitive to the uncertainty because of the matching condition, and thus the estimation error dynamics during sliding mode, $\mathbf{e}_y = \dot{\mathbf{e}}_y = 0$, is governed by,

$$\dot{\tilde{\mathbf{e}}}_1 = (\tilde{\mathbf{A}}_{11} + \mathbf{l}_o\tilde{\mathbf{A}}_{211})\mathbf{e}_1 \tag{3.64}$$

where $\tilde{\mathbf{A}}_{11}$ and $\tilde{\mathbf{A}}_{211}$ are the design parameters of the system and $\mathbf{l}_o$ is the design parameter which can be determined the sliding mode poles. The other parameter must be determined to guarantee the existence of the sliding mode. Then, the positive definite matrix $\mathbf{P}_o$ is designed to satisfy with

$$\mathbf{P}_o(\bar{\tilde{\mathbf{A}}}_{22} - \bar{\mathbf{G}}_{l2}) + (\bar{\tilde{\mathbf{A}}}_{22} - \bar{\mathbf{G}}_{l2})^T \mathbf{P}_o = -\mathbf{Q}_{po} \tag{3.65}$$

$\mathbf{P}_o > 0$, $\mathbf{Q}_{po} > 0$

which means $\mathbf{P}_o$ satisfies with a Lyapunov matrix for $(\bar{\tilde{\mathbf{A}}}_{22} - \bar{\mathbf{G}}_{l2})$.

$$\begin{aligned} \therefore \quad \bar{\tilde{\mathbf{A}}}_{22} - \bar{\mathbf{G}}_{l2} &= \tilde{\mathbf{A}}_{22} - \tilde{\mathbf{A}}_{21}\mathbf{L} - \mathbf{G}_{l2} \\ &= \tilde{\mathbf{A}}_{22} - \tilde{\mathbf{A}}_{21}[\mathbf{l}_o \quad \mathbf{0}] - \mathbf{G}_{l2} \end{aligned}$$

Considering the existence of the sliding mode, taking the positive definite matrix $\mathbf{P}_o$, such that

$$\rho \geq \left\| \mathbf{P}_o \tilde{\mathbf{d}}_2 \right\| \alpha + \eta_o \tag{3.66}$$

where ρ is the relay gain for the switching function. If the value of the relay gain ρ is large, the effect of the disturbance can not appeared. However, $\eta_o > 0$, $\alpha > |\xi_t|$, η_o is a small positive number, which means that α takes a larger value than the magnitude of the perturbation force.

The relationship between $\mathbf{P}_o$ and $\tilde{\mathbf{d}}_2$ is calculated as

$$\mathbf{P}_o \tilde{\mathbf{d}}_2 = \begin{bmatrix} P_{11} & P_{12} \\ P_{21} & P_{22} \end{bmatrix} \begin{bmatrix} 0 \\ \tilde{d}_{22} \end{bmatrix} \tag{3.67}$$

Therefore, the relay gain to be calculated as

$$\rho \geq \alpha \tilde{d}_{22} \sqrt{(P_{11} + P_{22})^2} + \eta_o \tag{3.68}$$

3.7 System Analysis

In this section, we apply the SRL (Symmetric Root locus) method, which gives the locus of the optimal poles with respect to the parameter W under the performance index eq (3.22), to analyze the optimal servo system designed in the section (3.4). By increasing the weighting factor W, the fluctuation of the contact force between pantograph and catenary can be reduced. The optimal poles are the stable roots in the left half plane of the SRL equation

$$1+\rho G_o(-s)G_o(s)=0 \tag{3.69}$$

where $G_o(s)$ is the transfer function of the control input to the contact force,

$$G_o(s)=\mathbf{c}(s\mathbf{I}-\mathbf{A})^{-1}\mathbf{b} \tag{3.70}$$

The symmetric root locus obtained for $W=10^{-1}\sim 10^{10}$ is shown in fig (3.8)., where a portion around the origin in the left figure is zoomed in the right figure.

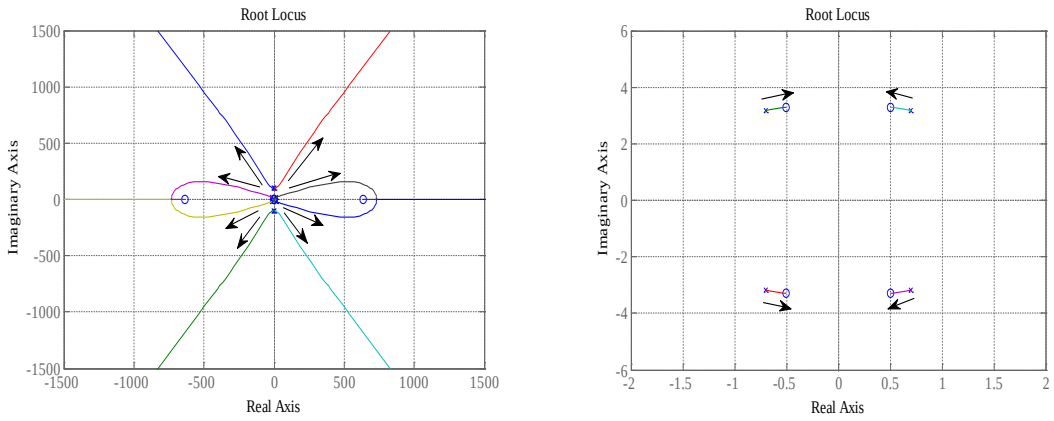

(a) Overall (b) around the origin

Fig 3.8 Root locus of linear optimal feedback poles

According to this figure, the stable roots converge to the zero of $G_o(s)$ as W increases. As described in chapter 2, the order of the relative degree from disturbance to contact force is smaller than the order of the relative degree from control input to the contact force, which means perfect output zeroing can not be achieved easily. In

this research, the weighting factor is set to $W = 10^7$, the poles and zeros in the transfer function from the reference signal to the contact force are obtained as follows:

$$\text{poles} = \begin{bmatrix} -34.29 \pm 142.25i & -90.79 \pm 85.56i & -0.50 \pm 3.28i & -113.10 \end{bmatrix}$$

$$\text{zeros} = \begin{bmatrix} -7.53 \pm 182.11i & -107.20 \pm 140.63i & -0.50 \pm 3.28i & -160.40 \end{bmatrix}$$

It should be noted that a pair of poles approximately cancel out a pair of zeros at $-0.50 \pm 3.28i$ which is the mode of the catenary subsystem given by eq (2.19). Taking these poles into account, the observer poles $\mathbf{l}_o$ during sliding mode were determined as

$$\text{Observer poles} = \begin{bmatrix} -70 \pm 10i & -50 \pm 10i \end{bmatrix}$$

after some trial and errors. According to this fact, perfect output zeroing can be achieved by exact pole-zero cancellations which make an unobservable subspace in the state space. From a physical point of view, in addition, these close-loop poles will make it possible that the pantograph head is following the catenary wire motion not to prevent its free motion, yielding a good regulation of the contact force.

According that the uncertainty ξ_t is an independent external disturbance, the frequency response from the disturbance ξ_t to the contact force f_c can be obtained as shown in fig (3.9) where the blue line is passive case (open loop) and the green line is the active (close loop). It can be expected from this figure that the active pantograph probably achieves the regulation of the contact force better than the passive pantograph, because the gain of the active pantograph is lower than the gain of the passive pantograph, in almost all frequencies especially at the disturbance frequency $(4\pi\ rad/s)$ without any resonances (much more stable).

In the rest of the simulation, the reference signal is given as follows:

$$r(t) = \begin{cases} 54 & for\ \ 0 \le t \le 11 \\ 64 & thereafter \end{cases}$$

to make sure the transient response.

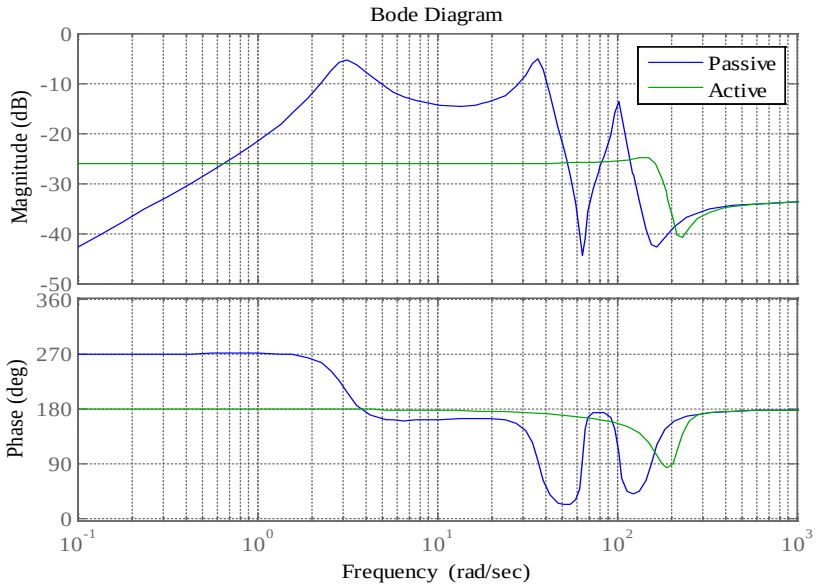

Fig 3.9 Bode diagram of the transfer function from the disturbance to the contact force

3.8 Simulation Results

In order to investigate the performance of the proposed linear state feedback controller, numerical simulation has carried out. Numerical simulation results are performed to confirm the effectiveness of the controller design. The parameter values of the pantograph-catenary system are shown in Table (2.2), where the parameter values of the pantograph are the estimates by identification experiments, and those of the catenary system are determined based on some references. The parameter values of the pantograph-catenary system as shown in this section obtained from the joint research with the Railway Technical Research Institute

When the train speed is 360 km/h and the span length of each cantilever is about 50 m, the catenary equivalent stiffness can be assumed to change periodically with 2Hz as shown in fig (3.10).

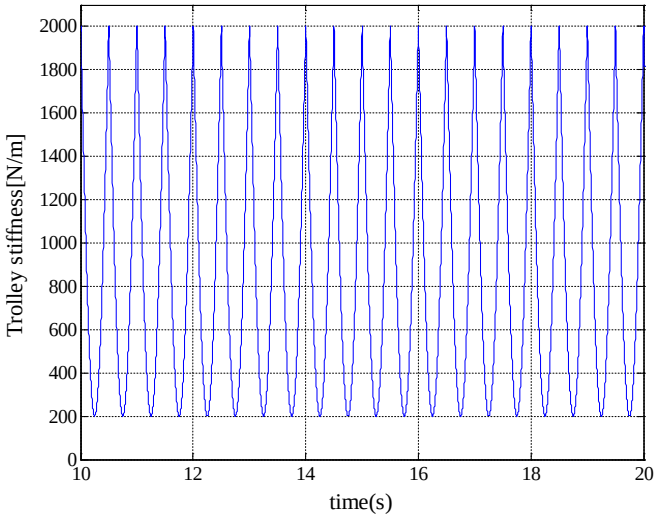

Fig 3.10 Catenary stiffness

Because the proposed controller achieved a good performance as expected for the simulation result, we carried out some simulations in more realistic situation. That is, although we neglected the actuator dynamics when designing the controller and observer, we inserted the following dynamic model of the pneumatic actuator

$$G(s) = \frac{1}{0.013s + 1} e^{-0.002s} \tag{3.71}$$

which had been obtained by some experiments. Furthermore, it was assumed that three measurements for the controller and observer were corrupted by white Gaussian noises whose maximum magnitude and some important parameters are as shown below:

Contact force: $\pm 4N$

Catenary equivalent stiffness: 2Hz

Displacement of the lower frame: $\pm 1 \times 10^{-4} m$

Velocity of the contact wire/shoe head: $\pm 1 \times 10^{-4} m/s$

Nominal value of stiffness fluctuation: $k_t = 1100 N/m$

The design parameters in the controller and observer were determined taking account of the above situation.

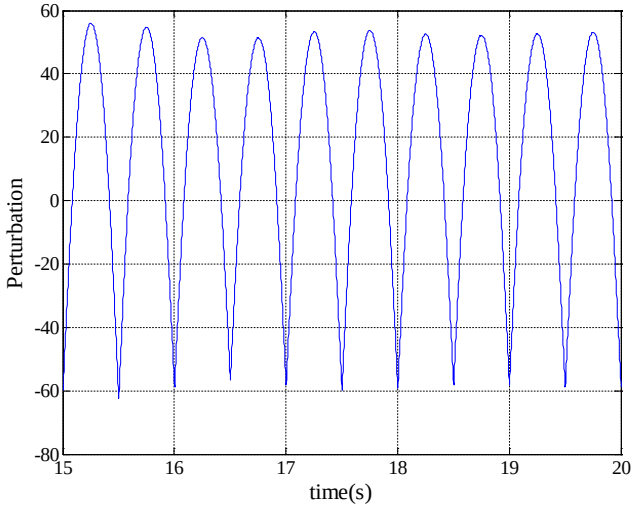

Fig 3.11 Perturbation force

Figure (3.12) and (3.13) shows the estimation errors, e_y, used in the observer eq (3.43) and eq (3.44), where the true state variables are used for control to evaluate only the observer performance. Figure (3.12) shows the simulation result of the estimation error of the linear optimal observer and Fig (3.13. a,b) shows the simulation result of the sliding mode observer. It can be seen from the chattering around the origin as shown in fig (3.12, a) that the quasi sliding mode takes place, and that the estimation accuracy is better than that of the linear optimal observer shown in fig (3.12).

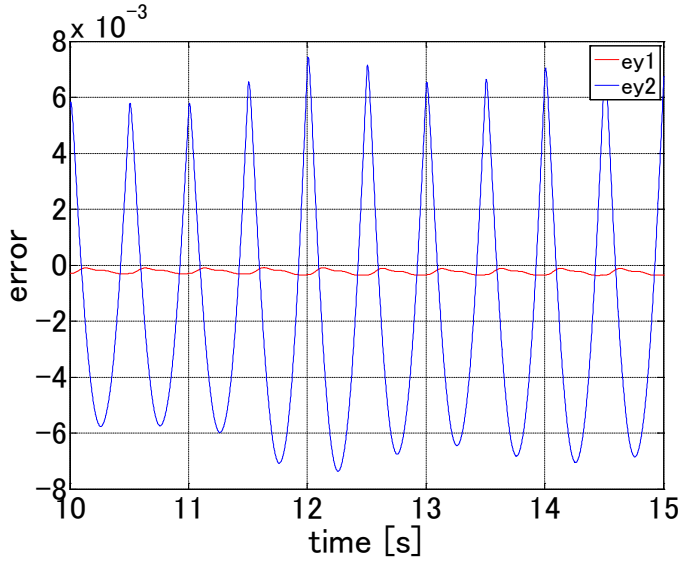

Fig 3.12 Estimation error, e_y for Linear optimal observer

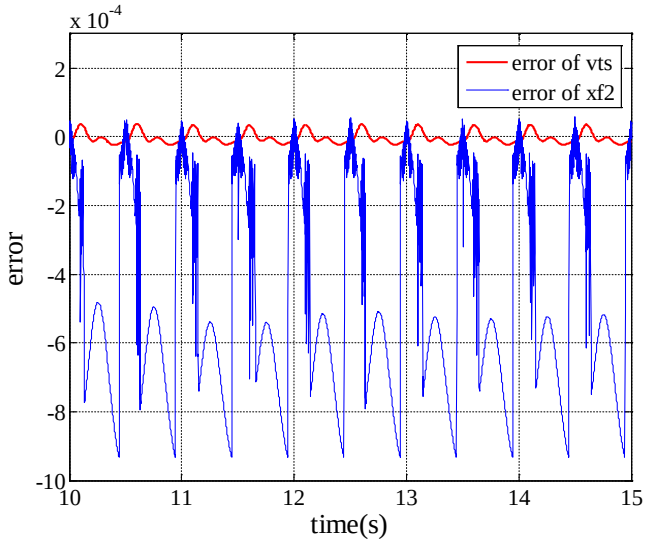

Fig 3.13 (a) Estimation error, e_y for Sliding mode observer (Without actuator)

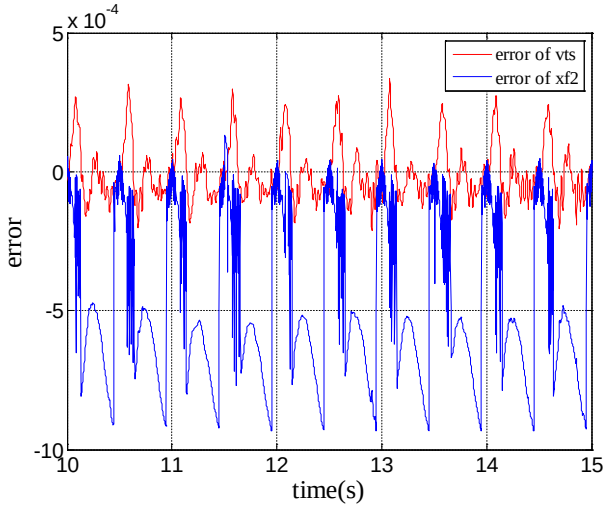

Fig 3.13 (b) Estimation error, e_y for sliding mode observer (With actuator)

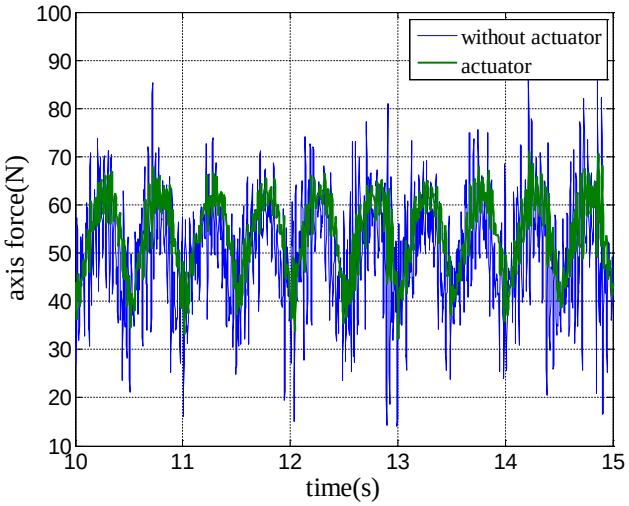

Fig 3.14 Control input

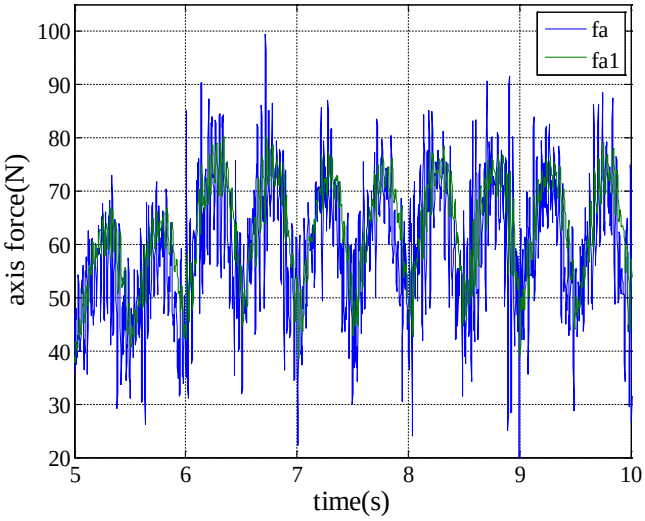

Fig 3.15 Control input in transient response

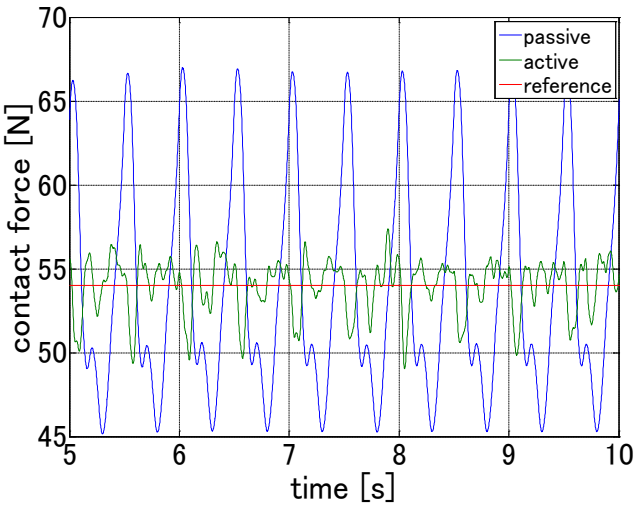

Fig 3.16 Contact force in steady state

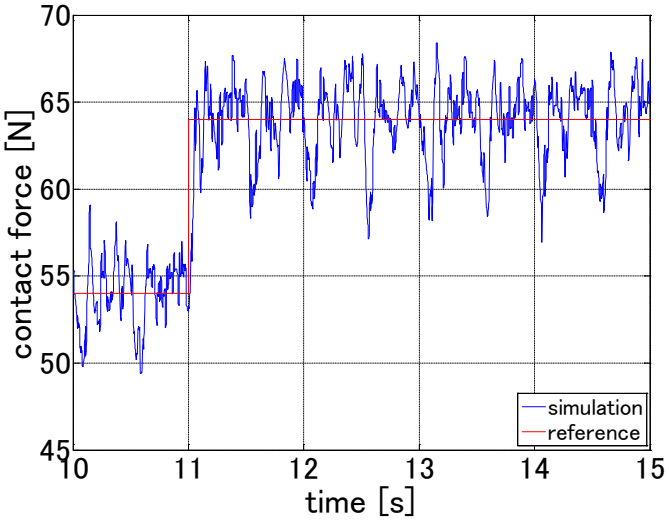

Fig 3.17 Step response of the contact force

Furthermore, it is assumed that the measurement of the contact force with a load cell is corrupted by a band limited white noise. It can be seen from fig 3.13 (b) that the quasi sliding mode takes place in spite of the existence of the actuator dynamics. Figure (3.14) and (3.15) show the simulation results of the control input with actuator control dynamics and the without actuator control dynamics. The simulation result of those two are almost the same, which means that the designed controller is appropriate for the actuator dynamics.

Figure (3.16) shows the contact force in the steady state in comparison with the passive case where the static uplift force is provided. It is clear that the active pantograph achieves much better regulation performance than the passive one. Figure (3.17) shows the step response of the contact force, from which it can be seen that the transient response is also good.

3.9 Summary

In this chapter, we proposed the linear state feedback controller together with the sliding mode observer, taking account of the flexibility of the articulated frame in our pantograph. It has emphasized that one of the key points to regulate the contact force in the nominal model without perturbation. A physical interpretation of this pole-zero cancellation is also given, that is, the pantograph head can follow the catenary motion not to prevent it free motion by assigning some of the closed loop poles on the catenary mode. Because it is found out through many simulation results that the observer plays a key role in the control performance, we are still under investigation on which physical variables to use for the observer and how to measure them precisely in severe environments.

Chapter 4

Sliding Mode Servo Controller Design

4.1 Introduction

Previous chapter was developed the linear state feedback controller together with a sliding mode observer and it can proved that the system have good performance according to the simulation results. However, It is always required to design a more robust controller for an active pantograph. Therefore, a sliding mode controller together with a sliding mode observer is proposed in order to regulate the robust contact force in the presence of variation with respect to the equivalent stiffness of the catenary system in this chapter. To regulate the robust contact force, we have developing an active pantograph with a pneumatic actuator, which described in chapter (2). Based on the same model design, sliding mode control strategy with the aim of achieving the robust contact force are investigated in this chapter.

As we mentioned above, the control system is developed with a sliding mode controller together with a sliding mode observer, is based on the same mathematical model of the pantograph. Figure (4.1) shows the overall block diagram of the control system where the reference r is the reference contact force, the contact force f_c is the control output, σ is the switching function of sliding mode control and *u* is the control input to the system. We use sliding mode control theory for both controller and observer design to regulate the robust contact force. At first, assuming that all the state variables are available, we design a sliding mode control law, and then design sliding mode observer to estimate the state.

The two different sections discuss in this chapter. The first section is how to design the sliding mode controller together with sliding mode observer and next

section is the stability analysis of the system. A design of the sliding mode controller for the pantograph-catenary system is mainly discussed even though a sliding mode observer is combined with the controller in the control system. Because we used the same design of sliding mode observer, which described in chapter (3). And the stability of the closed loop control system is proved by using Lyapunov method. In the design of sliding mode controller, the controlled variable is the contact force f_c between the pantograph and the catenary.

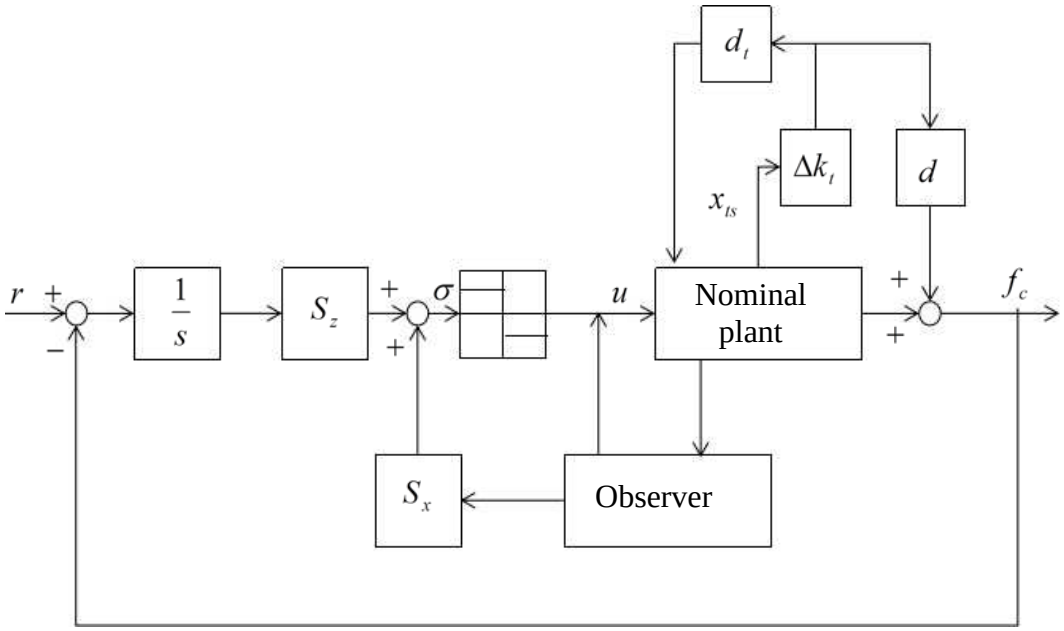

Fig 4.1 Overall block diagram of the control system

In section 4.2, a basic concept of the variable structure system with sliding mode control is introduced. Section 4.3 is devoted to the design of a sliding mode controller and section 4.4 is presented the stability analysis of the closed loop control system. Numerical simulation is carried out and the output reduction is discussed in section 4.5.

4.2 Variable Structure Control

The concepts of variable structure system originated in the Soviet literature in 1955 and got much attention in 1977 when Utkin published his famous paper in English. The variable structure control systems include a feedback control law which employs a discontinuous control action and decision rule. [15] The decision rule is often based upon the behavior of the switching function and determines which of the control law is activated at any instant times.

The basic idea of control systems are designed to drive the system state trajectory onto a specified surface in the state space, named sliding or switching surface and keep the system state on this manifold for all the subsequent times. In order to achieve the control objective, the control input must be designed with a sufficient to overcome the uncertainties and the disturbances acting on the system. [15, 16, 17, 18] There are two main advantages of sliding mode control approach. First, while the system is on the sliding manifold it behaves as a reduced order system with respect to the original plant. In the nonlinear systems, an appropriate selection of switching function may render the reduced order motion to be linear or almost linear. Secondly, the close loop response becomes totally insensitive to some particular uncertainties and disturbances, so called matched uncertainty.

For a variable structure control system with sliding mode control, the dynamical behavior of the system state is divided in to two stages. Firstly, the phase is to drives the states to the surface. During the motion, the system is effected by any unmatched disturbances present. Secondly, seek to maintain the states on the switching surface for the remaining period where it is insensitive to all the matched uncertainty.

In this thesis, linear uncertain systems of the following form are considered,

$$\dot{\mathbf{x}}(t) = \mathbf{A}\mathbf{x}(t) + \mathbf{b}u(t) + \mathbf{g}\xi_t(t) \tag{4.1}$$

where $\mathbf{A} \in \Re^{n\times n}$ and $\mathbf{b} \in \Re^{n\times m}$ are plant model matrices where n and m are the number of states of x, input u and ξ_t is considered to represent any uncertainty and disturbances in the system. The control input is discontinuous across the manifold $\sigma = 0$. The function of the control input is defined as

$$u(t) = -\gamma \operatorname{sgn}(\sigma) \tag{4.2}$$

where γ is the relay gain and $\operatorname{sgn}(\sigma)$ is denoted as signum function and indicates the positive and negative sign changes depending on the switching function, that is;

$$u(t) = \begin{cases} -\gamma & for\ \ \sigma > 0 \\ \gamma & for\ \ \sigma < 0 \end{cases} \tag{4.3}$$

where the switching function is defined by

$$\sigma(t) = Sx(t) \tag{4.4}$$

where $S \in \Re^{m \times n}$ and the system trajectories lie on

$$S = \left\{ x \in \Re^{n} \quad : \quad s(x) = 0 \right\} \tag{4.5}$$

The controller can be considered as a discontinuous at $s = 0$, due to the effects of sampling, switching and delays in the device. It is natural to choose the control action and the switching strategy such that sliding takes place on the switching surface S and remain on the surface S. It can be clearly understood by the following figure.

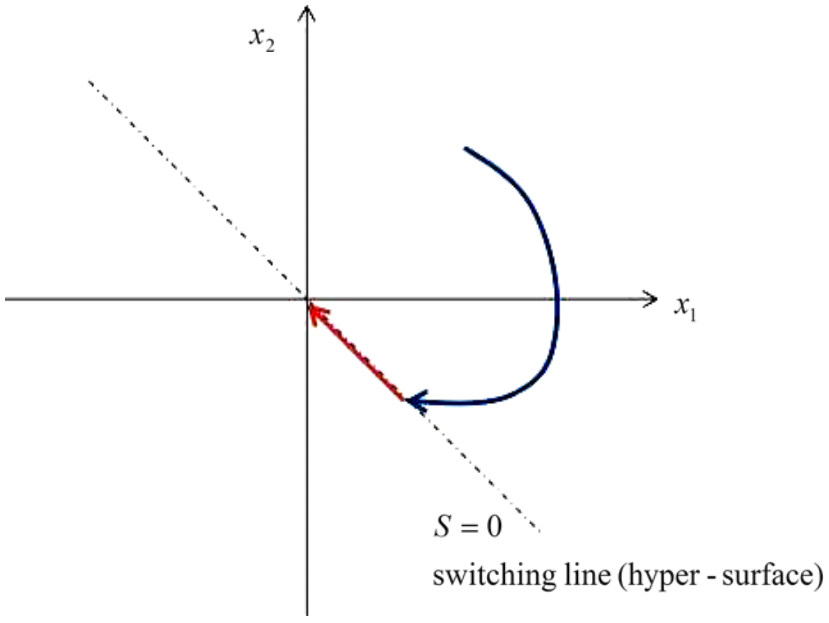

Fig 4.2 Sliding mode technique

In practice, an ideal sliding motion may not be attained due to the effects of imperfections such as delays, hysteresis and unmodelled dynamics and become the high frequency motion which called chattering effect. Chattering, which is a dangerous high frequency variations of an controlled system that become the main problem for sliding mode control.

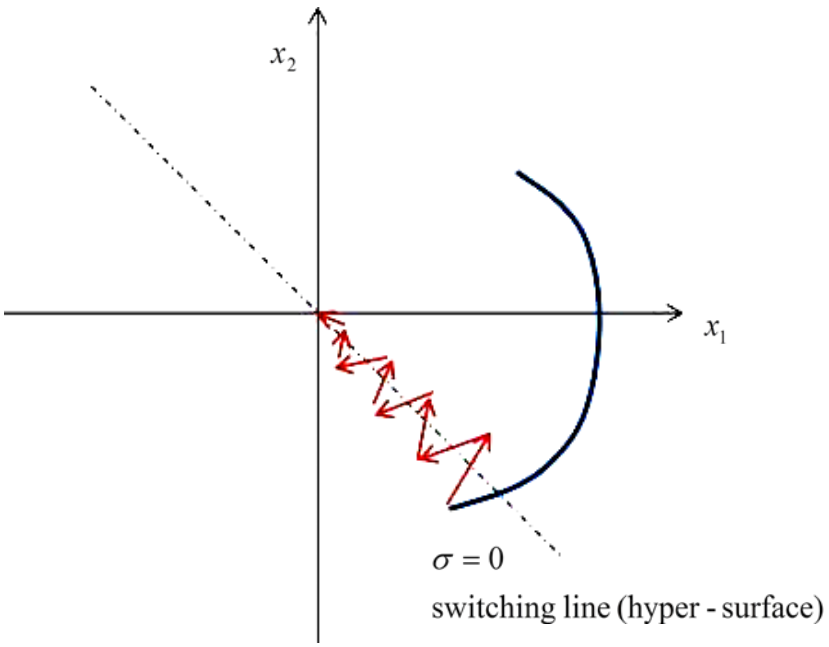

Fig 4.3 Chattering effect on the control switching line

Figure (4.3) show how delays can cause chattering. The chattering can be eliminated by replacing the discontinuity in the control law.

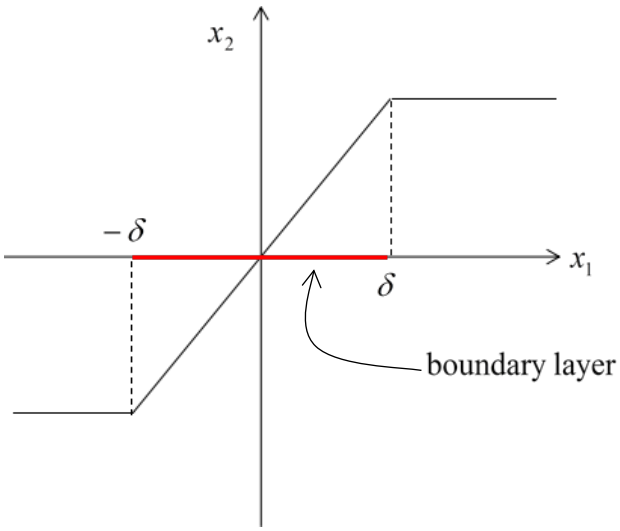

Fig 4.4 Boundary layer control

In such a case, we can design to add various control theories, such as boundary layer, adaptive switching function and low pass filtering. Among the various solutions to reduce the chattering: the boundary layer control is the most popular approach. Figure (4.4) shown the diagram of the boundary layer design. In a boundary layer design, a smooth continuous function is used to approximate the discontinuous sign function in a region called the boundary layer around the sliding surface.

4.2.1 Method of equivalent control

This section described a method of establishing the nominal control function required to maintain a sliding motion remain on the switching function S and the equations representing the dynamic behavior of the states, named 'equivalent dynamics'. In describing the method of equivalent control, it will initially be assumed that the uncertain function in eq (4.1) is identically zero. Therefore, equation (4.1) can be rewritten as

$$\dot{x}(t) = Ax(t) + bu(t) \tag{4.6}$$

At time $t = t_s$ the system output reaches the switching function S and an ideal sliding motion is attained. This can be expressed mathematically as $Sx(t) = 0$ and $\dot{s}(t) = S\dot{x}(t) = 0$ for all $t \geq t_s$. Substituting for $\dot{x}(t)$ from eq (4.6) gives

$$\dot{\sigma} = S\dot{x}(t) = SAx(t) + Sbu(t) \tag{4.7}$$

The equivalent control associated with the nominal system eq (4.6), written as u_{eq}

$$u_{eq}(t) = -(Sb)^{-1}SAx(t) \tag{4.8}$$

This shown that the matrix Sb is required to be the matrix of invertible if an 'equivalent control u_{eq}' is exist. The ideal sliding mode dynamics may be given by substituting the equivalent control u_{eq} into eq (4.6), which results in free motion

$$\dot{x}(t) = (I_n - b(Sb)^{-1}S)Ax(t) \qquad for\ all\ t \geq t_s \text{ and } Sx(t_s) = 0 \tag{4.9}$$

Define the linear projection operator is ,

$$P_s = (I_n - b(Sb)^{-1}S) \tag{4.10}$$

which satisfies

$$SP_s = 0 \quad \text{and} \quad P_s b = 0 \tag{4.11}$$

The system matrix governing the sliding motion $P_s A$, which is belongs to the $N(s)$ and consequently the sliding motion is a reduced order dynamic. Hence, the system can be decomposed into two sub-dynamics. One is called the Range space dynamics $R(s)$ and Null space dynamic $N(s)$. The stability and the invariance properties of the range space is explained in next section.[13, 16, 17]

4.2.2. Invariance properties of VSS

To consider the invariance properties of the range space, eq (4.1) is used

$$\dot{\mathbf{x}}(t) = \mathbf{A}\mathbf{x}(t) + \mathbf{b}u(t) + \mathbf{g}\xi_t(t)$$

where ξ_t is considered to represent any uncertainty and disturbances in the system. Suppose a controller exists which induces a sliding motion on the surface S, then the equivalent equation can be represented as

$$u_{eq}(t) = -(\mathbf{Sb})^{-1}(\mathbf{SA}\mathbf{x}(t) + \mathbf{Sg}\xi_t(t)) \qquad \text{for } t \geq t_s \tag{4.12}$$

Substituting eq (4.12) into the uncertain system in eq (4.1) yields the sliding motion

$$\dot{\mathbf{x}}(t) = P_s\mathbf{A}\mathbf{x}(t) + P_s\mathbf{g}\xi_t(t) \qquad \text{for all } t \geq t_s \text{ and } Sx(t_s) = 0 \tag{4.13}$$

where P_s is the projection operator defined in eq (4.10). Suppose $R(g) \subset R(b)$ then there exist a matrix $R \in \Re^{m\times 1}$ such that $g = bR$. This leads to $P_s g = 0$ and $P_s b = 0$ which described previous section. The reduced order motion as given in eq (4.13) reduces to

$$\dot{\mathbf{x}}(t) = P_s \mathbf{A}\mathbf{x}(t) \qquad \text{for all } t \geq t_s \text{ and } Sx(t_s) = 0 \tag{4.14}$$

where the function ξ_t does not effect the motion. The reduce order dynamics are insensitive to any disturbances occurring in the Range space $R(b)$. This class of uncertainty is called matched uncertainty. The invariance properties with respect to the matched uncertainty makes the 'VSS' a powerful tool for controlling uncertainties system.

4.2.3 Condition on the existence of sliding mode

According to the sliding mode control law, it is clear that the neighborhood of switching surface S must be directed towards to the sliding surface. The sliding surface is locally stable. Using Lyapunov approach, a sufficient condition for existence of a sliding motion is described. [13, 16, 17]. Lypunov approach is described in section (4.4). To consider the sliding reachability region, first, it is necessary to establish sufficient conditions which guarantee that an ideal sliding motion will take place. The sliding surface must be locally attractive, which may be expressed as

$$\lim_{\sigma\to 0^+} \dot{\sigma} < 0 \quad \text{and} \quad \lim_{\sigma\to 0^-} \dot{\sigma} > 0 \tag{4.15}$$

which can be clearly expressed as

$$\dot{\sigma}\sigma = 0 \tag{4.16}$$

The expressions in eq (4.15) and eq (4.16) are termed as reachability conditions. However, the eq (4.15) and (4.16) do not guarantee the existence of the ideal sliding

motion. For guaranteeing an ideal sliding motion, a stronger condition of η -reachability is given by

$$\dot{\sigma}\sigma \le -\eta|s| \tag{4.17}$$

where η is a strictly positive constant. The relay gain is generated by using η -reachability conditions which shown in fig (4.5).

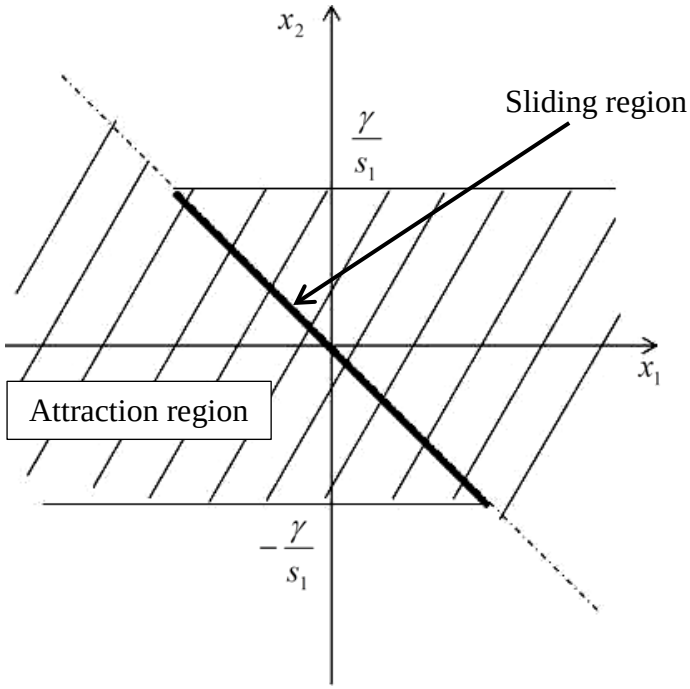

Fig 4.5 Reachability region

According to this facts, eq (4.17) is guarantee the system state to arrive the sliding surface at the finite time. Thus, the relay gain for the sliding mode is obtained

$$\begin{aligned}\sigma\dot{\sigma} &= \sigma\mathbf{S}(\mathbf{A}_a\mathbf{x}_a + \mathbf{b}_a u + \mathbf{d}_a\xi_t)\\ &= \sigma\mathbf{S}\left\{(\mathbf{I}-\mathbf{b}_a(\mathbf{S}\mathbf{b}_a)^{-1}\mathbf{S})\mathbf{A}_a\mathbf{x}_a + \mathbf{b}_a(\mathbf{S}\mathbf{b}_a)^{-1}\mathbf{S}\mathbf{V}_a\mathbf{r} - \mathbf{b}_a\gamma\,\mathrm{sgn}(\sigma) + \mathbf{d}_a\xi_t\right\}\\ &= \sigma\left\{\mathbf{S}\mathbf{V}_a r - \mathbf{S}\mathbf{b}_a\gamma\,\mathrm{sgn}(\sigma) + \mathbf{S}\mathbf{d}_a\xi_t\right\}\end{aligned} \tag{4.18}$$

Substitute eq (4.18) to eq (4.17),

$$\sigma\{\mathbf{SV}_a r - \mathbf{Sb}_a \gamma \,\mathrm{sgn}(\sigma) + \mathbf{sd}_a \xi_t\} \le -\eta|\sigma|$$

$$\gamma \,\mathrm{sgn}(\sigma) \ge (\mathbf{Sb}_a)^{-1}\left[\mathbf{SV}_a \mathbf{r} + \mathbf{Sd}_a \xi_t + \eta \frac{|\sigma|}{\sigma}\right] \tag{4.19}$$

Relay gain satisfies above equation. As mentioned above, chattering is the main problem of the sliding mode control. To reduced the chattering effect in this research, the boundary layer design is used. Therefore, in order to eliminate the influence of the chattering effects and suppress the influence of the uncertainty or disturbances, the saturation function using boundary layer δ is applied which shown in fig (4.6). The width of the boundary layer is completely depends on the relay gain. If the relay gain increases, the boundary layer become narrow and the system will be fast. If the relay gain decreases, the boundary layer become expense and the system will be slow. It is decided as the trial error so that a sliding mode occurs.

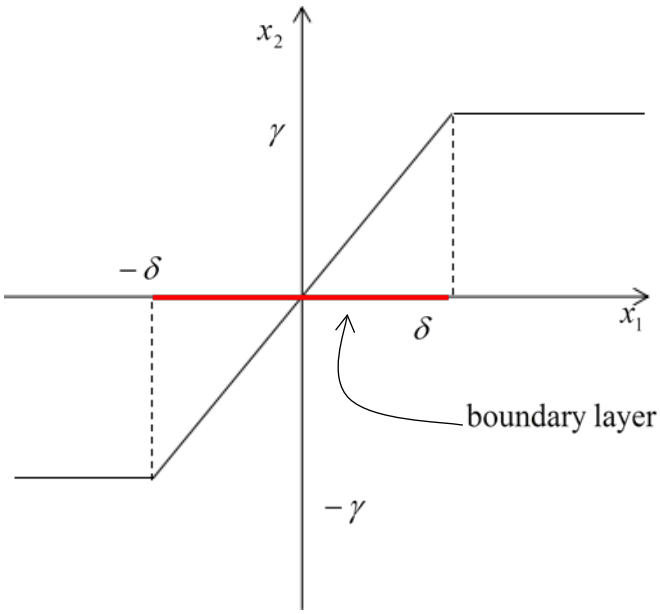

Fig 4.6 Boundary layer design with relay gain

4.2.4. Structure of control law

Based on the variable structure system with sliding mode control, the control law composed with two parts. This is given as

$$u = u_1 + u_2 \tag{4.20}$$

$$\begin{aligned} u_1 &= -(Sb)^{-1} S\left[A\hat{\hat{x}} - vr - g\xi_t\right] \\ u_2 &= -\gamma \,\mathrm{sgn}(\sigma) \\ \sigma &= Sx \end{aligned} \tag{4.21}$$

where u_1 is so-called the equivalent control of the system which is obtained by letting $\dot{\sigma} = 0$, and u_2 is the relay input to bring about the sliding motion. And σ is defined as the switching function of the system. It will precisely defined in controller section.

4.2.5 Regular form

For variable structure control design problem, a particular canonical form, the so-called regular form, is most useful for analysis. The system has considered as the matrices (A,b,c) to be controllable and observable. The configuration of eq (4.1) and eq (4.7) is expressed in regular form

$$\dot{x}_1(t) = A_{11}x_1(t) + A_{12}x_2(t) \tag{4.22}$$

$$\dot{x}_2(t) = A_{21}x_1(t) + A_{22}x_2(t) + b_2u(t) \tag{4.23}$$

with the switching surface is defined by

$$s(t) = S_N x_1(t) + S_R x_2(t) \tag{4.24}$$

where the change of coordinates is defined by an orthogonal matrix T_r as

$$\tilde{x}(t) = T_r x(t) \tag{4.25}$$

With a non-singular transformation $T_r \in \Re^{n\times n}$ exists, the plant matrices (A,b,c) have the following form. The system state matrix can be written as

$$T_r A T_r^T = \begin{bmatrix} A_{11} & A_{12} \\ A_{21} & A_{22} \end{bmatrix} \tag{4.26}$$

where $\mathbf{A}_{11} \in \Re^{(n-m)\times(n-m)}$, n is the number of the system states and m is the number of the measured states. The input matrix has the form

$$T_r b = \begin{bmatrix} 0 \\ b_2 \end{bmatrix} \tag{4.27}$$

where $b \in \Re^{m\times m}$ and is non-singular. The matrix of the switching function written as

$$S = \begin{bmatrix} S_N & S_R \end{bmatrix} \tag{4.28}$$

During sliding motion, the switching function $s(t)$ will be identically zero. Thus

$$S_N x_1(t) + S_R x_2(t) = 0 \tag{4.29}$$

$$\begin{aligned} x_2(t) &= -S_R^{-1} S_N x_1(t) \\ &= -M x_1(t) \end{aligned} \tag{4.30}$$

where $M \in \Re^{m\times(n-m)}$ is defined as

$$M = S_R^{-1} S_N \tag{4.31}$$

Therefore, the reduce order dynamics is governed by eq (4.20) and eq (4.28) as

$$\begin{aligned} \dot{x}_1(t) &= A_{11} x_1(t) - A_{12}(-M x_1(t)) \\ &= (A_{11} - A_{12} M) x_1(t) \end{aligned} \tag{4.32}$$

In particular, the reduce order dynamics eq (4.30) makes the system maximally robust to system uncertainty which occurs within the system has the effect of rendering the sliding mode dynamics minimally sensitive to the unmatched uncertainty in the system.

4.3 Design of Sliding Mode Controller

For the control system, we use sliding mode control theory for both controller and observer design to regulate the robust contact force. The overall block diagram shown in fig (4.1). Since an optimal type I servo system is designed, the system takes the error integration of the output where the controlled variable is the contact force f_c. The augmented state vector is defined as

$$x_a = \begin{bmatrix} \int r - y & x_{ts} & \dot{x}_{ts} & x_{f1} & \dot{x}_{f1} & x_{f2} & \dot{x}_{f2} \end{bmatrix} \tag{4.33}$$

The augmented state equation is expressed as

$$\dot{\mathbf{x}}_a = \begin{bmatrix} 0 & -\frac{k_t m_s - m_t k_s}{m_t + m_s} & -\frac{c_t m_s - m_t c_s}{m_t + m_s} & -\frac{m_t k_s}{m_t + m_s} & -\frac{m_t c_s}{m_t + m_s} \\ 0 & 0 & 1 & 0 & 0 \\ 0 & -\frac{k_t + k_s}{m_t + m_s} & -\frac{c_t + c_s}{m_t + m_s} & -\frac{k_s}{m_t + m_s} & -\frac{c_s}{m_t + m_s} \\ 0 & 0 & 0 & 0 & 1 \\ 0 & \frac{k_s}{m_{f1}} & \frac{c_s}{m_{f1}} & -\frac{k_s + k_{f1}}{m_{f1}} & -\frac{c_s + c_{f1}}{m_{f1}} \\ 0 & 0 & 0 & 0 & 0 \\ 0 & 0 & 0 & \frac{k_{f1}}{m_{f2}} & \frac{c_{f1}}{m_{f2}} \end{bmatrix}$$

$$\begin{bmatrix} 0 & 0 \\ 0 & 0 \\ 0 & 0 \\ 0 & 0 \\ -\frac{k_{f1}}{m_{f1}} & -\frac{c_{f1}}{m_{f1}} \\ 0 & 1 \\ -\frac{k_{f1}}{m_{f2}} & -\frac{c_{f1} + c_{f2}}{m_{f2}} \end{bmatrix} \mathbf{x}_a + \begin{bmatrix} 0 \\ 0 \\ 0 \\ 0 \\ 0 \\ 0 \\ \frac{1}{m_{f2}} \end{bmatrix} u + \begin{bmatrix} -\frac{m_s}{m_t + m_s} \\ 0 \\ \frac{1}{m_t + m_s} \\ 0 \\ 0 \\ 0 \\ 0 \end{bmatrix} \xi_t + \begin{bmatrix} 1 \\ 0 \\ 0 \\ 0 \\ 0 \\ 0 \\ 0 \end{bmatrix} r \tag{4.34}$$

$$= \begin{bmatrix} 0 & -\mathbf{c} \\ \mathbf{0} & \mathbf{A} \end{bmatrix} x_a + \begin{bmatrix} 0 \\ \mathbf{b} \end{bmatrix} u + \begin{bmatrix} d \\ \mathbf{d} \end{bmatrix} \xi_t + \begin{bmatrix} 1 \\ \mathbf{0} \end{bmatrix} r$$

$$= \mathbf{A}_a \mathbf{x}_a + \mathbf{b}_a u + \mathbf{d}_a \xi_t + \mathbf{j}_a r$$

From these equations, it follows the contact force equation is represented by

$$\begin{aligned} f_c &= \frac{1}{m_t + m_s}\begin{bmatrix} 0 & k_t m_s - m_t k_s & c_t m_s - m_t c_s & m_t k_s & m_t c_s & 0 & 0 \end{bmatrix}\mathbf{x}_a \\ &\qquad - \frac{m_s}{m_t + m_s}\xi_t \\ &= \mathbf{c}_a \mathbf{x}_a + d\xi_t \end{aligned} \tag{4.35}$$

From eq (4.34) and eq (4.35), the disturbance coefficient vector $\mathbf{d}_a$ does not satisfy the matching condition with the input vector $\mathbf{b}$, which is $\mathbf{d}_a \notin Range(\mathbf{b}_a)$. To get a good control performance, we design a sliding mode controller. First, we design a sliding mode control law eq (4.18), the switching function can be defined as

$$\sigma = \mathbf{S}\mathbf{x}_a \tag{4.36}$$

The first part, equivalent control law u_1 for this control design can be derived using eq (4.34) and eq (4.36) as

$$\begin{aligned} \dot{\sigma} &= \mathbf{S}\dot{\mathbf{x}}_a \\ &= \mathbf{S}(\mathbf{A}_a \mathbf{x}_a + \mathbf{b}_a u_{eq} + \mathbf{d}_a \xi_t + \mathbf{j}_a r) \end{aligned}$$

when the system enters to the sliding mode control $\sigma = \dot{\sigma} = 0$

$$\begin{aligned} \mathbf{S}\mathbf{b}_a u_{eq} &= -\mathbf{S}(\mathbf{A}_a \mathbf{x}_a + \mathbf{d}_a \xi_t + \mathbf{j}_a r) \\ u_{eq} &= -(\mathbf{S}\mathbf{b}_a)^{-1}\mathbf{S}(\mathbf{A}_a \mathbf{x}_a + \mathbf{d}_a \xi_t + \mathbf{j}_a r) \end{aligned} \tag{4.37}$$

For this controller design,we neglected the effect of the disturbance, the perturbation term from the plant system and consider as a nominal pantograph-catenary system. Removing the disturbance yields;

$$\tilde{u}_{eq} = -(\mathbf{S}\mathbf{b}_a)^{-1}\mathbf{S}(\mathbf{A}_a \mathbf{x}_a + \mathbf{j}_a r) \tag{4.38}$$

Recall the second part, relay gain is $u_2 = -\gamma \operatorname{sgn}(\sigma)$. The control law of sliding mode control can be written as

$$u = -(\mathbf{S}\mathbf{b}_a)^{-1}\mathbf{S}(\mathbf{A}_a\mathbf{x}_a + \mathbf{j}_a r) - \gamma \operatorname{sgn}(\sigma) \tag{4.39}$$

4.3.1 Switching Surface design for the plant

It is very important how to determine the switching function σ for a sliding mode controller design, because the sliding motion is prescribed by the switching function; an ideal sliding motion can be represented by $\sigma = \dot{\sigma} = 0$. To simplify the switching function design, the so-called regular form which described in section (4.2.5) is employed because this special form makes it possible to avoid the calculation of the $\dot{\sigma} = 0$.

According to the regular form technique, the system can be decomposed into two sub-dynamics. One is called the Range space dynamics and the another is Null space dynamic. To this end, the state equation eq (4.34) can be written with the divided state vector, partitioned system matrix, and coefficient vectors as follows:

$$\begin{bmatrix} \dot{\mathbf{x}}_N \\ \dot{x}_R \end{bmatrix} = \begin{bmatrix} \mathbf{A}_{N1} & \mathbf{a}_{N2} \\ \mathbf{a}_{R1} & a_{R2} \end{bmatrix} \begin{bmatrix} \mathbf{x}_N \\ x_R \end{bmatrix} + \begin{bmatrix} \mathbf{0} \\ b_R \end{bmatrix} u + \begin{bmatrix} \mathbf{d}_N \\ 0 \end{bmatrix} \xi_t + \begin{bmatrix} \mathbf{j}_N \\ 0 \end{bmatrix} r \tag{4.40}$$

where N is denoted for Null space and R is for Range space. The switching function is also partitioned as

$$\sigma = \mathbf{S}\mathbf{x}_a = \begin{bmatrix} \mathbf{S}_N & S_R \end{bmatrix} \begin{bmatrix} \mathbf{x}_N \\ x_R \end{bmatrix} \tag{4.41}$$

When system entering the sliding motion, the switching function can be written as

$$\mathbf{S}_N \mathbf{x}_N(t) + S_R x_R(t) = 0 \tag{4.42}$$

$$x_R(t) = -S_R^{-1}\mathbf{S}_N \mathbf{x}_N(t) \tag{4.43}$$

Since $\sigma = 0$, during ideal sliding motion, the dynamics of the sliding motion is given from eq (4.40) and eq (4.41) by

$$\dot{\mathbf{x}}_N = (\mathbf{A}_{N1} - \mathbf{a}_{N2} S_R^{-1} \mathbf{S}_N)\mathbf{x}_N + \mathbf{d}_N \xi_t + \mathbf{j}_N r \tag{4.44}$$

The coefficient vector of the switching function is determined by applying the LQR theory. In order to design an optimal switching function, the following quadratic minimization performance index is used

$$J = \frac{1}{2}\int_{t_s}^{\infty} \mathbf{x}_a(t)^T \mathbf{Q} \mathbf{x}_a(t) dt \tag{4.45}$$

where $\mathbf{Q}$ is weight matrix and is both symmetric and positive definite and t_s is the time which the sliding motion starts. To transform the performance index into the one used in the standard LQR problem, where the control effort is inclined, the matrix $\mathbf{Q}$ from eq (4.43) is partitioned as

$$\mathbf{Q} = diag\begin{vmatrix} q_1 & q_2 & \ldots & q_n \end{vmatrix} = \begin{bmatrix} \mathbf{Q}_{N1} & \mathbf{q}_{N2} \\ \mathbf{q}_{R1} & q_{R2} \end{bmatrix} \tag{4.46}$$

where $\mathbf{q}_{R1} = \mathbf{q}_{N2}^T$. Because of the plant system is used the regular form technique, the weight matrix also need to change with this conversation matrix to the regular form. However, pantograph-catenary system is originally the regular form, therefore, there is no need to change any situation. Consider the derivation of the optimal switching function in the sliding mode control state for the optimal control design of pantograph overhead system, the state equation where removing the disturbances yields can be written as

$$\dot{\mathbf{x}}_N = \mathbf{A}_{N1}\mathbf{x}_N + \mathbf{a}_{N2}\mathbf{x}_R \tag{4.47}$$

The situation of eq (4.47) can be regarded as a virtual control system, which will be discussed in next chapter. Then, the eq (4.47) can be seen as the similar as a general state equation

$$\dot{\mathbf{x}} = \mathbf{A}\mathbf{x} + \mathbf{b}u \tag{4.48}$$

From eq (4.45) and eq (4.46), the quadratic performance index can be rewritten as

$$\mathbf{J} = \int_{t_s}^{\infty} \left\{ \mathbf{x}_N(t)^T \mathbf{Q}_{N1} \mathbf{x}_N(t) + x_R(t)^T q_{R2} x_R(t) \right\} dt \tag{4.49}$$

After some algebraic manipulations on eq (4.47) and eq (4.49), Riccati equation to give the optimal solution is obtained by

$$\mathbf{P}_N \mathbf{A}_{N1} + \mathbf{A}_{N1}^T \mathbf{P}_N - q_{R2}^T \mathbf{P}_N \mathbf{a}_{N2} \mathbf{a}_{N2}^T \mathbf{P}_N + \mathbf{Q}_{N1} = 0 \tag{4.50}$$

where $\mathbf{P}$ is the unique positive definite and the following equation is obtained

$$x_R(t) = -q_{R2}^{-1} \mathbf{a}_{N2}^T \mathbf{P}_N \mathbf{x}_N(t) \tag{4.51}$$

From eq (4.41) and eq (4.51), the optimal switching function vector can be given by

$$S_R^{-1} S_N = q_{R2}^{-1} \mathbf{a}_{N2}^T \mathbf{P}_N \tag{4.52}$$

where S_R, the range space of the switching function does not directly effect the sliding mode state. In this controller design, let S_R is equal to the one. And the weight matrix Q from eq (4.46) is determined as follows

$$Q = \begin{bmatrix} 0.1 & 0 & 0 & 0 & 0 & 0 & 0 \\ 0 & 5 & 0 & 0 & 0 & 0 & 0 \\ 0 & 0 & 1 & 0 & 0 & 0 & 0 \\ 0 & 0 & 0 & 5 & 0 & 0 & 0 \\ 0 & 0 & 0 & 0 & 1 & 0 & 0 \\ 0 & 0 & 0 & 0 & 0 & 5 & 0 \\ 0 & 0 & 0 & 0 & 0 & 0 & 1 \end{bmatrix}$$

Note: Sliding mode observer design described in chapter (3).

4.4 Stability Analysis

The purpose of switching control law is to drive the system state trajectory onto a specified surface in the state space, named sliding or switching surface and keep the system state on this manifold for all the subsequent times. The most important task is to design a switched control that will drive the system state to the switching surface and maintain it on the manifold. A Lyapunov approach is used to characterize this task. Since the invariant property of the sliding mode observer which is described in chapter (3), we investigate the stability of ideal sliding motion given by eq (4.42). Deleting the reference signal from eq (4.42), it follows;

$$\begin{aligned}\dot{\mathbf{x}}_N &= (\mathbf{A}_{N1} - \mathbf{a}_{N2} S_R^{-1} \mathbf{S}_N)\mathbf{x}_N + \mathbf{d}_N \xi_t \\ &= \mathbf{A}_{sm}\mathbf{x}_N + \mathbf{d}_N \xi_t\end{aligned} \tag{4.53}$$

Lyapunov method is used to determine the stability properties of an equilibrium point without solving the state equation. Let $V(x)$ be a continuously differentiable scalar function defined in a domain that contain in the origin. A function $V(x)$ is said to be positive definite if $V(0) = 0$ and $V(x) > 0$ for x. It is said to be negative definite if $V(0) = 0$ and $V(x) > 0$ for x. Lyapunov method is to assure that the function is positive definite when the function is negative definite if is possible. Using this analogy, the stability is assured.

A Lyapunov function candidate can be taken as

$$V = \mathbf{x}_N^T \mathbf{P} \mathbf{x}_N \tag{4.54}$$

where the matrix $\mathbf{P} \in \Re^{n \times n}$ is symmetric positive definite. It is well known that $\mathbf{A}_{sm}$ has stable eigenvalues or $\mathbf{A}_{sm}$ is Hurwitz, there exists a unique positive definite matrix $\mathbf{P}$ satisfying the following Lyapunov equation

$$\mathbf{P}\mathbf{A}_{sm} + \mathbf{A}_{sm}^T \mathbf{P} = -\mathbf{Q} \tag{4.55}$$

Thus, any stable linear system is quadratically stable. A symmetric positive definite matrix $\mathbf{P}$ satisfying eq (4.53) will be referred to as a Lyapunov matrix for the matrix $\mathbf{A}_{sm}$. The pair of positive definite matrices $(\mathbf{P},\mathbf{Q})$ satisfy the Lyapunov equation, eq (4.53) and can be defined as

$$\mu = \frac{\lambda_{\min}(\mathbf{Q})}{\lambda_{\max}(\mathbf{P})} \tag{4.56}$$

and the uncertain function is satisfied

$$\|\xi_t\| \le \frac{1}{2}\mu\|\mathbf{x}_N\| \tag{4.57}$$

Then, the system state of the plant system, eq (4.51) is stable. The derivate along the trajectories using a Lyapunov equation, eq (4.52) satisfies

$$\begin{aligned}\dot{V} &= \mathbf{x}_N^T\mathbf{P}\mathbf{A}\mathbf{x}_N + \mathbf{x}_N^T\mathbf{A}^T\mathbf{P}\mathbf{x}_N + 2\mathbf{x}_N^T\mathbf{P}\mathbf{d}_N\xi_t \\ &= -\mathbf{x}_N^T\mathbf{Q}\mathbf{x}_N + 2\mathbf{x}_N^T\mathbf{P}\mathbf{d}_N\xi_t \\ &\le -\mathbf{x}_N^T\mathbf{Q}\mathbf{x}_N + 2\|\mathbf{P}\mathbf{x}_N\mathbf{d}_N\|\|\xi_t\|\end{aligned} \tag{4.58}$$

where the Cauchy-Schwarz inequality has been used to obtain the last inequality from eq (4.56) is

$$\|\mathbf{P}\mathbf{x}_N\| = \sqrt{\mathbf{x}_N^T\mathbf{P}^2\mathbf{x}_N} \le \sqrt{\lambda_{\max}(\mathbf{P}^2)\|\mathbf{x}_N\|^2} = \lambda_{\max}(\mathbf{P})\|\mathbf{x}_N\| \tag{4.59}$$

And the Rayleigh principle has been used to get the first inequality from eq (4.56)

$$-\mathbf{x}_N^T\mathbf{Q}\mathbf{x}_N \le -\lambda_{\min}(\mathbf{Q})\|\mathbf{x}_N\|^2 \tag{4.60}$$

With the above three equations, eq (4.56), eq (4.57) and eq (4.58), the time derivative of V along the state trajectory satisfies the boundedness.

$$\dot{V} \le -\lambda_{\min}(\mathbf{Q})\|\mathbf{x}_N\|^2 + \delta\|\mathbf{x}_N\|\|\xi_t\|$$

$$= -\|\mathbf{x}_N\|(\lambda_{\min}(\mathbf{Q})\|\mathbf{x}_N\| - \delta|\xi_t| \tag{4.61}$$

where δ is defined as

$$\delta = 2\sqrt{\lambda_{\max}(\mathbf{P}\mathbf{d}_N\mathbf{d}_N^T\mathbf{P})} \tag{4.62}$$

From eq (4.59), if the following inequality holds

$$|\xi_t| < \frac{\lambda_{\min}(\mathbf{Q})}{\delta}\|\mathbf{x}_N\| \tag{4.63}$$

then the system state in this thesis during sliding motion is asymptotically stable (sometime referred to as quadratically stable).

This result is a special case of the one Patel and Toda [22] obtained for general linear time invariant systems subject to linear growth uncertainty, where the uncertainty was represented by an n-th dimensional vector; $\mathbf{d}_N\xi_t \to \xi_t$. In their case, δ becomes $2\lambda_{\max}(P)$ and the condition on the uncertainty for the perturbed system to be asymptotically stable is given by

$$\|\xi\| < \frac{\lambda_{\min}(\mathbf{Q})}{2\lambda_{\max}(\mathbf{P})}\|\mathbf{x}_N\| \tag{4.64}$$

Furthermore, their research shows that the coefficient on the right hand side in eq (4.62) is maximized when $\mathbf{Q} = \mathbf{I}$. Although the condition given by eq (4.62) is clearly more conservative than the one by eq (4.61). In this research, we assume $\mathbf{Q} = \mathbf{I}$ to simplify further analysis.

Substituting the perturbation term in the present study

$$\xi_t(t, x_{ts}) = \Delta k_t x_{ts} \tag{4.65}$$

into eq (4.62), then it follows:

$$\left|\Delta k_t x_{ts}\right| < \frac{1}{\delta}\left\|\mathbf{x}_N\right\| \tag{4.66}$$

Therefore, if $\left|\Delta k_t\right| < \frac{1}{\delta}$, this inequality holds for the system. For example, we obtained $\delta \cong 85$ for some sliding mode controller. In this pantograph-catenary system, the actual fluctuation of the catenary stiffness is terribly large when the train speed is $360 km/h$ and the span length of each cantilever is about 50 m that can be seen in fig (4.7).

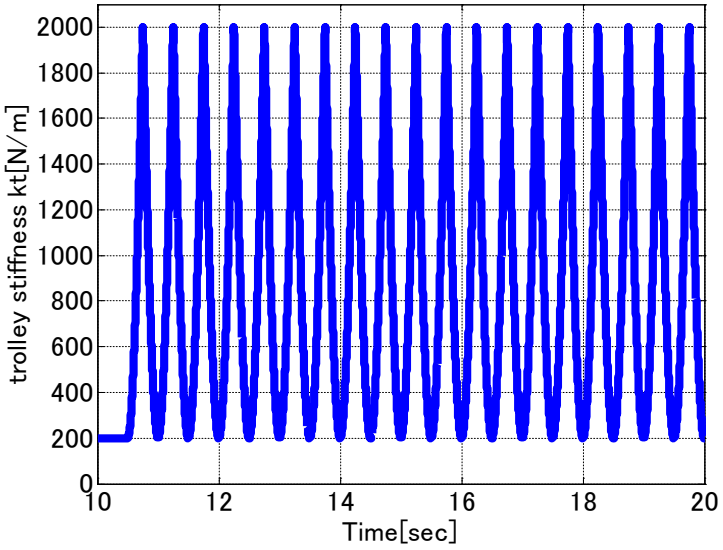

Fig 4.7 Catenary stiffness

Even if the values of the nominal stiffness k_t, was taken as $1{,}100 N/m$, when the maximum perturbation is about 900. Therefore, eq (4.64) gives a sufficient condition for asymptotically stability of the closed loop system of the system, this also implies that the control system that we have designed would not be asymptotically stable even if the design parameters are adjusted by some means. However, it might be able to guarantee ultimate stability and boundedness by making use of the periodicity of the perturbation.

4.5 Simulation Results

In order to investigate the performance of the proposed controller, numerical simulation has been carried out. The parameter values of the pantograph-catenary system are shown in Table 1, where the parameter values of the pantograph are estimated by identification experiments, and those of the catenary system are determined based on some references, e.g. Kobayashi et al. [20]. The design parameters in the controller were determined taking account of this situation so that sliding mode would take place. Because chattering may result in wear and tear on the actuator components, it is very important to reduce the chattering from the control system. To reduce chattering due to the relay component of the control law, we used saturation function with a boundary layer instead of the relay.

In this section, the numerical analysis of the sliding mode controller is performed. The transfer from the reference input r to the contact force f_c is

$$G_{ry}(s) = \frac{5.95\times10^4 s^3 + 3.78\times10^7 s^2 + 3.83\times10^7 s + 4.15\times10^8}{s^6 + 133s^5 + 1.87\times10^4 s^4 + 1.19\times10^6 s^3 + 3.9\times10^7 s^2 + 5.15\times10^7 s + 4.15\times10^8}$$

The design parameters in the controllers are as follows:

$$S = \begin{bmatrix} -0.32 & -92.02 & -3.18 & -28.17 & 2.31 & 121.53 & 1 \end{bmatrix}$$
$$\text{relay}: \ \rho = 100$$
$$\text{boundary layer}: \ \delta = \pm 3$$
$$\text{Weighting matrix}: \ Q = diag\begin{bmatrix} 0.1 & 5 & 1 & 5 & 1 & 5 & 1 \end{bmatrix}$$

With these parameters, the poles and zeros in the transfer function from the reference signal to the contact force are obtained as follows:

$$zeros = z_{ry} = \begin{bmatrix} 0 & -633 & -0.5 \pm 3.27i \end{bmatrix}$$
$$Poles = P_{ry} = \begin{bmatrix} 0 & -21.07 \pm 105.14i & -44.97 \pm 35.49i & -0.5 \pm 3.27i \end{bmatrix}$$

where *ry* represents the output value *y* and input reference value *r*. Hence, the sliding mode controller is used in this system, the zero eigenvalues are present. It

should be noted that a pair of poles approximately cancel out a pair of zeros at $-0.5 \pm 3.27i$ which is the mode of the catenary subsystem given by eq (2.19) from chapter 2. Therefore, a perfect output zeroing can be achieved by exact pole-zero cancellations which make an unobservable subspace in the state space of the control system. From a physical point of view, in addition, these closed-loop poles will make it possible that the pantograph head is following the catenary wire motion not to prevent its free motion, yielding a good regulation of the contact force.

Because the proposed controller achieved a good performance as expected for the simulation result, we carried out some simulations in more realistic situation. That is, although we neglected the actuator dynamics when designing the controller and observer, we inserted the following dynamic model of the pneumatic actuator

$$G(s) = \frac{1}{0.013s + 1} e^{-0.002s} \tag{4.67}$$

which had been obtained by some experiments. Furthermore, it was assumed that three measurements for the controller and observer were corrupted by white Gaussian noises whose maximum magnitude and some important parameters are as shown below:

Contact force: $\pm 4N$
Catenary equivalent stiffness: 2Hz
Displacement of the lower frame: $\pm 1 \times 10^{-4} m$
Velocity of the contact wire/shoe head: $\pm 1 \times 10^{-4} m/s$
Nominal value of stiffness fluctuation: $k_t = 1100 N/m$

The design parameters in the controller and observer were determined taking account of the above situation. Figure (4.8) shows the switching function, σ, where the switching function stays within the boundary layer that can prove that quasi-sliding mode exists. Figure (4.9) and fig (4.10) show the estimation errors of sliding mode observer, e_y, used in the observer eq (3.43) and eq (3.44) which described in chapter (3), where the true state variables are used for control to evaluate only the observer performance. Figure (4.9) shows the simulation result of the

estimation error without actuator dynamic and fig (4.10) shows the simulation result of the estimation error with actuator dynamic. It can be seen from the chattering around the origin as shown in fig (4.10) that the quasi sliding mode takes place in spite of the existence of the actuator dynamics.

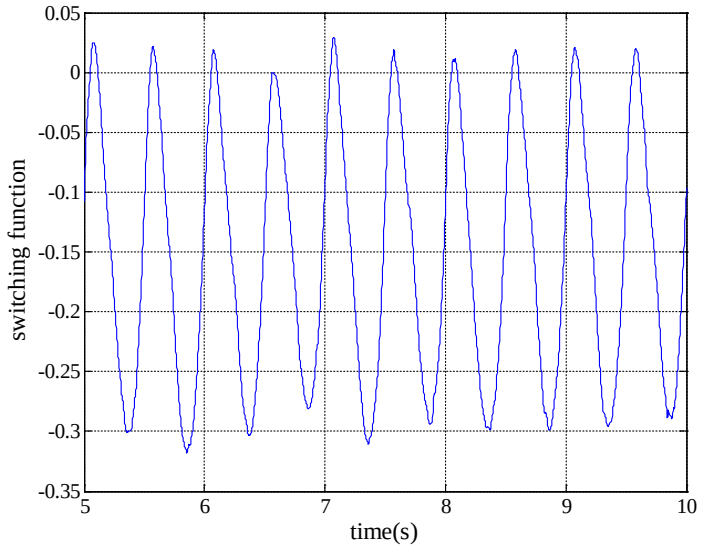

Fig 4.8 Switching function

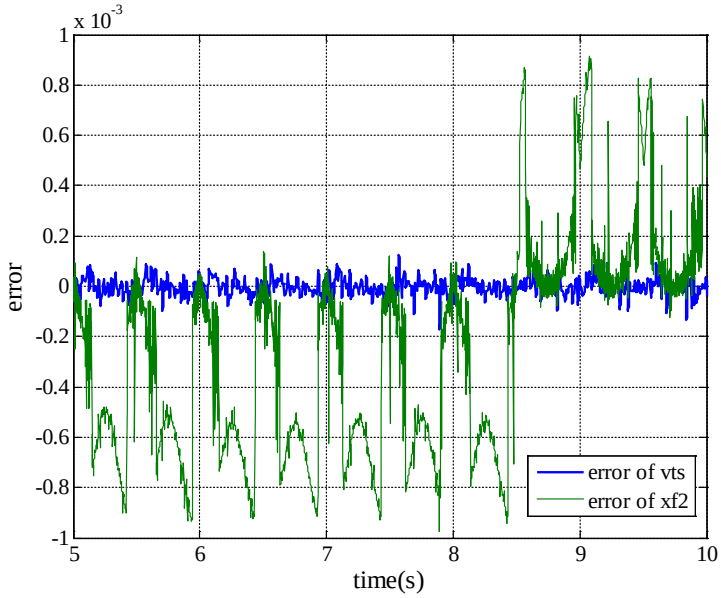

Fig 4.9 Estimation error, e_y without actuator

Figure (4.11) shows the simulation results of the steady state response of the control input with actuator control and the without actuator control. The simulation result of those two are almost the same, which means that the designed controller is appropriate for the actuator dynamics.

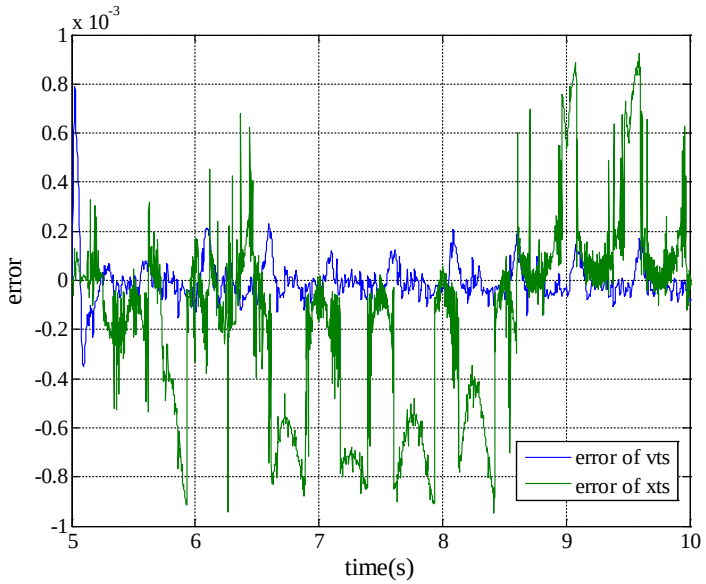

Fig 4.10 Estimation error e_y, with actuator

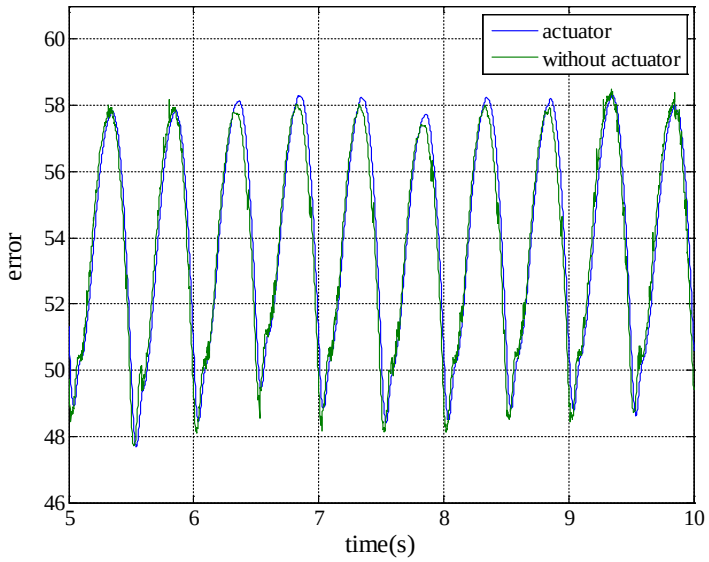

Fig 4.11 Control input

Figure (4.12 a,b) shows the steady state response of the contact force and the catenary displacement. Figure (4.12.a) shows the contact force in the steady state in comparison with the passive case where the static uplift force is provided. It is clear that the active pantograph achieves much better regulation performance than the passive one. Figure (4.13), fig (4.14) and fig (4.15) show the simulation result of the step response of the control input, contact force and catenary displacement, from which it can be seen that the transient response is also good.

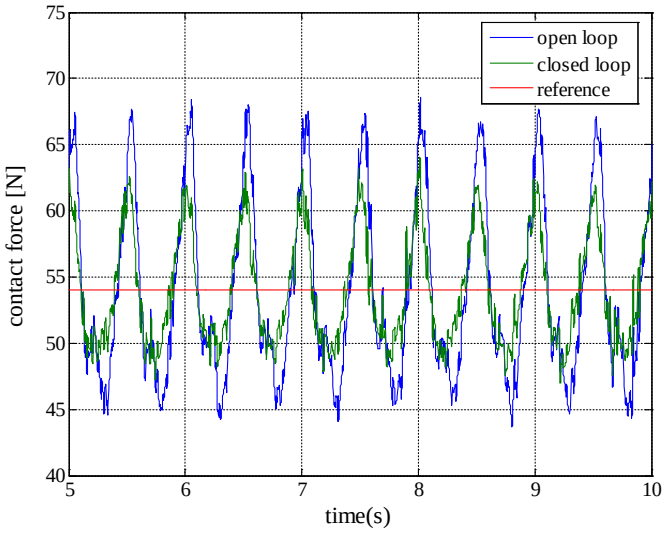

Fig 4.12. (a) Steady state response of Contact force

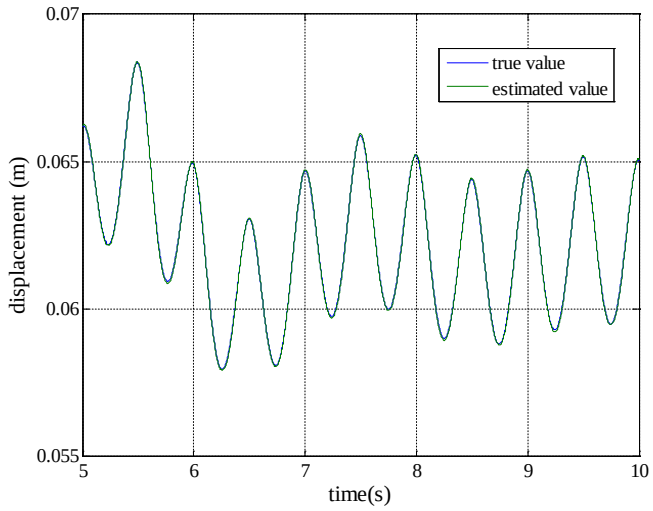

Fig 4.12. (b) Steady state response of Catenary displacement

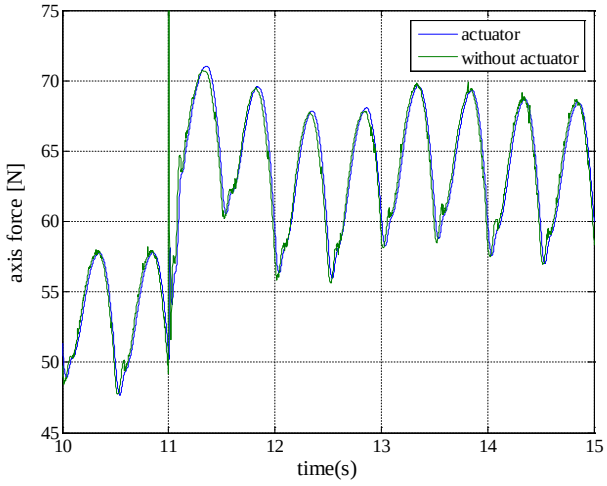

Fig 4.13 Control input in transient response

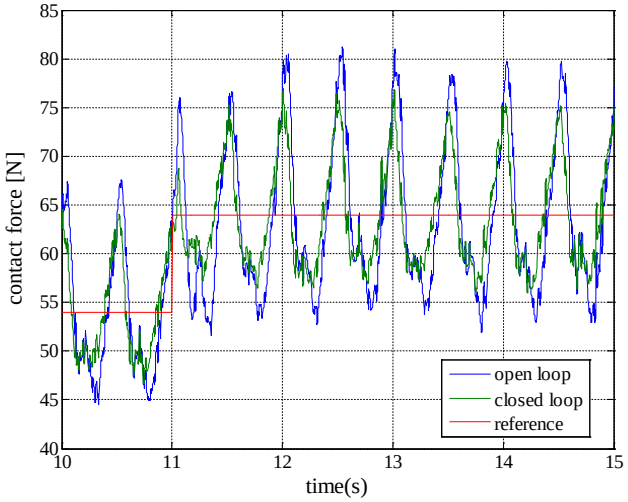

Fig 4.14 Contact force in transient response

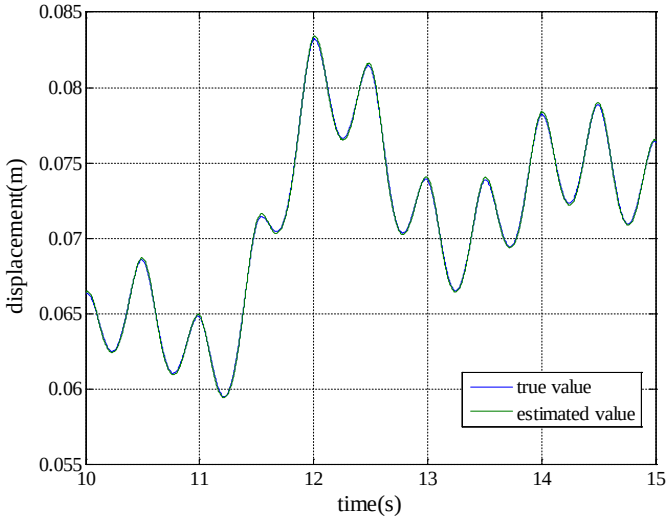

Fig 4.15 Catenary displacement in transient response

From fig (4.12. a), it can be numerically verified that eq (4.66) does not hold with the above switching function shown in fig (4.8). As can be seen from these results, however, the closed-loop system is not asymptotically stable but seems like ultimately bounded. Furthermore, the system was asymptotically stable under the condition, $\delta \cong 85, |\Delta k_t| < 10$. This means the condition $|\Delta k_t| < 1/\delta$ is conservative.

If the perturbation is strictly periodic just shown in fig (4.12. a) this system can be seem as a parametric excitation system and there are some other methods such as Floquet theory to analyze the system. However, actual perturbation is not strictly periodic, and other analyzing methods should be established to prove the ultimate boundness of the system. Figure (4.12 b) shows the catenary displacement of the

system where the true value and estimated value is the almost the same. It is clear from this figure that the pantograph head is following the catenary wire motion not to prevent its free motion.

4.6 Conclusions

In this chapter, we discussed two different section of pantograph-catenary system. In the first section, we proposed a sliding mode controller together with the sliding mode observer, taking account of the flexibility of the articulated frame in the actual pantograph. An introduction to the variable structure system (VSS) is described. The condition to ensure the switching surface, so-called reachability condition, is also described. The reduce order sliding dynamics is formulated. Here, it is also discussed about how to avoid the chattering effects of the system using boundary layer. The proposed controller achieves the robust output (contact force) by pole-zero cancellation during sliding mode. A physical interpretation of this pole-zero cancellation is also given, that is, the pantograph head follow the catenary mode without preventing its free motion.

Secondly, we analyzed the robust stability of the active pantograph system using Lyapunov method. Although one sufficient condition for asymptotic stability has been derived, but it is too conservative. Therefore, other methods to prove more practical stability such as the ultimate boundness of the system is still under investigation.

Chapter 5

Optimal Sliding Mode Servo Controller Design

5.1 Introduction

This work reported herein is a continuation of our early study which investigates the control of the contact force of an active pantograph. As an extension of chapter (4), in this chapter, we mainly discuss a design method of optimal servo systems based on sliding mode for an active pantograph with flexibility subject to the stiffness variation of the catenary. Uncertainties in dynamical and control systems are ineluctable. Robust controls represent a class of methods to handle uncertainties. In fact, the sliding mode control is a powerful robust nonlinear control technique for the systems with uncertainties. Therefore, an optimal sliding mode servo controller together with the sliding mode observer is proposed in order to regulate more robust contact force of an active pantograph.

The points for controller design in this research can be summarized as follows:

“ If the contact force can be used as a switching function in the sliding mode controller, the contact force would be regulate very well because sliding mode takes place when the switching function is forced to be zero by a relay control. In such a case, however, it is impossible to guarantee the existence of sliding mode because of the relative degree between the control input and the contact force, which must be one for the existence. In order to get around this problem, the switching function was constructed just to “approximate” the contact force by introducing a design parameter.”

In order to regulate the contact force, we have been developing an active pantograph with a pneumatic actuator which described in chapter (2). After that, however, it was found through some experiments that the frame had flexibility which could not be ignored to control the contact force. This flexibility increase not only the freedom of motion but also the relative degree mentioned above.

We employ sliding mode theory both controller and observer. The overall block diagram is shown in fig (5.1) where the reference r is the reference contact force, the contact force f_c is the control output, σ is the switching function of sliding mode control and u is the control input to the system. To compensate the tracking error in steady state, integral action with respect to the tracking error is used, although the tracking error cannot be kept zero due to the uncertainty as mentioned above. At first, assuming all the state variables are available for control, we design an optimal sliding mode control law applying a design method of optimal linear tracking system, and then design a sliding mode observer to estimate the state.

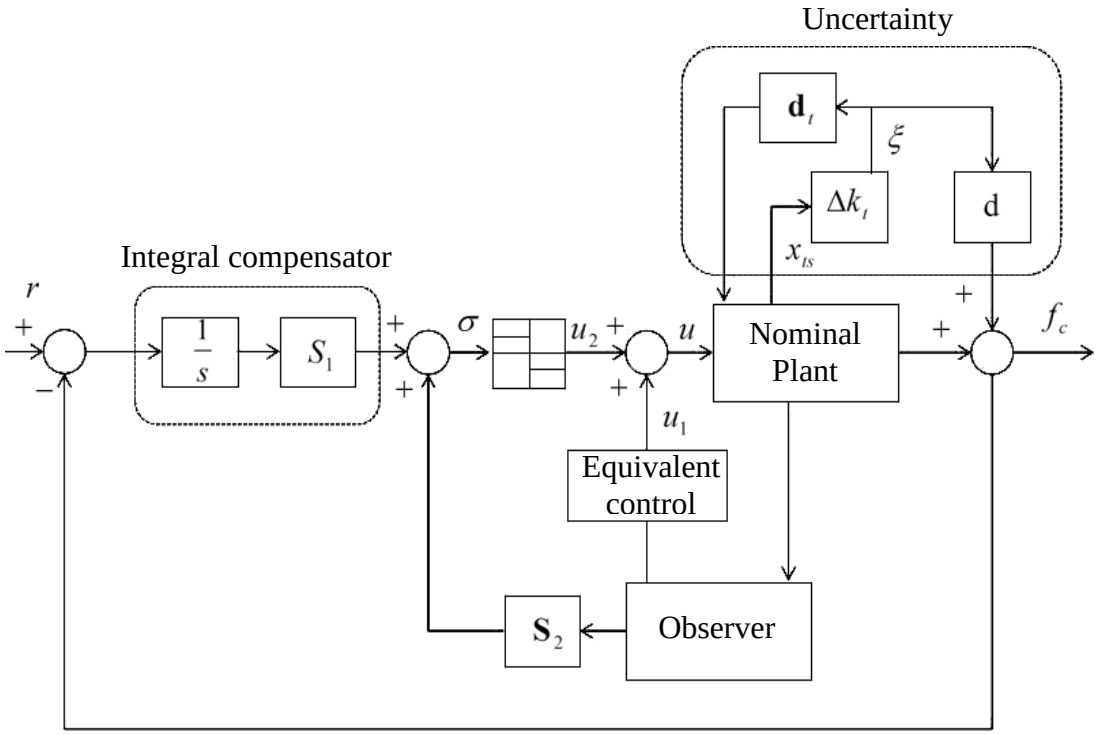

Fig 5.1 Overall block diagram

In this research, therefore, we present a design method of an optimal servo systems based on sliding mode taking account of the flexibility. Although most of the active pantograph systems in literature only regulate the contact force under model

uncertainty or disturbances, servo system should be realized by making efficient use of active force.

For example, the desired contact force might be changed due to some trouble in the catenary. In such a situation, transient response to a step command would be very important. LQR (Linear Quadratic Regulator) technique has been successively applied to not only linear servo systems but also sliding mode control systems. To our best knowledge, however, the reference signal must be assumed to be zero to treat it as a regulator design problem in the optimal design methods for sliding mode servo controllers [22, 23]. As a results, transient response such as step response cannot be taken into account explicitly. On the other hand, Takeda and Kitamori proposed a design method of linear optimal servo systems without such an assumption . We apply their method to design a sliding mode servo controller, which makes it possible to take the transient response into account and gives an important guidelines for controller design. Finally, we combine the controller with a sliding mode observer which described in chapter (3) [23, 24].

As an extension of the early chapter, here, we mainly discuss the design of the controller in which switching function, optimal linear gain and virtual plant system are include. Theoretical background which was explained in chapter (3) and chapter (4), therefore, here we mainly point out how to design the optimal based servo sliding mode controller. The main advantages of this optimal sliding mode servo control is that they can provide a more robust optimal control to the system. The optimal sliding mode control system works as follows:

- If the control system is dominated in the region of nominal part, the system behavior is mainly governed by optimal control.
- If the control system is dominated in the region of perturbations, sliding mode control will take over the main control task.

In section (5.2) describes the main controller design of the active pantograph system. Analysis of the optimal servo system is described in section (5.3). Finally, Numerical simulation results of the proposed controller is given.

5.2 Design of the controller

We employ the (VSS) sliding mode theory to design the controller. There are two main task in a variable structure control system with sliding mode control. The first one is that the phase is to drives the states to the surface. During the motion, the system is effected by any unmatched disturbances present. Secondly, seek to maintain the states on the switching surface for the remaining period where it is insensitive to all the matched uncertainty. To design the controller, the plant to be controlled is

$$\dot{\mathbf{x}} = \mathbf{A}\mathbf{x} + \mathbf{b}u + \mathbf{d}_t\xi_t \tag{5.1}$$

$$y = \mathbf{c}\mathbf{x} + d\xi_t \tag{5.2}$$

where $\mathbf{A} \in \Re^{6\times 6}$ and $\mathbf{b} \in \Re^{1\times 6}$ are plant model matrices where n and m are the number of states of x , input u and ξ_t is considered to represent any uncertainty and disturbances in the system. Recall the state vector to be controlled which described in chapter (2) is

$$\dot{\mathbf{x}} = \begin{bmatrix} x_{ts} & \dot{x}_{ts} & x_{f1} & \dot{x}_{f1} & x_{f2} & \dot{x}_{f2} \end{bmatrix} \tag{5.3}$$

Having introduced the integral action, the augmented state vector is defined as

$$\mathbf{z} = \begin{bmatrix} \int r - y & x_{ts} & \dot{x}_{ts} & x_{f1} & \dot{x}_{f1} & x_{f2} & \dot{x}_{f2} \end{bmatrix} \tag{5.4}$$

Rewrite the state equation of the augmented system for the pant system is expressed as

$$\dot{\mathbf{z}} = \begin{bmatrix} 0 & -\frac{k_t m_s - m_t k_s}{m_t + m_s} & -\frac{c_t m_s - m_t c_s}{m_t + m_s} & -\frac{m_t k_s}{m_t + m_s} & -\frac{m_t c_s}{m_t + m_s} \\ 0 & 0 & 1 & 0 & 0 \\ 0 & -\frac{k_t + k_s}{m_t + m_s} & -\frac{c_t + c_s}{m_t + m_s} & -\frac{k_s}{m_t + m_s} & -\frac{c_s}{m_t + m_s} \\ 0 & 0 & 0 & 0 & 1 \\ 0 & \frac{k_s}{m_{f1}} & \frac{c_s}{m_{f1}} & -\frac{k_s + k_{f1}}{m_{f1}} & -\frac{c_s + c_{f1}}{m_{f1}} \\ 0 & 0 & 0 & 0 & 0 \\ 0 & 0 & 0 & \frac{k_{f1}}{m_{f2}} & \frac{c_{f1}}{m_{f2}} \end{bmatrix}$$

$$\begin{bmatrix} 0 & 0 \\ 0 & 0 \\ 0 & 0 \\ 0 & 0 \\ -\frac{k_{f1}}{m_{f1}} & -\frac{c_{f1}}{m_{f1}} \\ 0 & 1 \\ -\frac{k_{f1}}{m_{f2}} & -\frac{c_{f1} + c_{f2}}{m_{f2}} \end{bmatrix} \mathbf{z} + \begin{bmatrix} 0 \\ 0 \\ 0 \\ 0 \\ 0 \\ 0 \\ \frac{1}{m_{f2}} \end{bmatrix} u + \begin{bmatrix} 1 \\ 0 \\ 0 \\ 0 \\ 0 \\ 0 \\ 0 \end{bmatrix} r + \begin{bmatrix} -\frac{m_s}{m_t + m_s} \\ 0 \\ \frac{1}{m_t + m_s} \\ 0 \\ 0 \\ 0 \\ 0 \end{bmatrix} \xi_t \qquad (5.5)$$

$$= \begin{bmatrix} 0 & \mathbf{-c} \\ \mathbf{0} & \mathbf{A} \end{bmatrix} z + \begin{bmatrix} 0 \\ \mathbf{b} \end{bmatrix} u + \begin{bmatrix} 1 \\ \mathbf{0} \end{bmatrix} r + \begin{bmatrix} d \\ \mathbf{d} \end{bmatrix} \xi_t$$

$$= \overline{\mathbf{A}}\mathbf{z} + \overline{\mathbf{b}} u + \overline{\mathbf{v}} r + \overline{\mathbf{d}}_t \xi_t$$

The output equation is expressed as

$$f_c = \frac{1}{m_t + m_s} \begin{bmatrix} 0 & k_t m_s - m_t k_s & c_t m_s - m_t c_s & m_t k_s & m_t c_s & 0 & 0 \end{bmatrix} \mathbf{z} - \frac{m_s}{m_t + m_s} \xi_t$$

$$= \begin{bmatrix} 0 & \mathbf{c} \end{bmatrix} \mathbf{z} + d\xi_t \qquad (5.6)$$

$$= \overline{\mathbf{c}}\mathbf{z} + d\xi_t$$

From eq (5.5) and eq (5.6), the disturbance coefficient vector $\mathbf{d}_t$ does not satisfy the matching condition with the input vector $\mathbf{b}$, which is $\mathbf{d}_t \notin Range(\mathbf{b})$. To get a good control performance, we design a sliding mode controller law.

5.2.1 Control law of the controller

Based on the standard sliding mode control theory, the control input u is composed of two components as follows:

$$u = u_1 + u_2 \tag{5.7}$$

where u_1 is the so-called equivalent control and u_2 is the relay input to bring about the sliding motion. Th equivalent control u_1 which is obtained by solving the switching equation shows in eq (5.8).

$$\dot{\sigma} = \mathbf{S}\dot{\mathbf{z}} = 0 \tag{5.8}$$

Equation (5.5) substitutes to eq (5.8) for the control u is

$$\dot{\sigma} = \mathbf{S}\overline{\mathbf{A}}\mathbf{z} + \mathbf{S}\overline{\mathbf{b}}u_1 + \mathbf{S}\overline{\mathbf{v}}r + \overline{\mathbf{d}}\xi_t$$

when system enters to the sliding mode $\dot{\sigma} = 0$

$$\mathbf{S}\overline{\mathbf{A}}\mathbf{z} + \mathbf{S}\overline{\mathbf{b}}u_1 + \mathbf{S}\overline{\mathbf{v}}r + \overline{\mathbf{d}}\xi_t = 0$$

$$\mathbf{S}\overline{\mathbf{b}}u_1 = -\mathbf{S}(\overline{\mathbf{A}}\mathbf{z} + \overline{\mathbf{v}}r + \overline{\mathbf{d}}\xi_t)$$

$$u_1 = -(\mathbf{S}\overline{\mathbf{b}})^{-1}\mathbf{S}(\overline{\mathbf{A}}\mathbf{z} + \overline{\mathbf{v}}r + \overline{\mathbf{d}}\xi_t) \tag{5.9}$$

For this controller design,we neglected the effect of the disturbance, the perturbation term from the plant system and consider as a nominal pantograph-catenary system. Removing the disturbance yields;

$$u_1 = -(\mathbf{S}\bar{\mathbf{b}})^{-1}\mathbf{S}(\bar{\mathbf{A}}\mathbf{z} + \bar{\mathbf{v}}r) \tag{5.10}$$

The relay input u_2 is defined as

$$u_2 = (\mathbf{S}\bar{\mathbf{b}})^{-1}\rho\,\mathrm{sgn}(\sigma) \tag{5.11}$$

The control law of the controller, eq (5.7) is rewritten as

$$u = -(\mathbf{S}\bar{\mathbf{b}})^{-1}\mathbf{S}(\bar{\mathbf{A}}\mathbf{z} + \bar{v}r) + (\mathbf{S}\bar{\mathbf{b}})^{-1}\rho\,\mathrm{sgn}(\sigma) \tag{5.12}$$

5.2.2 Switching surface design

As mentioned chapter (4), It is very important how to determine the switching function σ for the sliding mode controller because the sliding motion is prescribed by the switching function; an ideal sliding motion can be obtained from $\sigma = \dot{\sigma} = 0$. To simplified the switching function design, the so called regular form is employed because this special form makes it possible to use of complicated equivalent control to represent the dynamics during ideal sliding mode. To apply the regular form technique, the state equation eq (5.5) is divided into two subsystems, i.e. two sub-states $\mathbf{z}_N$ and z_R, which are sometimes referred to as “Null space dynamics” and “Range space dynamics” respectively.

$$\dot{\mathbf{z}} = \begin{bmatrix} \dot{\mathbf{z}}_N \\ \dot{z}_R \end{bmatrix} = \begin{bmatrix} \bar{\mathbf{A}}_{N1} & \bar{\mathbf{a}}_{N2} \\ \bar{\mathbf{a}}_{R1} & \bar{a}_{R2} \end{bmatrix} \begin{bmatrix} \mathbf{z}_N \\ z_R \end{bmatrix} + \begin{bmatrix} \mathbf{0} \\ \bar{b}_r \end{bmatrix} u + \begin{bmatrix} \bar{\mathbf{v}}_N \\ 0 \end{bmatrix} r + \begin{bmatrix} \bar{\mathbf{d}}_N \\ 0 \end{bmatrix} \xi_t \tag{5.13}$$

$$\dot{\mathbf{z}}_N = \bar{\mathbf{A}}_{N1}\mathbf{z}_N + \bar{\mathbf{a}}_{N2} z_R + \bar{\mathbf{v}}_N r + \bar{\mathbf{d}}_N \xi_t \tag{5.14}$$

$$\dot{z}_R = \bar{\mathbf{a}}_{R1}\mathbf{z}_N + \bar{a}_{R2} z_R + \bar{b}_r u \tag{5.15}$$

where $\mathbf{z}_N \in \Re^{6\times 1}$, $z_R \in \Re^1$, $\bar{\mathbf{A}}_{N1} \in \Re^{6\times 6}$, $\bar{\mathbf{a}}_{N2} \in \Re^{6\times 1}$, $\bar{\mathbf{a}}_{R1} \in \Re^{1\times 6}$, $\bar{a}_{R2} \in \Re^1$, $\bar{\mathbf{v}}_N \in \Re^{6\times 1}$, $\bar{b}_r \in \Re^1$ and $\bar{\mathbf{d}}_N \in \Re^{6\times 1}$.

The output equation in regular form is given as

$$f_c = \begin{bmatrix}\bar{\mathbf{c}}_N & 0\end{bmatrix}\begin{bmatrix}\mathbf{z}_N \\ z_R\end{bmatrix} + d\xi_t = \bar{\mathbf{c}}_N \mathbf{z}_N + d\xi_t \tag{5.16}$$

where $\bar{\mathbf{c}}_N \in \Re^{1\times 6}$ and $d \in \Re^1$.

The coefficient of the switching function is also partitioned corresponding to the subsystem as

$$\sigma = \begin{bmatrix}\mathbf{S}_N & 1\end{bmatrix}\mathbf{z} = \begin{bmatrix}\mathbf{S}_N & 1\end{bmatrix}\begin{bmatrix}\mathbf{z}_N \\ z_R\end{bmatrix} \tag{5.17}$$

where the last element in $\mathbf{S}$ is assumed to be 1 without any loss of generality because the switching function from the range space region does not directly effect the sliding mode state. Since $\sigma = 0$ and the system order is reduced by one during ideal sliding mode, the dynamics of the sliding mode is represented by eq (5.14) and and $\sigma = 0$ with eq (5.17) instead of the range space dynamics eq (5.15) as

$$z_R = -\mathbf{S}_N \mathbf{z}_N \tag{5.18}$$

During ideal sliding motion, the dynamics of the sliding motion is given from eq (5.14) and eq (5.18) by

$$\dot{\mathbf{z}}_N = (\bar{\mathbf{A}}_{N1} - \bar{\mathbf{a}}_{N2}\mathbf{S}_N)\mathbf{z}_N + \bar{\mathbf{v}}_N r + \bar{\mathbf{d}}_N \xi_t \tag{5.19}$$

One of the advantages of this form is that z_R can be though of as virtual linear state feedback control for the Null space eq (5.14) which will be discussed in next section, and thus the coefficient of the switching function, S_N can be determined by linear control theory as a feedback gain vector.

5.2.3 Design of a Linear feedback gain

The coefficient vector of the switching function is determined by applying the LQR theory. In order to design an optimal switching function, the following quadratic minimization performance index is used

$$J = \frac{1}{2}\int_{ts}^{\infty} \mathbf{z}^T \mathbf{Q}\mathbf{z}\, dt \tag{5.20}$$

where $\mathbf{Q}$ is weight matrix and is both symmetric and positive definite. To transform the performance index into the one used in the standard LQR problem, where the control effort is inclined, the matrix $\mathbf{Q}$ from eq (5.20) is partitioned as

$$\mathbf{Q} = diag\begin{vmatrix} q_1 & q_2 & \dots & q_n \end{vmatrix} = \begin{bmatrix} \mathbf{Q}_{11} & \mathbf{q}_{12} \\ \mathbf{q}_{12} & q_{22} \end{bmatrix} \tag{5.21}$$

where $\mathbf{Q}_{11} \in \Re^{6\times 6}$, $\mathbf{q}_{12} \in \Re^{1\times 6}$ $(\mathbf{q}_{12} = \mathbf{q}_{21}^T)$ and $q_{22} \in \Re^1$. After some algebraic manipulations eq (5.20) is seen

$$J = \frac{1}{2}\int_{ts}^{\infty} (\mathbf{z}_N^T \hat{\mathbf{Q}}\mathbf{z}_N + q_{22}\mathbf{v}^2)dt \tag{5.22}$$

where

$$\hat{\mathbf{Q}} = \mathbf{Q}_{11} - q_{22}^{-1}\mathbf{q}_{12}\mathbf{q}_{12}^T \tag{5.23}$$

$$v = z_R + q_{22}^{-1}\mathbf{q}_{12}^T \mathbf{z}_N \tag{5.24}$$

To simplify the analysis, letting $\mathbf{Q}$ be diagonal, so that

$$\mathbf{Q}_{11} = \begin{bmatrix} q_{11} & 0 & 0 & 0 & 0 & 0 \\ 0 & q_{22} & 0 & 0 & 0 & 0 \\ 0 & 0 & q_{33} & 0 & 0 & 0 \\ 0 & 0 & 0 & q_{44} & 0 & 0 \\ 0 & 0 & 0 & 0 & q_{55} & 0 \\ 0 & 0 & 0 & 0 & 0 & q_{66} \end{bmatrix}, \ \mathbf{q}_{12} = 0 \tag{5.25}$$

Yielding, $\hat{\mathbf{Q}} = \mathbf{Q}_{11}$, $v = z_R$. Finally, the quadratic performance index is

$$J = \frac{1}{2}\int_{ts}^{\infty} (\mathbf{z}_N^T \mathbf{Q}_{11}\mathbf{z}_N + q_{22} z_R^2)dt \tag{5.26}$$

Using Riccati equation to give the optimal solution is obtained by

$$\mathbf{P}_N\overline{\mathbf{A}}_{N1}+\overline{\mathbf{A}}_{N1}^T\mathbf{P}_N-q_{22}^T\mathbf{P}_N\overline{\mathbf{a}}_{N2}\overline{\mathbf{a}}_{N2}^T\mathbf{P}_N+\mathbf{Q}_{11}=0 \tag{5.27}$$

where $\mathbf{P}$ is the unique positive definite and the following equation is obtained

$$z_R=-q_{22}^{-1}\mathbf{a}_{N2}^T\mathbf{P}_N\mathbf{z}_N \tag{5.28}$$

The optimal switching function vector can be given by

$$\mathbf{S}_N=q_{22}^{-1}\mathbf{a}_{N2}^T\mathbf{P}_N\mathbf{z}_N \tag{5.29}$$

5.2.4 Design of Virtual Linear State Feedback Control

As we mentioned above, the advantage of the optimal servo sliding mode form is that z_R can be thought of as virtual linear state feedback control for the Null space dynamics. Figure 5.2 shows the system block diagram of the virtual linear servo system.

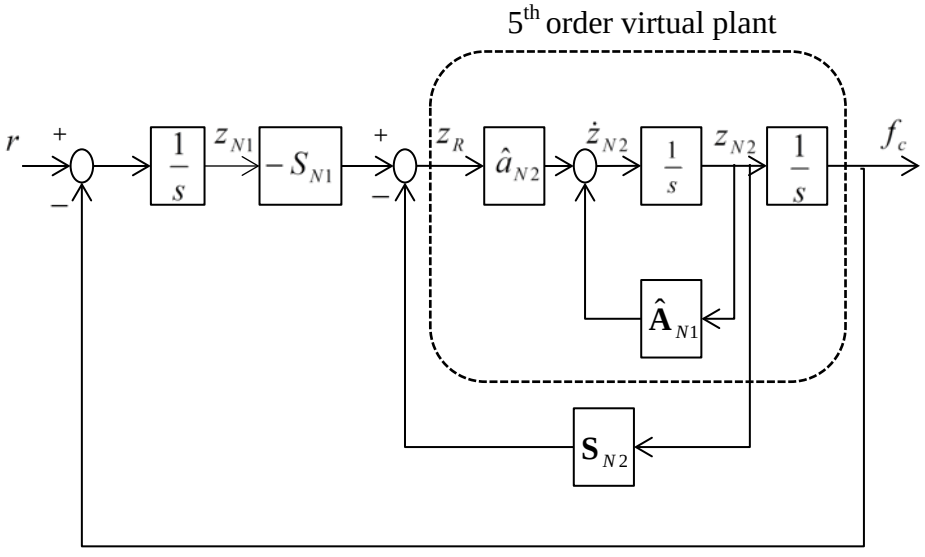

Fig 5.2 Virtual linear servo system equivalent to ideal sliding mode

In this research, therefore, we divide the Null space dynamics further into two subsystems. The state equation of the sliding mode dynamics eq (5.5) for Null space region is partitioned as

$$\mathbf{z}_N = \begin{bmatrix} z_{N1} \\ \mathbf{z}_{N2} \end{bmatrix} \tag{5.30}$$

The system state matrix is divided as

$$\overline{\mathrm{A}}_{N1} = \left[\begin{array}{ccccc|c} 0 & -\frac{k_t m_s - m_t k_s}{m_t + m_s} & -\frac{c_t m_s - m_t c_s}{m_t + m_s} & -\frac{m_t k_s}{m_t + m_s} & -\frac{m_t c_s}{m_t + m_s} & 0 \\ \hline 0 & 0 & 1 & 0 & 0 & 0 \\ 0 & -\frac{k_t + k_s}{m_t + m_s} & -\frac{c_t + c_s}{m_t + m_s} & -\frac{k_s}{m_t + m_s} & -\frac{c_s}{m_t + m_s} & 0 \\ 0 & 0 & 0 & 0 & 1 & 0 \\ 0 & \frac{k_s}{m_{f1}} & \frac{c_s}{m_{f1}} & -\frac{k_s + k_{f1}}{m_{f1}} & -\frac{c_s + c_{f1}}{m_{f1}} & \frac{k_{f1}}{m_{f1}} \\ 0 & 0 & 0 & 0 & 0 & 0 \end{array}\right]$$

where $\overline{\mathbf{A}}_{N1}$ is divided as,

$$\hat{\mathbf{A}}_{N1} = \begin{bmatrix} 0 & 0 & 1 & 0 & 0 \\ 0 & -\frac{k_t + k_s}{m_t + m_s} & -\frac{c_t + c_s}{m_t + m_s} & -\frac{c_s}{m_t + m_s} & 0 \\ 0 & 0 & 0 & 0 & 1 \\ 0 & \frac{k_s}{m_{f1}} & \frac{c_s}{m_{f1}} & -\frac{k_s + k_{f1}}{m_{f1}} & -\frac{c_s c_{f1}}{m_{f1}} \\ 0 & 0 & 0 & 0 & 0 \end{bmatrix},$$

$$\overline{\mathbf{a}}_{N2} = \begin{bmatrix} 0 \\ \hat{\mathbf{a}}_{N2} \end{bmatrix} \text{ where } \quad \hat{\mathbf{a}}_{N2} = \begin{bmatrix} 0 \\ 0 \\ 0 \\ -\frac{k_{f1}}{m_{f1}} \\ 0 \end{bmatrix}$$

The output equation is

$$\overline{c}_N = \begin{bmatrix} 0 & \frac{k_t m_s - m_t k_s}{m_t + m_s} & \frac{c_t m_s - m_t c_s}{m_t + m_s} & \frac{m_t k_s}{m_t + m_s} & \frac{m_t c_s}{m_t + m_s} & 0 \end{bmatrix} \tag{5.31}$$

$$\bar{\mathbf{c}}_N = \begin{bmatrix} 0 & \hat{\mathbf{c}}_N \end{bmatrix} \text{ where } \hat{\mathbf{c}}_N = \begin{bmatrix} \frac{k_t + m_s}{m_t + m_s} & \frac{c_t m_s + m_t c_s}{m_t + m_s} & \frac{m_t k_s}{m_t + m_s} & \frac{m_t c_s}{m_t + m_s} & 0 \end{bmatrix}$$

where $z_{N1} \in \Re^1$, $\mathbf{z}_{N2} \in \Re^{5\times1}$, $\hat{\mathbf{a}}_{N2} = \Re^{5\times1}$, $\hat{\mathbf{c}}_N = \Re^{1\times5}$ and $\hat{\mathbf{A}}_{N1} \in \Re^{5\times5}$. According to above calculation, the state vector of the virtual plant system is almost the same as the augmented state vector equation which described in eq (5.5) without disturbance/uncertainties . The virtual state matrix $\overline{\mathbf{A}}_{N1}$ can be defined as

$$\overline{A}_{N1} = \begin{bmatrix} 0 & -\hat{\mathbf{c}}_N \\ 0 & \overline{\mathbf{A}}_{N1} \end{bmatrix} \tag{5.32}$$

The switching function is also partitioned as

$$\mathbf{S}_N = \begin{bmatrix} S_{N1} & \mathbf{S}_{N2} \end{bmatrix} \tag{5.33}$$

where $S_{N1} \in \Re^1, \mathbf{S}_{N2} \in \Re^{1\times5}$. Where we use $\hat{\mathbf{c}}_N$ in $\overline{\mathbf{A}}_{N1}$ noting that the first row in $\overline{\mathbf{A}}$ given in eq (5.5) originally contains the coefficient of the output in eq (5.6). Using these matrices and assuming $\xi_t = 0$ to get a nominal model for controller design. And then, equation (5.14) is rewritten as

$$\begin{aligned} \dot{z}_{N1} &= r - \hat{\mathbf{c}}_N \\ \mathbf{z}_{N2} &= r - f_c \end{aligned} \tag{5.34}$$

$$\dot{\mathbf{z}}_{N2} = \hat{\mathbf{A}}_{N1}\mathbf{z}_{N2} + \hat{\mathbf{a}}_{N2} z_R \tag{5.35}$$

where we use the fact that

$$\begin{aligned} f_c &= \mathbf{cx} = \bar{\mathbf{c}}_N \mathbf{z}_N \\ &= \begin{bmatrix} 0 & \hat{\mathbf{c}}_N \end{bmatrix} \begin{bmatrix} z_{N1} \\ \mathbf{z}_{N2} \end{bmatrix} = \hat{\mathbf{c}}_N \mathbf{z}_{N2} \end{aligned} \tag{5.36}$$

which is easily derived from eq (5.16) under the assumption $\xi_t = 0$. In a similar way the virtual control eq (5.18) can be rewritten as

$$\begin{aligned} z_R &= -\mathbf{S}_N \mathbf{z}_N \\ &= -S_{N1} z_{N1} - \mathbf{S}_{N2} \mathbf{z}_{N2} \\ &= -S_{N1} \int (r - f_c) d\tau - \mathbf{S}_{N2} \mathbf{z}_{N2} \end{aligned} \tag{5.37}$$

Equation (5.34) and (5.37) are represented by the block diagram of the virtual linear servo system which shown in fig (5.2), from which it turns out that the coefficient of the switching function can be though of as a feedback gain vector for the virtual plant eq (5.35) with an integral compensator by eq (5.34) and eq (5.37).

5.2.5 Design of an Optimal Switching function for the virtual plant

In order to determine an optimal switching function for the virtual plant, we apply the design method of optimal linear tracking systems proposed by Takeda and Kitamori. There are two features in their approach. One of them is to use the control input instead of the output of the integral compensator as a state variable, i.e. z_R instead of z_{N1} in the equivalent system shown in fig (5.2). Another one is use to a deviation system from the steady state under the assumption the reference signal is a step function or constant. As a result, the tracking error, $r - f_c$, can be thought of as the system output, and it can be weighted in the quadratic performance function as below.

Recall the virtual linear equation to be controlled;

$$\dot{z}_{N1} = r - \hat{\mathbf{c}}_N \,, \mathbf{z}_{N2} = r - f_c$$

$$z_R = -S_{N1} \int (r - f_c) d\tau - \mathbf{S}_{N2} \mathbf{z}_{N2}$$

In order to formulate the tracking problem to LQR, the state vector of the virtual linear servo system is defined as $\begin{bmatrix} \mathbf{z}_{N2} & z_R \end{bmatrix}$. Using the above equation, we can derive the deviation system from the steady state for the virtual linear servo system as follows;

$$\begin{bmatrix} \dot{\mathbf{z}}_{N2} \\ \dot{z}_R \end{bmatrix} = \begin{bmatrix} \mathbf{I} & \mathbf{0} \\ -\mathbf{S}_{N2} & S_{N1} \end{bmatrix} \begin{bmatrix} \hat{\mathbf{A}}_{N1} & \hat{\mathbf{a}}_{N2} \\ \hat{\mathbf{c}}_N & 0 \end{bmatrix} \begin{bmatrix} \mathbf{z}_{N2} \\ z_R \end{bmatrix} + \begin{bmatrix} \mathbf{0} \\ S_{N1} \end{bmatrix} z_R \tag{5.38}$$

$$f_c = \begin{bmatrix} \hat{\mathbf{c}}_N & 0 \end{bmatrix} \begin{bmatrix} \mathbf{z}_{N2} \\ z_R \end{bmatrix} \tag{5.39}$$

Assuming the both reference signal and the disturbance are constant in the steady state, the equilibrium point can be obtained as follows:

$$\begin{bmatrix} 0 \\ 0 \end{bmatrix} = \begin{bmatrix} \mathbf{I} & \mathbf{0} \\ -\mathbf{S}_{N2} & S_{N1} \end{bmatrix} \begin{bmatrix} \hat{\mathbf{A}}_{N1} & \hat{\mathbf{a}}_{N2} \\ \hat{\mathbf{c}}_N & 0 \end{bmatrix} \begin{bmatrix} \mathbf{z}_{N2}(\infty) \\ z_R(\infty) \end{bmatrix} + \begin{bmatrix} \mathbf{0} \\ S_{N1} \end{bmatrix} z_R$$

$$\begin{aligned} \begin{bmatrix} \mathbf{z}_{N2}(\infty) \\ z_R(\infty) \end{bmatrix} &= -\begin{bmatrix} \hat{\mathbf{A}}_{N1} & \hat{\mathbf{a}}_{N2} \\ \hat{\mathbf{c}}_N & 0 \end{bmatrix} \begin{bmatrix} \mathbf{I} & \mathbf{0} \\ -\mathbf{S}_{N2} & S_{N1} \end{bmatrix}^{-1} \left\{ \begin{bmatrix} \mathbf{0} \\ S_{N1} \end{bmatrix} z_R \right\} \\ &= \begin{bmatrix} \hat{\mathbf{A}}_{N1} & \hat{\mathbf{a}}_{N2} \\ \hat{\mathbf{c}}_N & 0 \end{bmatrix} \begin{bmatrix} \mathbf{0} \\ 1 \end{bmatrix} z_R \end{aligned} \tag{5.40}$$

$$f_c(\infty) = \begin{bmatrix} \hat{\mathbf{c}}_N & 0 \end{bmatrix} \begin{bmatrix} \mathbf{z}_{N2}(\infty) \\ z_R(\infty) \end{bmatrix} \tag{5.41}$$

Define the new state and output for the tracking problem, which are perturbations from the equilibrium.

$$\begin{aligned} \mathbf{z}_{N2e} &= \mathbf{z}_{N2} - \mathbf{z}_{N2}(\infty) \\ \mathrm{z}_{\mathrm{Re}} &= z_R - z_R(\infty) \end{aligned} \tag{5.42}$$

Defining $\mathbf{z}_{N2e}$ and z_{Re} as the deviation of the state and the control, respectively, and taking $\mathbf{z}_{N2w} = \begin{bmatrix} \mathbf{z}_{N2e} & z_{\mathrm{Re}} \end{bmatrix}^T$ as the augmented state vector. The augmented deviation system can be represented by

$$\begin{bmatrix} \dot{\mathbf{z}}_{N2e} \\ \dot{z}_{\mathrm{Re}} \end{bmatrix} = \begin{bmatrix} \dot{\mathbf{z}}_{N2} \\ \dot{z}_{R} \end{bmatrix} = \begin{bmatrix} \mathbf{I} & \mathbf{0} \\ -\mathbf{S}_{N2} & S_{N1} \end{bmatrix} \begin{bmatrix} \hat{\mathbf{A}}_{N1} & \hat{\mathbf{a}}_{N2} \\ \hat{\mathbf{c}}_{N} & 0 \end{bmatrix} \begin{bmatrix} \mathbf{z}_{N2e} \\ z_{\mathrm{Re}} \end{bmatrix} + \begin{bmatrix} \mathbf{0} \\ S_{N1} \end{bmatrix} z_{R}$$

$$= \begin{bmatrix} \hat{\mathbf{A}}_{N1} & \hat{\mathbf{a}}_{\mathrm{N2}} \\ \mathbf{0} & 0 \end{bmatrix} \begin{bmatrix} \mathbf{z}_{N2e} \\ z_{\mathrm{Re}} \end{bmatrix} - \begin{bmatrix} \mathbf{0} \\ 1 \end{bmatrix} \omega \tag{5.43}$$

where,

$$\omega = \dot{z}_{\mathrm{Re}} = -\mathbf{f}_{\mathbf{e}} \begin{bmatrix} \mathbf{z}_{N2e} \\ z_{\mathrm{Re}} \end{bmatrix} \tag{5.44}$$

Define the matrix $\mathbf{f}_{\mathbf{e}}$ as;

$$\mathbf{f}_{\mathbf{e}} = \begin{bmatrix} \mathbf{S}_{N2} & -S_{N1} \end{bmatrix} \begin{bmatrix} \hat{\mathbf{A}}_{N1} & \hat{\mathbf{a}}_{N2} \\ \hat{\mathbf{c}}_{N} & 0 \end{bmatrix} \tag{5.45}$$

The tracking error is defined as;

$$e = r - f_{c} = \begin{bmatrix} \hat{\mathbf{c}}_{N} & 0 \end{bmatrix} \begin{bmatrix} \mathbf{z}_{N2e} \\ z_{\mathrm{Re}} \end{bmatrix} \tag{5.46}$$

Equation (5.43) can be though of as a plant to be controlled with the control input ω which is linear state feedback eq (5.44) and eq (5.46) can be thought of as the output equation. Because the feedback gain $\mathbf{f}_{\mathbf{e}}$ includes the coefficient vector of the switching function in eq (5.45), it is given by

$$\begin{bmatrix} \mathbf{S}_{N2} & -S_{N1} \end{bmatrix} = \begin{bmatrix} \hat{\mathbf{A}}_{N1} & \hat{\mathbf{a}}_{N2} \\ \hat{\mathbf{c}}_{N} & 0 \end{bmatrix}^{-1} \mathbf{f}_{\mathbf{e}} \tag{5.47}$$

once $\mathbf{f}_{\mathbf{e}}$ is obtained. The matrix on the right-hand side in eq (5.47) is non-singular because the virtual plants eq (5.35), eq (5.36) does not have any zeros at the origin as the original plant eq (5.1), eq (5.2). Finally, applying the LQR technique with the performance index

$$J = \int_0^\infty \left\{ e^T q e + \omega^2 \right\} dt$$

$$= \int_0^\infty \left\{ \begin{bmatrix} \mathbf{z}_{N2e}^T & z_{\mathrm{Re}}^T \end{bmatrix} \begin{bmatrix} \hat{\mathbf{c}}_N^T \mathbf{q} \hat{\mathbf{c}}_N & \mathbf{0} \\ \mathbf{0} & 0 \end{bmatrix} \begin{bmatrix} \mathbf{z}_{N2e} \\ z_{\mathrm{Re}} \end{bmatrix} + \omega^2 \right\} dt \tag{5.48}$$

The optimal feedback gain $\mathbf{f_e}$ is obtained by solving the standard Riccati equation.

$$\mathbf{P}_N \hat{\mathbf{A}}_{N1} + \hat{\mathbf{A}}_{N1}^T \mathbf{P}_N - \omega \mathbf{P}_N \hat{\mathbf{a}}_{N2} \hat{\mathbf{a}}_{N2}^T \mathbf{P}_N + q = 0 \tag{5.49}$$

It should be noted here that the tracking error is directly weighted by q, and the virtual control input is $\omega = \dot{z}_{\mathrm{Re}} = \ddot{x}_{f2}$. That is, the optimal control obtained under the performance index achieves the trade-off between the tracking error and the acceleration of the lower frame. However, evaluating the acceleration of the lower frame means to penalize the use of control effort implicitly, because the equation of motion eq (2.8) which described in chapter (2), implies that it is highly depend on the control force f_a.

5.3 Analysis of the Optimal Servo System

In this section, we will apply the SRL (Symmetric Root Locus) method, which gives the locus of the optimal poles with respect to the parameter q under the performance index eq (5.48), to analyze the optimal servo system designed in the previous subsection. The optimal poles are the stable roots in the left half plane of the SRL equation,

$$1+\rho G_N(-s)G_N(s)=0 \tag{5.50}$$

where $G_N(s)$ is the transfer function of the virtual control input ω to the tracking error e,

$$G_N(s)=\begin{bmatrix}\hat{\mathbf{c}}_N & 0\end{bmatrix}\left(\mathbf{SI}-\begin{bmatrix}\hat{\mathbf{A}}_{N1} & \hat{\mathbf{a}}_{N2}\\ \mathbf{0} & 0\end{bmatrix}\right)\begin{bmatrix}\mathbf{0}\\ 1\end{bmatrix} \tag{5.51}$$

$$G_N(s)=\frac{1.88\times10^5 s^3+1.19\times10^8 s^2+1.21\times10^8 s+1.31\times10^9}{s^5+11.57s^4+99.29\times10^2 s^3+1.13\times10^4 s^2+1.29\times10^6 s}$$

The symmetric root locus is obtained for $q=10^{-2}\sim10^5$ is shown in fig (5.3), where a portion around the origin in the left figure is zoomed in the right figure.

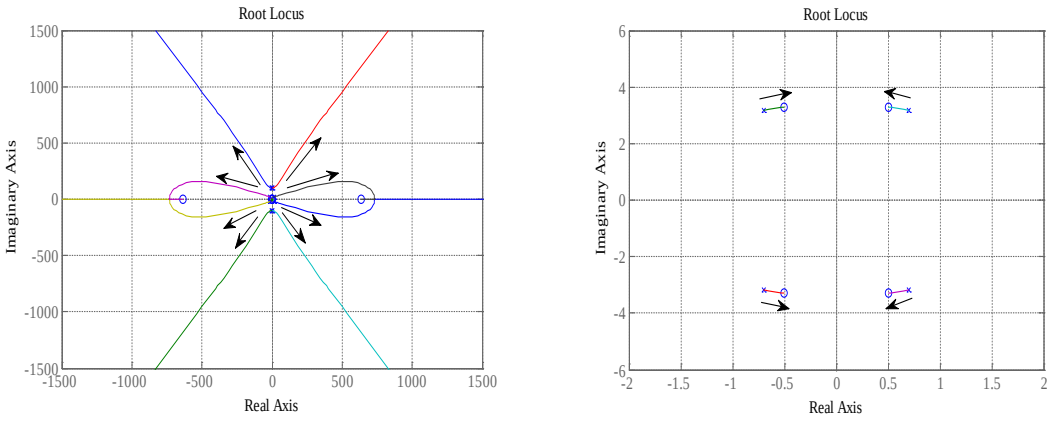

(a) Overall (b) around the origin

Fig 5.3 Root locus of optimal sliding mode poles

As shown in this figure, the stable roots converge to the zeros of $G_N(s)$ as ρ increases, which is the same property as normal roots. In this research, the weighting factor is set to $W = 10^7$, the poles and zeros in the transfer function from the reference signal to the contact force are obtained as follows:

$$\text{Poles} = \begin{bmatrix} -633.33 & -0.5 \pm 3.28i \end{bmatrix}$$

$$\text{zeros} = \begin{bmatrix} 0 & -5.28 \pm 98.78i & -0.5 \pm 11.49i \end{bmatrix}$$

Noting that these zeros are identical to those of the virtual plant in fig (5.2), they must satisfy the determinant equation with respect to s

$$\begin{vmatrix} \hat{\mathbf{A}}_{N1} - s\mathbf{I} & \hat{\mathbf{a}}_{N2} \\ \hat{\mathbf{c}}_N & 0 \end{vmatrix} = 0 \tag{5.52}$$

On the other hand, the determinant equation for the zeros of the original plant eq (2.18) which described in chapter (2) can be written by expending the determinant with respect to the last column as

$$\begin{aligned} \begin{vmatrix} A - sI & b \\ c & 0 \end{vmatrix} &= \begin{vmatrix} -s & 1 & 0 & 0 & 0 & 0 & 0 \\ a_{12} & a_{22} - s & a_{23} & a_{24} & 0 & 0 & 0 \\ 0 & 0 & -s & 1 & 0 & 0 & 0 \\ a_{41} & a_{42} & a_{43} & a_{44} - s & a_{45} & a_{46} & 0 \\ 0 & 0 & 0 & 0 & -s & 1 & 0 \\ 0 & 0 & a_{63} & a_{64} & a_{65} & a_{66} - s & b_6 \\ c_1 & c_2 & c_3 & c_4 & 0 & 0 & 0 \end{vmatrix} \\ &= b_6 \begin{vmatrix} \hat{\mathbf{A}}_{N1} - s\mathbf{I} & \hat{\mathbf{a}}_{N2} \\ \hat{\mathbf{c}}_N & 0 \end{vmatrix} = 0 \end{aligned} \tag{5.53}$$

where a_{ij} is an element of $\mathbf{A}$, b_i is an element of $\mathbf{b}$, and c_i is an element of $\mathbf{c}$. It can be seen from eqs (5.52), (5.53) that the optimal poles converge to the zeros of

the original plant eq (2.19) which described in chapter (2). As mentioned below eq (2.19), the complex zeros near the origin are identical to the poles of the nominal catenary system eq (2.11). The asymptotic property reveals that two optimal poles converge to the catenary poles as ρ increases so that pole-zeros cancellation are approximately brought about. This analytical result is very sound from a physical point of view, because the pantograph should follow the catenary motion to reduce the contact force variation.

5.4 Simulation results

In this section, the numerical analysis of the optimal servo system based sliding mode controller is performed. The transfer from the reference input r to the contact force f_c is

$$G_{ry}(s) = \frac{1.88\times10^5 s^3 + 1.18\times10^8 s^2 + 1.21\times10^8 s + 1.31\times10^9}{s^6 + 211.9s^5 + 3.23\times10^4 s^4 + 2.80\times10^6 s^3 + 1.22\times10^8 s^2 + 1.49\times10^8 s + 1.31\times10^9}$$

In order to investigate the performance of the proposed controller, numerical simulation has been carried out. The parameter values of the pantograph-catenary system are shown in Table 1, where the parameter values of the pantograph are the estimates by identification experiments, and those of the catenary system are determined based on some references, e.g. Kobayashi et al. [13]. The designed parameters in the in the controller is as follows:

$\text{weighting factor}: \ q = 1$
$\text{switching function}: \ S = \begin{bmatrix} -1 & -385.068 & -7.143 & 185.998 & 6.262 & 200.286 & 1 \end{bmatrix}$
$\text{relay gain}: \ \rho = 100$
$\text{boundary layer}: \ \pm 0.05$

With these parameters, the poles and zeros in the transfer function from the reference signal to the contact force are obtained as follows:

$$\text{zeros} = \begin{bmatrix} -633.33 & -0.5 \pm 3.28\text{i} \end{bmatrix}$$

$$\text{poles} = \begin{bmatrix} -29.89 \pm 119.69i & -75.54 \pm 46.09i & -0.5 \pm 3.28i \end{bmatrix}$$

It should be noted that a pair of poles approximately cancel out a pair of zeros at $-0.5 \pm 3.28i$ which is the mode of the catenary subsystem given by eq (2.19) from chapter 2. Therefore, a perfect output zeroing can be achieved by exact pole-zero cancellations which make an unobservable subspace in the state space of the control system. From a physical point of view, in addition, these closed-loop will make it possible that the pantograph head is following the catenary wire motion not to prevent its free motion, yielding a good regulation of the contact force.

Because the proposed controller achieved a good performance as expected for the simulation result, we carried out some simulations in more realistic situation. That is, although we neglected the actuator dynamics when designing the controller and observer, we inserted the following dynamic model of the pneumatic actuator

$$G(s) = \frac{1}{0.013s + 1} e^{-0.002s} \tag{5.54}$$

which had been obtained by some experiments. Furthermore, it was assumed that three measurements for the controller and observer were corrupted by white Gaussian noises whose maximum magnitude and some important parameters are as shown below:

Contact force: $\pm 4N$
Catenary equivalent stiffness: 2Hz
Displacement of the lower frame: $\pm 1 \times 10^{-4} m$
Velocity of the contact wire/shoe head: $\pm 1 \times 10^{-4} m/s$
Nominal value of stiffness fluctuation: $k_t = 1100 N/m$

The design parameters in the controller and observer were determined taking account of the above situation. Figure (5.4) shows the switching function, σ, in the controller and observer in steady state. It can be seen from fig (5.4, a) that the switching function in the controller stays within the small boundary layer, which can prove that quasi-sliding mode takes place in spite of the existence of the actuator dynamics eq (5.54). It can be seen from fig (5.4, b) that the estimation errors, $\mathbf{e}_y$,

which is the switching function vector as well, contains high frequency components due to the sensor noise but quite small, yielding the sliding mode.

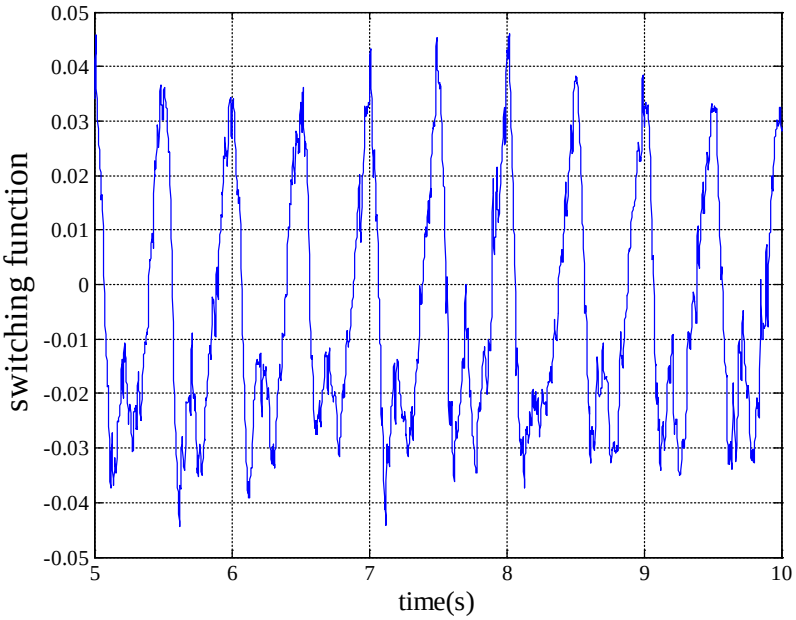

Fig 5.4 (a) Switching function in steady state: In controller

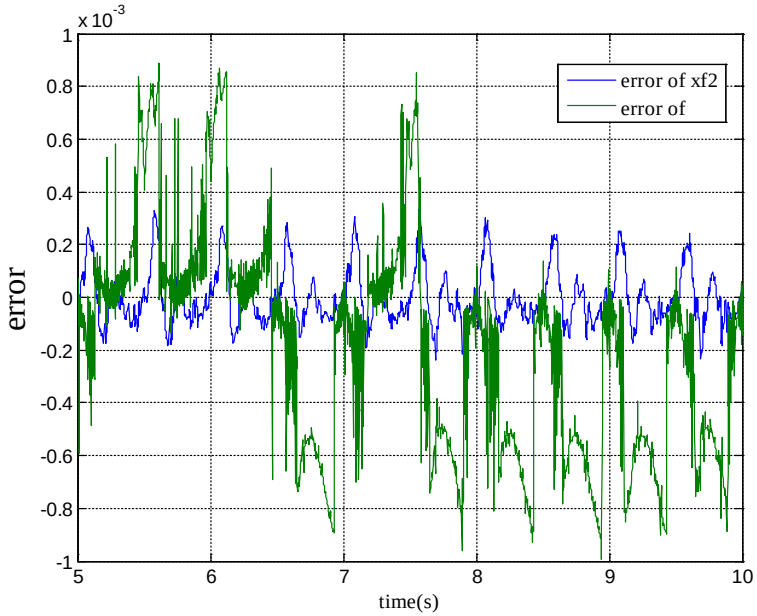

Fig 5.4 (b) Switching function in steady state : In observer

Figure (5.5) shows the simulation result of the steady state response. As shown in fig (5.5, a), two control inputs, one is with the actuator and the other is without actuator, are almost the same, which means that the controller demands appropriate

control force for the actuator dynamics. Consequently, as shown in figs (5.5, b) and (5.5, c), the active pantograph regulates the contact force much better than the passive case, where the static uplift force is provided, by keeping the variation of the catenary displacement very small with the highly accurate estimates by the observer.

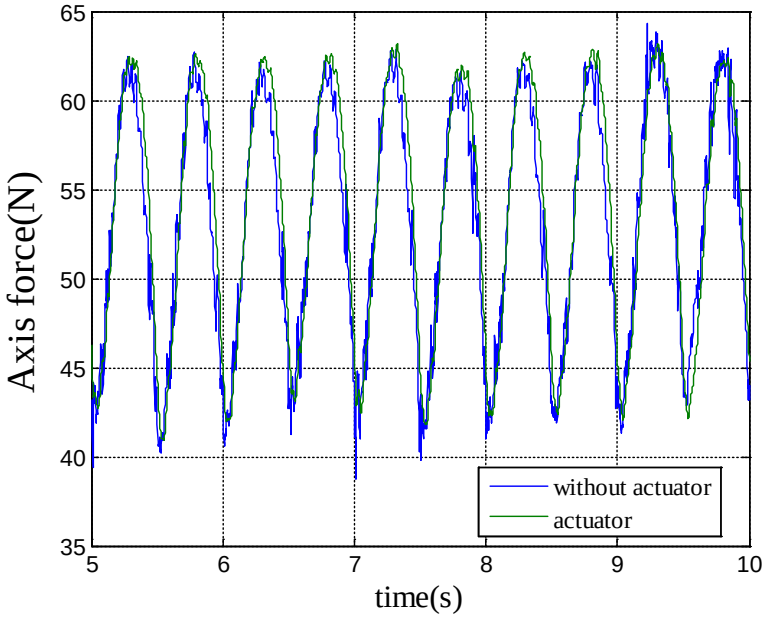

Fig 5.5 (a) Steady state response: For control input

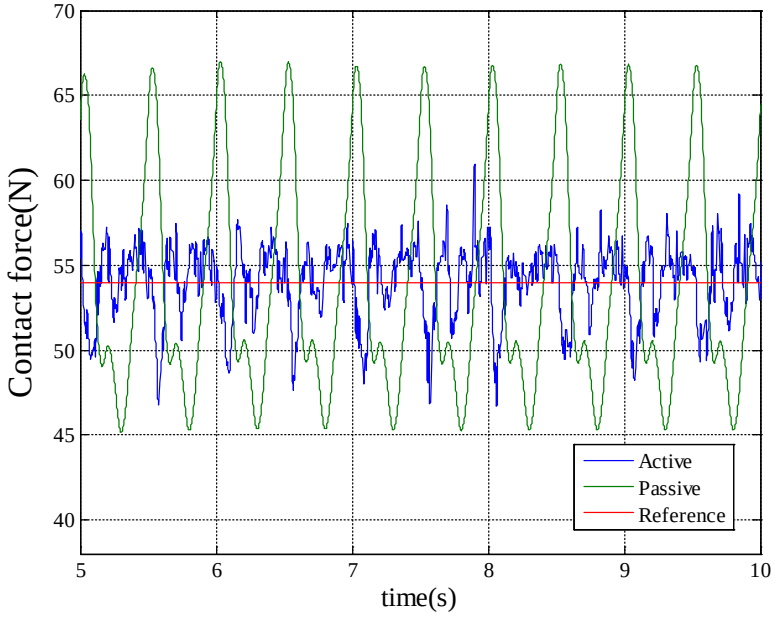

Fig 5.5 (b) steady state response: For contact force

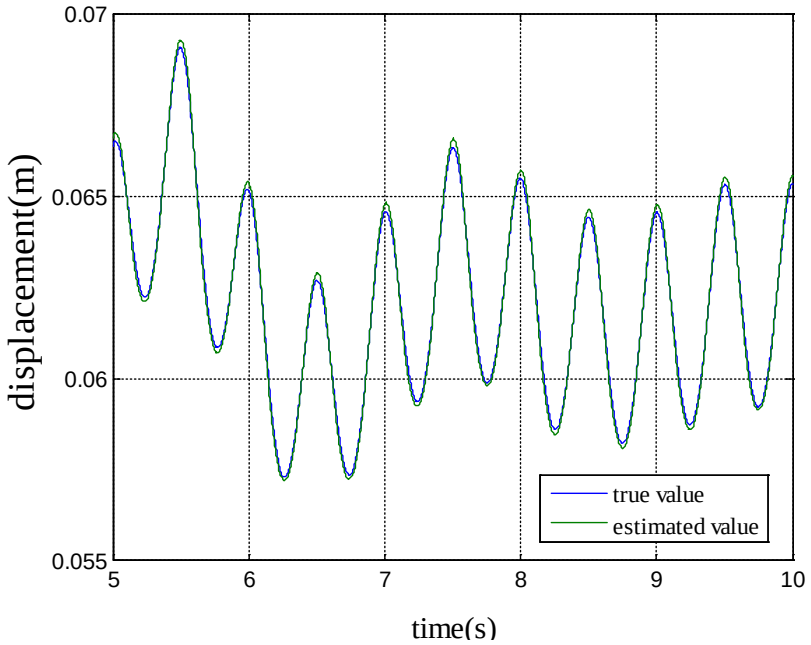

Fig 5.5 (c) Steady state response: for catenary displacement

Figure (5.6) shows the step response of the catenary displacement and contact force, from which it can be seen that the transient response is also good with small rise time and no overshoot expect for that due to the steady variation.

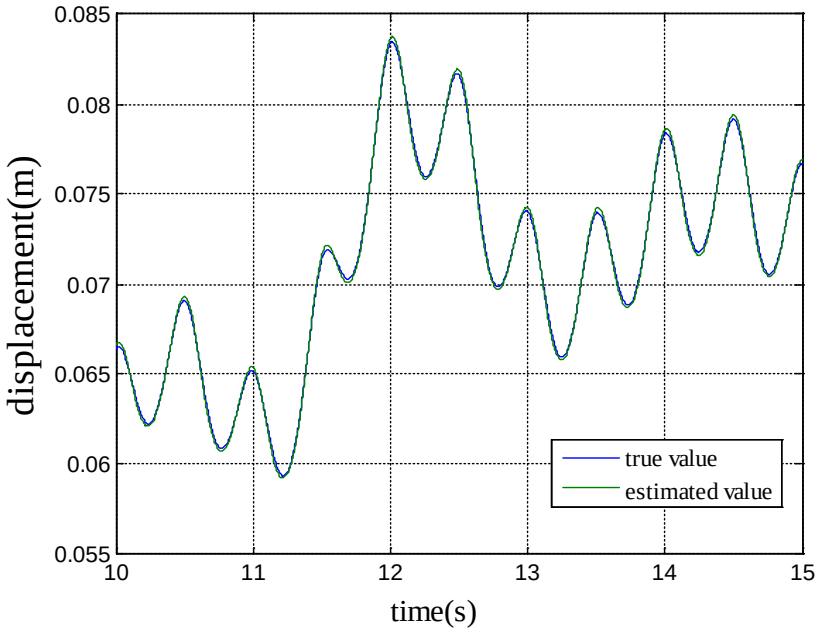

Fig 5.6 (a) Step response: For catenary displacement

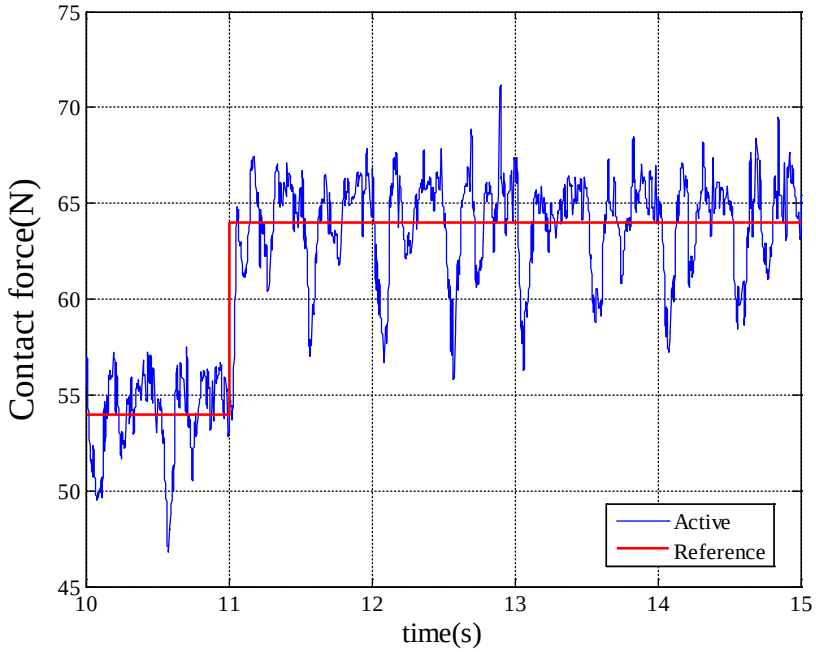

Fig 5.6 (b) Step response: For contact force

5.5 Conclusion

In this chapter, we proposed a sliding mode controller using optimal servo control theory and sliding mode observer, taking account of the flexibility of the articulated frame in the actual pantograph. It has been pointed out through our analysis of the plant and the closed-loop system using SRL (symmetric root locus) technique that pole-zero cancellations play an important role to control the contact force. A physical interpretation of the pole-zero cancellations is that the pantograph head should follow the catenary motion to reduce the variation of the contact force. The simulation results has confined the good performance and robustness of the proposed control system in the presence of variation of the catenary stiffness.

Although the measurements for the observer which described in section (3.6) of chapter(3), were assumed to be the velocity of the contact-wire/shoe and the displacement of the lower frame, other choices should be investigated taking more practical situations such as noise level into account. Much more rigorous analysis of the closed-loop stability dealing the plant as a time-varying system which described in section (4.4) of chapter (4) is still under investigation.

Chapter 6

Conclusion

6.1 Summary of Study

The main objective of this thesis is to investigate the robust contact force of an active pantograph for high speed trains. The work includes the studies on the structures and the dynamics behavior of the active pantograph-catenary system. Three different control strategies have proposed, taking account of the flexibility of the articulated frame in the actual pantograph. Firstly, the development of the contact force control of an active pantograph using a linear state feedback controller together with the sliding mode observer has been considered and secondly, the development of an active pantograph using sliding mode controller together with the sliding mode observer has been improved where the disturbances and uncertainties were neglected. Finally, the development of a robust contact force control of an active pantograph using optimal servo system based sliding mode controller together with the sliding mode observer has been developed. It has been pointed out through our analysis that the pole-zero cancellations play an important role to control the contact force.

In chapter 2, the construction of mathematical model of the pantograph head and the catenary system is described. An active pantograph using pneumatic actuator is developed in this chapter, which is considered for the entire thesis. It is very important to control the contact force between the pantograph head and the overhead contact wire because the active pantograph system for the high speed train in this research is considered as moving state. After that, however, it was found through some experiments that the frame had flexibility which could not be ignored to control the contact force. The stiffness of the overhead contact wire in catenary system is a main

source of the variation of the pantograph. Hence, the fluctuation of the equivalent stiffness between the pantograph head and the overhead contact wire, make it happen a problem to control the contact state of the system. The important measurements which are used in this thesis is also described. The problem formulation of the pantograph-catenary system is proposed.

Chapter 3 has mainly discussed the design of a linear state feedback controller together with the sliding mode observer. The main objective of this controller design is that the active pantograph can resist the disturbances/ uncertainties using optimal force, which is derived from the feedback state and can achieved the best theoretical performance. The theoretical background for both controller and observer are discussed with the figures. LQR (linear quadratic regulator) technique has been successively applied to the linear servo system. The problem of designing the sliding mode observer using VSS (variable structure control system) is considered. It has been emphasized that one of the key points to regulate the contact force is pole-zero cancellation in the nominal model without perturbation. Finally, the simulation results of the controller and observer, which is described with good performance results.

Chapter 4 has discussed two different sections: the sliding mode controller design and the stability of the system. Firstly, a sliding mode controller together with the sliding mode observer is proposed, taking account of the flexibility of the articulated frame in the actual pantograph. An introduction to the variable structure control system with sliding mode control is described. The reduce order sliding dynamics is formulated. It is also discussed the use of boundary layer design to avoid the chattering effects. The proposed controller achieves the robust output (contact force) by pole-zero cancellation during sliding mode. A physical interpretation of this pole-zero cancellation is also given, that is, the pantograph head follow the catenary mode without preventing its free motion. Then, the robust stability approach for the active pantographs system is analyzed. Lyapunov theory for stability analysis is used. One sufficient condition for asymptotic stability has been derived but still need other methods to prove more practical stability.

Chapter 5 has proposed a sliding mode controller using optimal servo control theory and sliding mode observer. The design of the controller in which switching function is mainly discussed, optimal linear gain and virtual plant system are included. LQR (linear quadratic regulator) technique has been successively applied to not only linear servo systems but also sliding mode control systems. The main advantages of

this optimal sliding mode servo control is that they can provide a more robust optimal control to the system. The function of an optimal sliding mode control system is as follows: if the control system is dominated in the region of nominal part, the system behavior is mainly governed by optimal control. If the control system is dominated in the region of perturbations, sliding mode control will take over the main control task. A physical interpretation of this pole-zero cancellation is also given, that is, the pantograph head can follow the catenary motion not to prevent its free motion by assigning some of the closed loop poles on the catenary mode. The simulation results has confined the good performance and robustness of the proposed control system in the presence of variation of the catenary stiffness.

6.2 Future Work

There are some subjects to investigate in the future as follows:

1. To make sure of the effectiveness of the proposed controllers with some experimental setup such as HILS.
2. To choose more appropriate measurements (output variables) for the observer taking practical situations such as noise level into account.
3. To analyze the closed-loop stability much more rigorously dealing the plant as a time-varying system.

References

(1) https://en.wikipedia.org/wiki/Railway_electrification_system

(2) https://en.wikipedia.org/wiki/Pantograph_(transport)

(3) https://en.wikipedia.org/wiki/current_corrector

(4) Arnold, M. and Simeon, B., Pantograph and catenary dynamics, A benchmark problem and it's numerical solution, Applied Numerical Mathematics, 34, pp.345-362, 2000

(5) Makino, T., Yoshida, K., Seto, S. and Makino, K., Running test on current collector with contact force controller for high-speed railways, JSME International Journal Series, Vol. C 40, No. 4 (1997), pp. 671-80.

(6) Yamashita, Y., Ikeda, M., Masuda, A., Iba, D. and Sone, A., Advanced active control of a contact between a pantograph and a catenary for a high speed train, Proc. Of 9th world congress of railway research (2011).

(7) Chater, E., Ghani, D., Giri, F., Rachid, A., Chaoui, F.Z. and Haloua, m., Output feedback control of pantograph-catenary system 5th IFAC International Workshop on Periodic Control Systems, Vol. 5, No. 1 (2013), pp.131-36.

(8) Allotta, B., Pisano, A., Pugi, L. and Usai, E., VSC of a servo-actuated ATR 90-type pantograph, Proc. Of the 44th IEEE Conference on Decision and Control, and the European Control Conference (2005), pp.590-95.

(9) Pisano, A. and Usai, E., Contact force regulation in wire-actuated pantographs via variable structure control and frequency-domain techniques, International Journal of Control, 1st series, Vol. 81, No. 11 (2008), pp.1747-62.

(10) Pisano, A. and Usai, E., Output-feedback regulation of the contact-force in high-speed train pantographs, Transactions of the ASME, Vol. 126, March (2004), pp.82-7.

(11) Sanchez-Rebolloa, C., jimenez-Octaviob, J.R. and Carnicerob, A., Active control strategy on a catenary-pantograph validated model vehicle system dynamics, Vol. 51, No.4 (2013), pp.554-69.

(12) Kiessling, F., Puschmann, R., Schmieder, A. and Schmieder, E, Contact lines for electric railways, (2001) 5.

(13) Edwards, C. and Spurgeon, S., Sliding mode control-Theory and applications (1998), Taylor and Francis.

(14) Franklin, G.F., Powell, J.D. and Emami-Naeini, A., Feedback Control of Dynamics Systems (2010), pp.475-483 Pearson.

(15) Utkin, V.I., Variable structure systems with sliding mode, IEEE Transactions on Automatic control, Vol. 22, No. 2 (1977), pp.212-222.

(16) Raymond, A.D., Stanislaw H.Z. and Gregory, M., Variable Structure Control of Nonlinear Multivariable Systems: A Tutorial., Proceedings of the IEEE, Vol. 76, No. 3 (1988).

(17) Utkin, V.I., Sliding modes in control optimization. Springer-Verlag, Berlin (1992).

(18) Hung, J.Y., Gao, W. and Hung, J.C., Variable Structure Control: A survey, IEEE Transactions on Nonlinear Industrial Electronics, Vol. 40, No 1 (1993).

(19) Edwards, C. and Spurgeon, S., Sliding mode stabilization of uncertain systems using only output information, International journal of control, 62: 1129-1144 (1995).

(20) Kobayashi, S., Usuda, T. and Ikeda, M., Applications of HILS technique to pantograph-catenary system, RTRI Report, Vol. 28, No. 12 (2014), pp.5-10.

(21) Usuda, T. and Ikeda, M., Estimation method of static height of contact wire using pantograph contact force RTRI Report, Vol. 28, No. 12 (2014), pp.35-40.

(22) Patel, R., V. and Toda, M., Quantitative measures of robustness for multivariable systems, Proc. Of ACC, (1980), pp. TP8-Aning of a sentence, e.g.

(23) Shtessel, Y., Edwards, C., Fridman, L. and Levant, A., Sliding mode control and observation (2014), New York: Birkhauser.

(24) Yokoyama, M., Yokoyama, S., Sakakibara, H., Kobayashi, S., Usuda, T. and Ikeda, M., Modeling and robust control of a high speed train pantograph, Bulletin of the JSME Mechanical Eng. J., Vol. 23, No. 3 (2015), 15-00041.

(25) Myat Thiri Ko, Yokoyama, M., Yamashita, Y., Kobayashi, S. and Usuda, T., Contact force control of an active pantograph for high speed trains, Proc. of Movic/RASD (2016a).

(26) Myat Thiri Ko, Yokoyama, M. and Nagayoshi, S., Robust contact force control of an active pantograph via sliding mode controller and sliding mode observer, Proc. of SII (2016b).

(27) Myat Thiri Ko, Yokoyama, M. and Nagayoshi, S., Stability analysis of the active pantograph with sliding mode controller and sliding mode observer, Proc. of ICSE (2016c).

(30) Perruquetti, W. and Barbot, J.P. (eds), Sliding Modes in Automatic Control, Marcel Dekker, New York (2001).

(31) Utkin, V., Gulder, J. and Shi, J., Sliding Mode Control in Electromechanical Systems, Taylor & Francis, Abington (1999).

(32) Pisano, A. and Usai, E., Output-feedback regulation of the contact force in High-speed train pantograph. Dynamic Systems, Measurement and control, 126: 82-87 (2004).

(33) Utkin, V., Guldner, J. and Shi, J., Sliding Mode Control in Electro-Mechanical Systems. Automation and control engineering, CRC press (2009).

(34) Takeda, T. and kitamori, T., A design method of linear multi-input-output optimal tracking systems, Transactions of the society of Instrument and control engineers, Vol. 14, No. 4 (1977), pp.359-364.

(35) Ambrosio, J., pombo, J., Pereia, m., Antunes, P. and Mosca, A., Recent developments pantograph-catenary interaction modelling and analysis, International journal of railway technology, 1(1), pp. 249-278, (2012).

(36) Zhai, WM. And Cai, CB., Effect of locomotive vibrations on pantograph catenary system dynamics, Journal of vehicle system dynamics, 28, pp. 47-58, (1998).

(37) Collina, A., Facchinetti, A., Fossati, F. and Resta, F., An application of active control to the collector of High-speed pantograph: Simulation and Laboratory tests, Proc. Of 2001 IEEE/ ASME International conference, 1:243-248, 2005.

(38) Wu, TX. and Brennan, MJ., Active vibration control of railway pantograph, Journal of Rail and Rapid transit, 211, 117-130, 1997.

(39) Tieri, R., Collina, A., Carnevale, M., Stichel, S. and Jonsson, PA., Pneumatic active control system for pantograph-catenary interaction, 10th World congress on railway research, Sidney, 25-28, 2013.

(40) Cho, YH., Lee, K., Park, Y., Kang, B. and Kim, KN., Influence of contact wire pre-sag on the dynamics of pantograph railway catenary, International journal of mechanical sciences, 52(11), pp. 1471-1490, 2010.

(41) Harell, P., Drugge, L. and Reijm, M., Study of critical sections in catenary systems during multiple pantograph operation, Journal of Rail and rapid transit, 219, 203-211, 2005.

(42) Zhai, W. M. and Cai, C. B., Effect of locomotive vibrations on pantograph-catenary system dynamics, The dynamics vehicles on roads and on tracks, 29, 47-58, 2000.

(43) Hartland, D. J., Developments towards an active pantograph current collections for high speed trains seminar (Ref. No. 1998/509), IEEE, Current collections for high speed trains seminar: 5/1-5/5, 1998.

(44) Poetsh, G., Evans, J., Meisinger, R., Kortum, W., Baldauf, W., Veitl., A. and Wallaschek, J., Pantograph/ catenary dynamics and control vehicle system dynamics, pp 159-195, 7, 1997.

(45) Aldo Balestrino, Ottorino Bruno, Alberto Landi and Luca Sani., Innovative solutions for overhead catenary-pantograph systems: Wire actuated control and observed contact force, Journal of vehicle system dynamics, Vol (33), pp 69-89, (2000).

(46) Wu, TX. And Brennan, MJ., Basic analytical study of pantograph-catenary system dynamics, Journal of vehicle system dynamics, Vol (30), pp 443-456, (1998).

(47) Song, Y., Ouyang, H., Liu, Z. and et al., Active control of contact force for high-speed railway pantograph-catenary based on multi-body pantograph model, Mechanism and Machine Theory 2017, 115: 35-39.

(48) Song, Y., Ouyang, H., et al., Sliding mode control with PD sliding surface for high-speed railway pantograph-catenary contact force under strong stochastic wind field, Shock and vibration, 2017, 2017:4895321.

(49) Song, Y., Liu, Z., Ouyang, H., et al., Nonlinear modelling of high-speed catenary based on analytical expressions of cable and truss elements, Vehical system dynamics, 2015, 53(10): 1-25.

(50) Song, Y., Liu, Z., Wang, H., et al., Nonlinear analysis of wind-included vibration of high-speed railway catenary and its influence on pantograph-catenary interaction, Vehicle system dynamics, 2016, 54(6): 1-25.

(51) O'Connor, D.N., Eppinger, S.D., Seering, W.P. and Wormley, D.N., Active Control of a High-Speed Pantograph, Trans. ASME. J. Dyn. Syst. Meas. Control, Vol (119), pp. 1-4, 1997.

(52) Ding, T., Chen, GX., Bu, J. and Zhang, WH., Effect of temperature and arc discharge on friction and wear behaviors of carbon strip/ cooper contact wire in pantograph catenary system, Journal of wear, 271, 1629-1636, 2011.

(53) Ambrosio, J., Pombo, J. and Pereira, M., Optimization of high-speed railway pantographs for improving pantograph-catenary contact, Theoretical and Applied Mechanics letters, 3, 013006, 2013.